nuclear fusion
IAEA

REVIEW PAPER

Microinstability theory in tokamaks

To cite this article: W.M. Tang 1978 *Nucl. Fusion* **18** 1089

View the article online for updates and enhancements.

Related content

- Measurements of microturbulence in tokamaks and comparisons with theories of turbulence and anomalous transport
  Paulett C. Liewer
- Finite-beta and resonant-electron effects on trapped-electron instabilities
  W.M. Tang, C.S. Liu, M.N. Rosenbluth et al.
- Survey of theories of anomalous transport
  J W Conner and H R Wilson

Recent citations

- Nonlinear trapping in wave–particle interactions in tokamaks
  K.C. Shaing *et al*
- Numerical study of ubiquitous modes in tokamak plasmas in the presence of impurities
  Yong Shen *et al*
- Stabilization of Short Wavelength Resistive Ballooning Modes by Ion-to-Electron Temperature and Gradient Ratios in Tokamak Edge Plasmas
  Jian-Qiang Xu *et al*

IOP ebooks™

Bringing together innovative digital publishing with leading authors from the global scientific community.

Start exploring the collection–download the first chapter of every title for free.

This content was downloaded from IP address 172.8.128.60 on 14/05/2021 at 06:31

REVIEW PAPER

MICROINSTABILITY THEORY IN TOKAMAKS*

W.M. TANG
Princeton University,
Plasma Physics Laboratory,
Princeton, New Jersey,
United States of America

ABSTRACT. Significant investigations in the area of tokamak microinstability theory are reviewed. Special attention is focused on low-frequency electrostatic drift-type modes, which are generally believed to be the dominant tokamak microinstabilities under normal operating conditions. The basic linear formalism including electromagnetic (finite-beta) modifications is presented along with a general survey of the numerous papers investigating specific linear and non-linear effects on these modes. Estimates of the associated anomalous transport and confinement times are discussed, and a summary of relevant experimental results is given. Studies of the non-electrostatic and high-frequency instabilities associated with the presence of high-energy ions from neutral-beam injection (or with the presence of alpha-particles from fusion reactions) are also surveyed.

1. INTRODUCTION

1.1. Motivation and scope of review

In recent years, favourable progress in tokamak research [1] has stimulated continued interest in the area of microinstability theory. The basic reason is the well-known fact that even if the large-scale MHD instabilities are suppressed, there still remains sufficient free energy in the confined plasma to drive micro-instabilities. These small-scale disturbances, in turn, can be a serious obstacle to efficient confinement because they can give rise to "anomalous" transport levels well above those associated with classical Coulomb scattering. Hence, it is important (i) to determine relevant stability criteria for normal tokamak operation, (ii) to investigate possible configurations and conditions which could inhibit the onset of the instabilities, and (iii) to obtain estimates of particle and thermal transport if such modes cannot be avoided.

It is generally believed that under normal operating conditions the dominant tokamak microinstabilities are the low-frequency drift-type modes. These instabilities are driven by the non-uniformity in both the spatial distribution and the temperature of the particles. In the presence of small fluctuating electric fields, the density and temperature gradients cause particles to move in an oscillatory manner with a characteristic frequency called the diamagnetic drift frequency. At the simplest level, $\vec{E}$ (electric field) $\times \vec{B}$ (magnetic field) drifts of the electrons and ions are the same. Since this leads to no effective momentum or energy exchange, there is no instability. However, when the electrons and ions are driven out of phase by dissipative processes such as collisions and wave-particle resonances, the particles can give up energy to the waves and cause them to grow. The resultant unstable modes are the dissipative and collisionless ("universal") drift instabilities.

* This work was supported by US Department of Energy Contract No.EY-76-C-02-3073.

In tokamaks, the available free energy driving the drift modes is made more accessible by the presence of a trapped-particle population. This results from the fact that the inherent non-uniformity in the magnetic field causes particles to be trapped in local magnetic wells. These particles, in turn, are more susceptible to de-stabilizing collisional processes. In addition, unlike the circulating (untrapped) particles, which are free to sample many oscillations in a typical wave period, the trapped particles are constrained to sample only a small portion of the wave. Unstable modes associated with these trapping effects were discovered by Kadomtsev and Pogutse in 1966 and named trapped-particle instabilities. Since that time, a major portion of the theoretical investigations of anomalous transport in tokamaks has been focused on these dangerous modes.

The status of tokamak microinstability theory up to 1970 has been extensively reviewed by Kadomtsev and Pogutse [2,3]. In the subsequent six years, there have been many important new developments in this area. These have primarily involved (i) the inclusion of essential geometric and collisional effects in the theory of low-frequency drift-type modes and (ii) the detailed studies of effects related to the use of energetic neutral beams in so-called two-component tokamak (TCT) systems. The first has led to significant changes in stability criteria, growth rates, and estimates of anomalous diffusion, while the second has stimulated much interest in high-frequency instabilities driven by velocity-space anisotropy. In addition, as progress is made towards reactor conditions, the ratio of plasma pressure to magnetic pressure is expected to increase. The resultant "finite-β", non-electrostatic effects have accordingly become an important subject of research. Finally, it should be noted that computer codes modelling anomalous transport have been developed and considerably refined in recent years.

The present review article is intended to survey significant work in tokamak microinstability theory covering the period from 1970 through 1977. To clarify the discussion of these developments and to view them in proper perspective, the following approach is adopted. After briefly recalling the properties of tokamak systems in Section 1.2, the instabilities of interest are classified and their essential features reviewed in Section 1.3. The theory of low-frequency electrostatic modes, together with finite-β (electromagnetic) modifications, is then treated in some detail in Section 2. This section presents the basic linear formalism and highlights the fundamental problems encountered in this area. The numerous papers investigating specific linear effects on these modes are then surveyed in Section 3. In Section 4, the consequences of low-frequency instabilities on confinement are discussed. This section includes a review of the various approaches to the problem of determining the non-linear evolution of such modes. Rough estimates of confinement in the presence of microinstabilities, the basic features of one-dimensional computer codes modelling anomalous transport, and relevant experimental results are also presented in this section. Investigations of possible high-frequency and non-electrostatic modes in tokamaks are discussed in Section 5. Finally, in Section 6, a summary of the current status of tokamak microinstability theory is given along with some comments on the outstanding linear and non-linear problems in this area.

1.2. Properties of tokamak systems

Before discussing the various types of micro-instabilities which can occur in a toroidal device, it is helpful to recall a few fundamental features of tokamaks and the orbits of particles in such systems. As shown on Fig.1, the toroidal plasma is confined in a helical magnetic field produced by the superposition of a strong toroidal field, B_t, generated by external coils, and a poloidal field, B_p, produced by a current within the plasma itself. The variables r, θ, ζ are, respectively, the radial position co-ordinate, the angle in the poloidal direction, and the angle in the toroidal direction, R and a are the major and minor radius, and ι, the rotational transform, is the angle through which a field line passes in the θ-direction on passing once around in the ζ-direction. This last quantity is also expressed in terms of the "safety factor," $q(r) = 2\pi/\iota = rB_t/RB_p$, which in turn is used in the description of several basic tokamak properties. First, the well-known constraint for MHD stability, $q(r) > 1$, places an upper limit on the current, I, flowing within a radius, r, in the plasma. In addition, the location of the rational surfaces, $r = r_s$, and the magnitude of the shear in the system are also generally expressed in terms of q(r). At the rational surfaces, the magnetic field lines close on themselves, and the safety factor satisfies the condition, $q(r_s) = m/n$, with m and n being integers. With regard to shear (i.e. the radial variation in the pitch of the magnetic field lines), the magnitude in terms of the shear length, L_s, is related to q(r) by the expression, $L_s = [(\epsilon/q^2)(dq/dr)]^{-1}$, with $\epsilon \equiv r/R$.

A primary distinguishing feature of charged-particle motion in toroidal systems is the "banana-shaped" bounce orbit executed by the trapped particles and

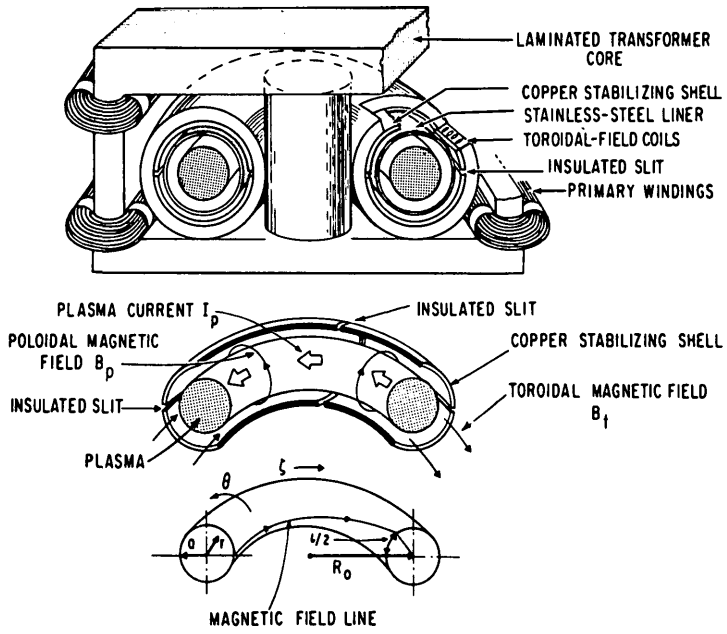

FIG.1. Basic tokamak system: a toroidal plasma confined in a helical magnetic field consisting of a strong, externally generated toroidal field and a poloidal field generated by the current in the plasma.

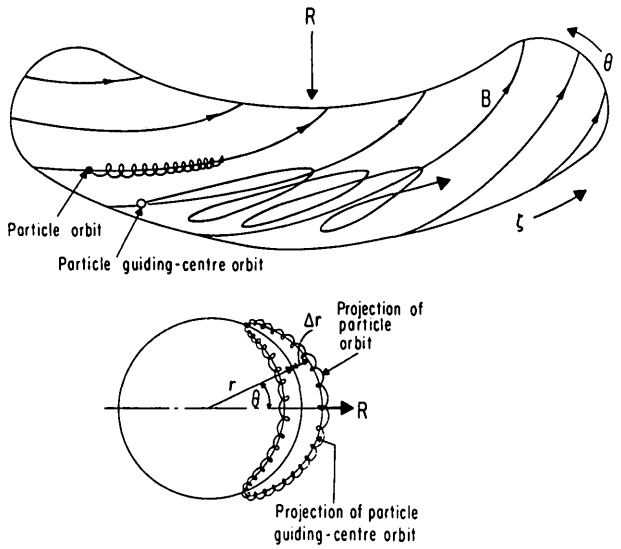

FIG.2. Schematic of trapped-particle orbits in a tokamak. Here the banana width is $r_B = 2\Delta r$.

depicted in Fig.2. Here the bounce motion along the field line is a consequence of magnetic trapping, and the radial or "banana" excursion, Δr, is due to the cross-field drifts produced primarily by the gradient of the magnetic field. Since the field is non-uniform and varies roughly as $B \cong B_0(1 - \epsilon \cos\theta)$, there is a maximum, B_{max}, on the inside of the torus and a minimum, B_{min}, on the outside. Invoking conservation of energy, E, and magnetic moment, μ, it is clear that particles with $E > \mu B_{max}$ pass freely along the field line while those with $E < \mu B_{max}$ will be reflected from the high-magnetic-field region and become trapped. The fraction of trapped particles, f_T, just corresponds to the fraction of velocity space they occupy. At the magnetic-field minimum ($\theta = 0$), this fraction is $[(B_{max}/B_{min}) - 1]^{1/2} \cong (2\epsilon)^{1/2}$, and, averaged over the magnetic surface (i.e. averaged over θ), $f_T \cong \epsilon^{1/2}$. The mean parallel velocity of these particles is approximately $\epsilon^{1/2} v_j$ with $v_j \equiv (2T/M)_j^{1/2}$ being the thermal velocity and T the temperature. Noting that the connection length along a field line between turning points is roughly qR, the average bounce frequency, ω_{bj}, can then be approximated by $\omega_{bj} = \epsilon^{1/2} v_j/qR$. For cross-field drifts the characteristic velocity is the magnetic drift velocity, which is approximately given by $\vec{v}_{Dj} \cong A_{Dj}(\vec{B} \times \nabla B)/B^2$ with $A_{Dj} = [(v_\perp^2/2) + v_\parallel^2]/\Omega_j$ and $\Omega_j = (eB/Mc)_j$. The poloidal or θ-component here is associated with the toroidal gradient drift, and the radial component with the "banana" drift which causes the excursion, Δr, shown in Fig.2. Taking $v_{Dj} \cong v_j \rho_j/R$, this radial half width of the banana orbit can be estimated by $\Delta r \cong v_{Dj}/\omega_{bj} \cong \rho_j q/\epsilon^{1/2}$ where $\rho_j = v_j/\Omega_j$. A much more detailed analysis of particle

orbits in tokamaks can be found, e.g. in Ref.[4], and a comprehensive summary of the main features of such orbits appears in Ref.[2].

For trapped particles, the "effective" collision frequency is given by $\nu_{eff,j} = \nu_j/\epsilon$, where $\nu_j \equiv 4\pi n Z_j^2 e^4 \times \ln\Lambda/[M_j^{1/2}(2T_j)^{3/2}]$ is the usual Spitzer collision frequency for 90°-scattering, and the $1/\epsilon$ enhancement factor comes from velocity-space pitch-angle scattering. Specifically, since deflections much less than 90° can cause de-trapping, the relevant quantity here is the time it takes a trapped particle to scatter through the pitch angle, $\Theta \equiv \tan^{-1}(v_\parallel/v_\perp) \cong \epsilon^{1/2}$. The appearance of trapped-particle instabilities requires that this effective collision frequency be small enough to allow the trapped particles to execute many bounce orbits before being collisionally de-trapped. In terms of the well-known collisionality parameter, $\nu_{*j} \equiv \nu_{eff,j}/\omega_{bj}$, the basic requirement here is just $\nu_{*j} < 1$. Particles satisfying this criterion are said to be in the "banana regime." At higher collisionality, the trapped orbits lose their significance because particles on the average are scattered into passing (circulating) orbits in less than a bounce period. If the circulating particles can complete many transit orbits before encountering Coulomb scattering, then they fall in the "plateau regime." Taking the average connection length of such particles to again be approximately qR, the requirement here is just $\nu_j < v_j/qR$. In terms of ν_*, this plateau regime criterion is $1 < \nu_{*j} < \epsilon^{-3/2}$. The so-called "collisionless" or "universal" drift instabilities can appear in this intermediate range of collisionality. Finally, for the collisional or "Pfirsch-Schlüter regime", the criterion is $\nu_{*j} > \epsilon^{-3/2}$. The relevant microinstabilities, which can appear here, are the collisional or dissipative drift modes. In the absence of micro-instabilities, the transport in the various collisional regimes described has been analysed in great detail [5,6] and has recently been reviewed in Ref.[7].

1.3. Classification of tokamak microinstabilities

It is well known that the primary source of free energy available to drive microinstabilities in low-beta toroidal devices is the expansion energy associated with the density and temperature gradients of the confined plasma. Under normal conditions, the velocity distributions common to such systems are isotropic to a good approximation. As shown in standard derivations [8, 9], the expansion free energy can give rise to drift and shear-Alfvén modes. Most of the relevant tokamak microinstabilities are related to the drift branch, which can be analysed in the electrostatic limit. Non-electrostatic modes associated with the shear-Alfvén branch can also be de-stabilized but generally under more restrictive conditions.

The principal categories of drift instabilities are (i) the collisional or dissipative drift modes, (ii) the collisionless or "universal" drift modes, and (iii) the trapped-particle modes. Both the dissipative and universal-type drift instabilities are characterized by parallel phase velocities which lie between the ion and electron thermal velocities, $v_i < \omega/k_\parallel < v_e$. At long wavelengths, the characteristic mode frequencies are close to the electron diamagnetic drift frequency; i.e. $\omega \cong \omega_{*e} = (mcT_e)/(eBrr_n)$ where m is the poloidal mode number, r is the radial co-ordinate, and $r_n = |d\ln n/dr|^{-1}$ is the density gradient scale length. Most studies of these instabilities have been carried out in the slab limit ignoring toroidal effects.

The dissipative drift modes, which are derivable [3,9] from the Braginskii fluid equations [10], are primarily de-stabilized by electron-Coulomb-type collisions, ν_e, and require $\nu_e > k_\parallel v_e$. In the high-collision-frequency regime, the dominant modes have long perpendicular wavelengths ($k_\perp \sim r_n$) and can give rise to a Bohm-like diffusion rate. At lower collision frequencies, the relevant perpendicular wavelengths become of the order of the ion gyroradius, and the resultant diffusion rate exhibits a pseudoclassical-type scaling [11]. These modes can be further de-stabilized by the presence of a parallel current along the magnetic field [12].

In the "collisionless" regime, where $\nu_e < k_\parallel v_e$, the primary de-stabilizing process for drift waves is inverse electron-Landau damping. These instabilities are called collisionless or universal drift modes and can be readily derived by following well-known kinetic-theory treatments [13–16]. Electron temperature gradients in the same direction as the density gradients (i.e. $\eta_e \equiv d\ln T_e/d\ln n_e > 0$) can exert a significant stabilizing influence [16]. The opposite case, $\eta_e < 0$, is de-stabilizing, but such configurations only occur under very special situations [17]. Other possible conditions, which can further de-stabilize these drift waves, are (i) the presence of impurities and (ii) the distortion of the Maxwellian electron velocity distribution by the current in the plasma. In the first case, impurity-driven drift instabilities can result provided the impurity density gradient and the density gradient of the main plasma are oppositely directly [18]. For the latter case, current-driven drift instabilities can become significant if the current-drift velocity, u_0, is sufficiently large. Specifically, the growth rate here

is proportional to the ratio, u_0/v_e, with v_e being the electron thermal velocity [19].

When radially non-local effects are taken into account, it was found in early work that the influence of magnetic shear together with ion viscosity could stabilize dissipative drift modes provided the shear is sufficiently strong [3], i.e. if $r_n/L_s > (m_e/m_i)^{1/4}$. For universal modes it was concluded that the instabilities could be suppressed if the condition $r_n/L_s > (m_e/m_i)^{1/3}$ is satisfied [15]. However, it has been reported in very recent calculations [19a] that, in the absence of toroidal effects, the collisionless drift modes are actually always stable. Similar conclusions have recently been obtained for the case of the dissipative drift instabilities [19b]. These results were derived by ignoring impurity and current-driven effects and are applicable only in the electrostatic limit. It should also be recalled that, for highly peaked density profiles, unstable drift eigenmodes can persist even in the absence of toroidal effects [14].

In a toroidal system, the relatively simple picture of drift waves just described remains valid only if the collisionality of the electrons is high enough to eliminate trapped-electron effects. The basic requirement here is just $\nu_{*j} > 1$. If this condition is not satisfied, then important de-stabilizing effects associated with trapped particles must be considered. Moreover, even for $\nu_{*j} > 1$, the toroidal contributions from the ∇B-drift of the ions can lead to important de-stabilizing effects in the radially non-local theory.

Since ν_{*j} is independent of mass and is proportional to n_j/T_j^2, the fact that electron temperatures are typically higher than those of ions in present-day experiments implies that the electrons should be the first to enter the banana regime. The associated instabilities here are the trapped-electron modes [20]. Basically, these again are unstable drift waves which are now primarily driven by positive temperature gradients ($\eta_e > 0$) together with collisional dissipation. In addition, they can be further de-stabilized by finite-ion-gyroradius effects (analogous to the universal mode) [21] and by both resonant [22, 23] and non-resonant [24, 25] interactions associated with the ∇B-magnetic drift. For sufficiently short wavelengths (i.e. large $k_\perp \rho_i$) and for particular profiles, the ∇B drifts can give rise to so-called "ubiquitous"-type drift modes which propagate in the ion rather than the usual electron diamagnetic direction [24]. Standard one-dimensional radial calculations [26] as well as two-dimensional treatments including multiple rational surface effects [27] indicate that the magnetic shear in tokamaks is insufficient to stabilize the trapped-electron modes. However, the reversed density gradient profiles ($\nabla n \cdot \nabla T < 0$), which are possible under certain modes of tokamak operation, can exert a strong stabilizing influence [22]. Effects associated with finite β ($\beta \equiv$ plasma pressure/magnetic pressure) and with Landau resonances by circulating electrons are also found to favour stability [28].

At the higher ion temperatures, where T_i is comparable to T_e, it becomes possible for both ions and electrons to be in the banana regime ($\nu_i^*, \nu_e^* < 1$). Since the mode frequency of trapped-electron instabilities falls above the ion bounce and transit frequencies ($\omega_{bi}, k_\parallel v_i < \omega$), trapped-ion effects have a negligible influence on them. However, additional unstable drift waves with characteristic frequencies below the ion bounce and transit frequencies ($\omega < \omega_{bi}, k_\parallel v_i$) can now be generated. These instabilities are known as trapped-ion modes [2,3] and are primarily driven by electron collisional dissipation in the presence of radial density gradients. They are usually associated with the electron diamagnetic drift branch ($\omega \propto \omega_{*e}$) and can be further de-stabilized by temperature gradients [29]. Among the more prominent stabilizing mechanisms are ion-collisional damping [2, 29], transit resonance damping by untrapped ions [30], and both bounce [31] and magnetic drift [32] resonance damping by trapped ions. In the transit and bounce resonance cases, the effects can become unfavourable if the temperature gradients are sufficiently large ($\eta_i > 2/3$). It should be noted, however, that for such situations the dominant unstable branch of the trapped-ion modes is the ion diamagnetic branch ($\omega \propto \omega_{*i}$) rather than the usual electron branch [33]. Both resonant and non-resonant effects associated with ∇B-magnetic drifts can be strongly de-stabilizing for this ion branch. For the special case of reversed density gradient profiles, the usual trapped-ion instabilities are easily stabilized [22], but the ion branch of these modes can persist as residual instabilities with reduced growth rates [33]. Analysis of the radial mode structure of the familiar electron branch indicates that radially non-local effects can reduce the growth rate but cannot effect a complete stabilization of the modes [34]. Impurity effects can also exert a significant stabilizing influence [35]. For example, Landau damping by impurity ions in the plateau regime can be quite favourable [36]. More generally, collisions with impurities increase the ion-collisional damping and reduce the de-stabilizing effect of electron collisions.

In the limit of very high temperatures where the plasma can essentially be treated as collisionless

($\nu_{eff,j} < \omega < \omega_{bi}$, $k_\parallel v_i$) the trapped-ion mode evolves to a fluid-like interchange mode known as the "collisionless" trapped-particle instability [2, 37]. This is a purely growing, non-resonant flute mode driven by the unfavourable magnetic drifts of trapped particles in the presence of radial density gradients. It is quite similar to the familiar MHD interchange mode in simple mirror machines, except that in tokamaks charge separations are severely retarded by the high dielectric constant of the plasma. Stabilizing effects can come from radially non-local effects associated with magnetic shear [38] and from impurity effects [39]. A more obvious source of stabilization is the reduction or elimination of the regions where the average magnetic drifts are unfavourable. This can result from finite-beta effects which generate a diamagnetic well [40] and also from a vertical elongation of the plasma cross-section [41]. Although the rough estimates of diffusion for the modes indicate a rapid Bohm-like scaling, the actual conditions for their existence are unlikely to be met even in the reactor regime.

Two basic features common to the instabilities covered in the preceding discussion are that the associated perturbed potentials are well extended along the magnetic field line and that such potentials have predominantly even symmetry around the field minimum (B_{min}). In contrast to the first characteristic, a class of trapped-electron instabilities, which are strongly localized along the field line by ion magnetic drift effects, have also been considered [42]. Although the growth rates here are generally smaller, these modes are far less susceptible to the stabilizing influences of shear and Landau damping by circulating electrons. With regard to the question of symmetry, trapped-particle modes with odd symmetry around the field minimum have been analysed in the collisionless ($\nu_{eff,j} \ll \omega$) limit [43, 44]. These instabilities are driven by inverse Landau damping in the presence of positive temperature gradients which must fall in a very narrow range, $2/3 < \eta_j < 1$. Electron modes of this type have been found with characteristic frequencies close to the average electron bounce frequency, ω_{be}, and typically short wavelengths, $k_\perp \rho_i > 1$ [43]. Ion modes are found to occur at longer wavelengths, $k_\perp \rho_i < 1$, with characteristic frequencies close to the average ion-bounce frequency [44]. Since the electric field due to odd modes is maximum at B_{min}, the scattering of deeply trapped particles can be quite effective [45]. Collisions and radially non-local effects do not appear to alter the basic features of these instabilities [46], which can be further de-stabilized by the presence of impurities [47].

As noted earlier in this section, the expansion free energy in toroidal systems can give rise to shear-Alfvén modes as well as the familiar electrostatic drift waves. The presence of such modes becomes significant when β_p, the ratio of plasma pressure to the pressure of the poloidal magnetic field, begins to exceed unity. Their effect on the electrostatic drift modes has generally been found to be stabilizing [48, 28]. However, radially local calculations indicate that for $\beta_p > 1$, electromagnetic (non-electrostatic) shear-Alfvén modes can be de-stabilized by toroidal effects [49, 50]. In the lower frequency range, $\omega < v_i/qR$, such modes can be driven by the inverse Landau damping of ions in the presence of density and temperature gradients [49]. At higher frequencies where $v_i/qR < \omega \sim v_A/qR < \omega_{be}$ (with v_A being the Alfvén speed), the primary driving mechanism appears to be trapped-electron collisions [50].

The rapid development of very high-powered neutral-beam sources in recent years has stimulated much interest in the use of such beams to heat toroidal plasmas [1]. Basically, this involves injecting high-energy neutrals which interact with the plasma by ionization or charge exchange. The energetic ions generated by this process then gradually slow down by collisions with the main plasma ions and electrons. In addition to plasma heating, it has been emphasized that for sufficiently high injection energy, the energetic ions can produce fusion energy directly while thermalizing with the bulk plasma [51, 1]. This beam-plasma system or TCT (two-energy component torus) has a required density-confinement-time product below the "Lawson-breakeven" value, i.e. $n\tau_E < 10^{14}\,cm^{-3} \cdot s$. An extensive review of neutral-beam-injected tokamak fusion reactor concepts has recently been presented in Ref.[52].

It is clear that the injection of high-energy neutral beams will tend to introduce velocity space anisotropy as another major source of free energy in a toroidal plasma. The resultant non-Maxwellian ion distributions can generate unstable high-frequency modes which could greatly increase the energy loss rate of the beam [53, 54]. It is found, however, that if the beams are injected parallel to the magnetic field, the system should be stable against most high-frequency modes [55]. As shown in Ref. [55], detailed calculations, carried out in the infinite-uniform-medium limit for representative steady-state distributions, indicate that

ion acoustic modes are easily stabilized by background ion-Landau damping, and that both shear and compressional Alfvén instabilities can be avoided. In the latter cases, the coupling between the beam and the Alfvén waves is effectively suppressed because the injection velocity is typically less than the Alfvén speed. With regard to the well-known high-frequency electrostatic instabilities associated with ion-cyclotron, lower hybrid, and electron plasma waves, it is found that typical steady-state distributions lack the required degree of perpendicular velocity space anisotropy to excite such modes. If the variation in the guiding-centre trajectories of the fast ions is taken into account, ordinary electromagnetic ion-cyclotron instabilities are also unlikely to appear [56].

When the spatial anisotropy (i.e. density gradients) in the beam-plasma system is considered, the most prominent instability appears to be the shear-Alfvén mode [55, 57]. Here the shear-Alfvén waves are de-stabilized by Landau resonances with fast ions that have unfavourable magnetic (∇B) drifts. Finite-medium calculations, which include the spatial variation along the field line of the beam drift velocity, the presence of trapped electrons, and radially non-local effects such as magnetic shear, indicate a reduced but still substantial growth rate [57]. It has also been noted that short-wavelength ion-diamagnetic drift waves can be de-stabilized by resonant interactions with the beam [55, 58].

For ordinary plasma systems without energetic neutral beams, the velocity space anisotropy present is usually insufficient to drive modes of any major consequence. In particular, the threshold for exciting high-frequency current-driven instabilities such as the current-driven ion-acoustic mode cannot be reached for typical tokamak parameters. However, it has recently been noted that for the case of a collisionless toroidal plasma in the presence of an applied electric field, "slide-away"-type distributions for electrons can result. Such distributions are found to be sufficiently anisotropic to drive high-frequency instabilities [59].

Just as in the case of the fast-ion population generated by the injection of energetic neutral beams, alpha-particles produced in thermonuclear reactions can also be a prominent source of velocity space anisotropy. For the case of highly anisotropic (δ-function) α-particle velocity distributions, radially local calculations indicate that fast magnetosonic (compressional Alfvén) waves can be de-stabilized by resonant interactions with trapped α-particles at the α-particle cyclotron frequency [60]. The growth rates of these "thermonuclear cyclotron instabilities" are found to be proportional to the α-particle density and can be considerably reduced by a thermal spread of the distribution [61]. However, even for an isotropic velocity distribution, these modes, along with the shear-Alfvén modes discussed earlier, can still be unstable if $v_\alpha > v_A$ and if the density gradient of the α-particles is taken into account [62].

2. BASIC THEORY OF LOW-FREQUENCY ELECTROSTATIC MODES

2.1. Fundamental considerations

2.1.1. Ordering

It is well known that the kinetic-theory analysis of microinstabilities entails solving the Boltzmann equation together with Maxwell's equations. In dealing with low-frequency, electrostatic modes, this basic set of equations can be considerably simplified. Specifically, for mode frequencies, ω, much smaller than the gyrofrequency, $\Omega_j \equiv (eB/Mc)_j$, it is convenient to adopt a small-gyroradius ordering [63, 64], $\rho_j/L \equiv \delta \ll 1$, where $\rho_j \equiv v_j/\Omega_j$ is the gyroradius, v_j the thermal velocity, j denotes particle species, L is a characteristic scale length of equilibrium variations and δ the smallness parameter. Hence, to determine the equilibrium (F) and perturbed (f) distribution functions, the following ordering of terms in the Boltzmann equation is invoked:

$$\frac{\partial \hat{F}}{\partial t} + \vec{v}\cdot\nabla\hat{F} + \frac{e}{M}\left(\vec{\mathcal{E}} + \frac{1}{c}\vec{v}\times\vec{B}\right)\nabla_v\hat{F} = C(\hat{F},\hat{F}) \qquad (1)$$

$$\begin{array}{ccccccc} & \delta & & \delta & 1 & & \delta \quad (F) \\ \delta & 1 & & 1 & 1 & & \delta \quad (f) \end{array}$$

where $\hat{F} \equiv F + f$, $\vec{\mathcal{E}} = -\nabla(\Phi_0 + \Phi)$ with Φ_0 being the equilibrium potential and $C(\hat{F},\hat{F})$ a collision operator.

The velocity variables can be expressed in terms of the conserved quantities, the energy per unit mass

$$E = v^2/2 + e\Phi_0/M$$

and the magnetic moment per unit mass, $\mu = v_\perp^2/2B$, where

$$\vec{v} = v_{||}\hat{n} + \vec{v_\perp}, \quad \hat{n} \equiv \vec{B}/B$$

$$v_{||} = \pm (2)^{1/2} (E - \mu B - e\Phi_0/M)^{1/2}$$

$$\vec{v}_\perp = v_\perp (\cos\phi\, \hat{e}_1 + \sin\phi\, \hat{e}_2)$$

$\hat{e}_1$ and $\hat{e}_2$ are any two unit vectors perpendicular to $\hat{n}$, and ϕ is the azimuth (gyrophase) angle in velocity space. In terms of these variables, the ∇ and ∇_v operators in Eq.(1) become

$$\nabla = \frac{\partial}{\partial \vec{x}} + \frac{e}{M} \nabla\Phi_0 \frac{\partial}{\partial E} - (\mu \nabla B + v_{||} \nabla \hat{n} \cdot \vec{v}_\perp) \frac{1}{B} \frac{\partial}{\partial \mu}$$

$$+ \left[\nabla \hat{e}_2 \cdot \hat{e}_1 + \frac{v_{||}}{v_\perp^2} \nabla \hat{n} \cdot (\vec{v}_\perp \times \hat{n})\right] \frac{\partial}{\partial \phi} \qquad (2)$$

and

$$\nabla_v = \vec{v} \frac{\partial}{\partial E} + \vec{v}_\perp \frac{1}{B} \frac{\partial}{\partial \mu} + \frac{1}{v_\perp^2} (\hat{n} \times \vec{v}_\perp) \frac{\partial}{\partial \phi} \qquad (3)$$

With regard to the spatial variables, it is convenient to define them in terms of the magnetic field configuration, i.e.

$$\vec{B} = B\hat{n} = B_p \hat{\chi} + B_t \hat{\zeta} \qquad (4)$$

where

$$B_p \hat{\chi} = \nabla\chi = \nabla\zeta \times \nabla\psi$$

ψ is the poloidal magnetic flux, ζ is the angle about the axis of symmetry, and $B_t = I/R$ with I being a constant and R being the distance to the axis of symmetry.

2.1.2. *Equilibrium*

For the equilibrium distribution, $F = F^{(0)} + F^{(1)} + \ldots$, Eq.(1), to lowest order, yields $\partial F^{(0)}/\partial\phi = 0$, and to first order it gives

$$\vec{v} \cdot \nabla F^{(0)} - \vec{v} \cdot (\mu \nabla B + v_{||} \nabla \hat{n} \cdot \vec{v}_\perp) \frac{1}{B} \frac{\partial}{\partial \mu} F^{(0)}$$

$$- \frac{e}{M} \nabla\Phi_0 \cdot \vec{v}_\perp \frac{1}{B} \frac{\partial}{\partial \mu} F^{(0)}$$

$$- \Omega \frac{\partial}{\partial \phi} F^{(1)} = C[F^{(0)}, F^{(0)}] \qquad (5)$$

The superscripts here denote the order in δ. Averaging Eq. (5) over ϕ gives

$$v_{||} \hat{n} \cdot \nabla F^{(0)} = C[F^{(0)}, F^{(0)}]$$

which is satisfied by the Maxwellian solution,

$$F^{(0)}(\psi, E) = F_M$$

$$= N_0(\psi) [M/2\pi T(\psi)]^{3/2} \exp[-ME/T(\psi)] \qquad (6)$$

where N_0 is the particle density and T is the temperature. Substitution of this result back into Eq.(5) then gives

$$\Omega \partial F^{(1)}/\partial\phi = \vec{v}_\perp \cdot \nabla F_M = (\partial/\partial\phi)(\vec{v}_\perp \times \hat{n} \cdot \nabla F_M)$$

Here the solution is just $F^{(1)} = F_D + \bar{F}^{(1)}$, where the diamagnetic contribution, F_D, is

$$F_D = (1/\Omega) \vec{v} \times \hat{n} \cdot \nabla F_M \qquad (7)$$

and the gyrophase-independent function, $\bar{F}^{(1)}$, must be determined from the second-order form of Eq.(1). Taking the ϕ-average of this equation then yields the usual neoclassical result [6],

$$v_{||} \hat{n} \cdot \nabla \bar{F}^{(1)} + \vec{v}_D \cdot \nabla F_M = C[F_M, \bar{F}^{(1)}] \qquad (8)$$

with the magnetic drift velocity, $\vec{v}_D$, defined as

$$\vec{v}_D \equiv \frac{1}{\Omega} \hat{n} \times (\mu \nabla B + v_{||}^2 \hat{n} \cdot \nabla \hat{n} + \frac{e}{M} \nabla\Phi_0) \qquad (9)$$

2.1.3. *Perturbations*

In determining the perturbed distribution, $f = f^{(0)} + f^{(1)} + \ldots$, the ratio of parallel to perpendicular wavenumbers for perturbations is generally treated as small, i.e. $k_{||}/k_\perp = O(\delta)$ with $k_\perp \rho_i = O(1)$. Using this gyro-kinetic ordering with $F^{(0)} = F_M$ in Eq.(1) then yields, to lowest order,

$$\left(\vec{v}_\perp \cdot \nabla - \Omega \frac{\partial}{\partial \phi}\right) h = 0 \qquad (10)$$

where $h = f^{(0)} + F_M e\Phi/T$. Here it is convenient to transform to a co-ordinate system displaced by a gyro-orbit from a flux surface, i.e.

$$\psi' = \psi - \frac{1}{\Omega} \hat{n} \times \vec{v}_\perp \cdot \nabla\psi$$

$$\chi' = \chi - \frac{1}{\Omega} \hat{n} \times \vec{v}_\perp \cdot \nabla\chi$$

$$\phi' = \phi \qquad (11)$$

Now Eq. (10) becomes $\partial h/\partial\phi' = 0$, so that $h = h(E,\mu,s,\psi',\chi')$ with s being the position co-ordinate along the field line. Proceeding as before, the specific form of h is calculated from the constraint equation obtained by taking the gyrophase (ϕ') average of the first-order form of Eq.(1). After some straightforward but lengthy algebraic steps [65], this procedure leads to the result

$$\left[\frac{\partial}{\partial t} + v_{||}\hat{n}\cdot\nabla s\frac{\partial}{\partial s} + \vec{v}_D\cdot\left(\nabla\psi\frac{\partial}{\partial\psi} + \nabla\chi\frac{\partial}{\partial\chi}\right)\right]h$$

$$= \frac{e}{T}F_M\frac{\partial}{\partial t}\left\langle\Phi\right\rangle_{\phi'}$$

$$+ \frac{e}{M}\frac{1}{\Omega}B\left(\frac{\partial}{\partial\psi}F_M\right)\left(\frac{\partial}{\partial\chi}\left\langle\Phi\right\rangle_{\phi'}\right) + \left\langle C(F_M,h)\right\rangle_{\phi'} \tag{12}$$

where

$$\left\langle A\right\rangle_{\phi'} \equiv (1/2\pi)\int_0^{2\pi} d\phi' A(\phi')$$

represents the gyrophase average. Note here that, to this order, $\bar{F}^{(1)}$, the neoclassical portion of the equilibrium distribution function, does not contribute to $f^{(0)}$ [65, 66]. Equation (12) is then solved for h, and the result used in the perturbed Poisson equation

$$\nabla^2\Phi = -4\pi\sum_j Z_j e_j \int d^3v f_j^{(0)} \tag{13}$$

to give the basic mode equation for low-frequency electrostatic instabilities in a system which is MHD-stable. Here Z is the charge number and

$$\int d^3v = \sum_\sigma \iiint dE\, d\mu\, d\phi\, B/|v_{||}|$$

with $\sigma = v_{||}/|v_{||}|$ being the sign of the longitudinal velocity. Since the Debye length, $\lambda_D = (4\pi N_0 e^2/T)^{1/2}$, is typically much shorter than the wavelengths of interest, Eq.(13) just reduces to the familiar quasi-neutrality condition:

$$\sum_j Z_j e_j \int d^3v f_j^{(0)} = 0 \tag{14}$$

with

$$f_j^{(0)} = -(Ze\Phi F_M/T)_j + h_j$$

In dealing with toroidal systems, the r,θ,ζ-co-ordinates, as shown in Fig.1, are commonly employed. The equilibrium magnetic field can be expressed as

$$\vec{B} = B_T\hat{e}_\zeta + B_p\hat{e}_\theta \tag{15}$$

where $\hat{e}_\zeta$ and $\hat{e}_\theta$ are unit vectors in the ζ- and θ-directions and B_T and B_p are the toroidal and poloidal components of the field with B_T being typically much greater than B_p. For simplicity, it is often assumed that the device is an axisymmetric, large-aspect-ratio, ($R/r \equiv 1/\epsilon > 1$), torus with magnetic surfaces which are circular and concentric. The guiding-centre co-ordinates given in Eq.(11) can then be expressed as

$$\begin{aligned} r' &= r - \frac{1}{\Omega}v_\perp\sin\phi \\ \theta' &= \theta - \frac{1}{r\Omega}v_\perp\cos\phi \\ \phi' &= \phi \end{aligned} \tag{16}$$

with $\zeta' = \zeta$.

Without loss of generality, we can introduce the following ansatz for the perturbed quantities:

$$\begin{pmatrix}\Phi\\ f^{(0)}\end{pmatrix} = \begin{pmatrix}\hat{\Phi}(r,\theta)\\ \hat{f}^{(0)}(r,\theta)\end{pmatrix} \times \exp\left(-i\omega t + i(m\theta - \ell\zeta)\right) \tag{17}$$

where $\hat{\Phi}$ and $\hat{f}^{(0)}$ contain the slow poloidal (θ) variation. This implies that perturbed quantities must satisfy the requirement, $|(1/\hat{\Phi})(\partial\hat{\Phi}/\partial\theta)| \ll m$, and that, to lowest significant order, the θ-variation in $\hat{\Phi}$ and $\hat{f}^{(0)}$ is unaffected by the guiding-centre transformation given in Eq.(16).

To obtain the perturbed distribution function, Eq. (12) must be solved for h subject to boundary conditions ensuring that it be single valued. Regarding this point, Connor and Hastie [67] have emphasized that any ansatz considered must satisfy not only the basic ordering requirement for long parallel wavelengths ($k_{||}\rho_j \sim \delta$) but also the periodicity requirements for θ and ζ in the presence of magnetic shear. Periodicity in the toroidal angle (ζ) is easily satisfied in the axisymmetric systems of interest. The boundary conditions in the poloidal angle (θ) are

$$h(\theta, \pm v_{||}) = h(\theta + 2\pi, \pm v_{||}) \tag{18}$$

for untrapped particles, and

$$h(\theta_0, \pm v_{||}) = h(\theta_0, \mp v_{||}) \tag{19}$$

for trapped particles. Here, θ_0 designates a trapped-particle turning point (i.e. the position where $v_{||} = 0$).

In accordance with Eqs (15), (16) and (17), the function h has the form

$$h(r',\theta',\zeta') = \hat{h}(r',\theta)\exp[-i\omega t + i(m\theta' - \ell\zeta')]$$

and

$$(\hat{n}\cdot\nabla s)(\partial/\partial s) = (1/Rq)(\partial/\partial\theta + q\partial/\partial\zeta)$$

Hence, Eq.(12) can be expressed as

$$\left(\omega - \frac{v_{||}}{Rq}(m - \ell q - i\frac{\partial}{\partial\theta})\right.$$

$$\left. + i(v_{Dj})_r \frac{\partial}{\partial r'} - k_\theta (v_{Dj})_\theta - iC_j\right)\hat{h}_j(r',\theta)$$

$$= (Z\frac{e}{T}F_M)_j(\omega - \omega^*_{Tj})$$

$$\times\left\langle \hat{\Phi}(r' + \frac{1}{\Omega}v_\perp \sin\phi', \theta)\right.$$

$$\left.\times \exp(ik_\theta \frac{1}{\Omega} v_\perp \cos\phi')\right\rangle_{\phi'}, \tag{20}$$

where

$$C_j\hat{h}_j = \left\langle C_j(F_{Mj}, \hat{h}_j)\right\rangle_{\phi'}$$

$(v_D)_r$ and $(v_D)_\theta$ are the r and θ components of $\vec{v}_D$ given in Eq.(9), $E \equiv M_j v^2/2$,

$$\omega^*_{Tj} \equiv \omega^*_j[1 + \eta_j(E/T_j - 3/2)]$$

$$\eta_j \equiv d\ell nT_j/d\ell nn_j, \quad \omega^*_j \equiv (k_\theta cT/eBr_n)_j$$

$$(r_n^{-1})_j \equiv -d\ell nn_j/dr, \quad n_j \equiv N_{0j}$$

$k_\theta = m/r$, and m and ℓ are the poloidal and toroidal mode numbers. It is useful to note here that the characteristics of this differential equation suggest the transformation

$$r_1 = r' - r_{Bj}(\theta)$$
$$\theta_1 = \theta \tag{21}$$

where

$$r_{Bj}(\theta) \equiv \int^\theta d\theta' \frac{1}{v_{||}} Rq(v_{Dj})_r \tag{22}$$

Physically, $r_{Bj}(\theta)$ just represents the radial "banana" excursion of a particle away from a magnetic surface (at $r' = r_1$). Equation (20) then reduces to an ordinary differential equation in one independent variable (θ_1) and has the form

$$\left[\omega + \omega_{Dj} - iC_j - \frac{v_{||}}{Rq}\right.$$

$$\left.\times\left(m - \ell q - i\frac{\partial}{\partial\theta_1}\right)\right]\hat{h}_j = A_j \tag{23}$$

with $\omega_{Dj} \equiv -k_\theta(v_{Dj})_\theta$ and A_j defined as the right-hand side of Eq.(20).

For $\Phi_0 = 0$ the magnetic drift velocity in the vacuum field limit becomes

$$\vec{v}_D = (\mu B + v_{||}^2)(\hat{n}\times\nabla B)/(\Omega B)$$

Taking $B \cong B_0(1 - \epsilon\cos\theta)$ then yields

$$\omega_{Dj} = k_\theta \cos\theta(\mu B + v_{||}^2)/(R\Omega_j)$$

Since the toroidal canonical angular momentum, P_ζ, is a constant of the motion for axisymmetric systems, the expression for $r_{Bj}(\theta)$ can also be simplified. Specifically,

$$P_\zeta \simeq M_j R(v_\zeta - \Omega_{\theta j} r)$$

so that

$$r' - r_1 \simeq [v_\zeta - (v_\zeta)_1]/\Omega_{\theta j}$$
$$\simeq [v_{||} - (v_{||})_1]/\Omega_{\theta j}$$

with $\Omega_{\theta j} \equiv e_j B_p/M_j c$. Hence, from Eq.(21),

$$r_{Bj}(\theta) = r' - r_1 \simeq [v_{||} - (v_{||})_1]/\Omega_{\theta j} \tag{24}$$

This result can now be used in Eq.(23) to express the factor $m - \ell q(r')$ in terms of r_1. Expanding around

$r' = r_1$ and employing the approximation in Eq.(24) then yields

$$\left(\omega + (\omega_{D1})_j - iC_j - \frac{v_{||}}{Rq}\left[m - \ell q(r_1) - i\frac{\partial}{\partial\theta_1}\right]\right)\hat{h}_j = A_j \tag{25}$$

where $(\omega_{D1})_j$, the effective magnetic drift frequency, has the form

$$(\omega_{D1})_j = (\hat{\omega}_D \cos\theta + \tilde{\omega}_D)_j \tag{26}$$

with

$$\hat{\omega}_D \equiv k_\theta (\mu B + v_{||}^2)/(R\Omega)$$

$$\tilde{\omega}_D \equiv (\varepsilon/q)(k_\theta q'/\Omega q)[v_{||}^2 - v_{||}(v_{||})_1]$$

and $q' = dq/dr$.

Before proceeding with the analysis of Eq.(25), it is necessary to specify the appropriate model for the linearized, gyrophase-averaged collision operator, C_j. The most general form relevant to plasma physics problems is the complete Fokker-Planck operator introduced by Rosenbluth, et al. [68]. However, for investigating low-frequency toroidal microinstabilities, it is sufficient to either use reduced forms of this very complicated operator or to employ much simpler collision models.

In the banana and plateau regimes, the primary effect of collisions is velocity-space pitch-angle scattering [7, 29]. Hence, to a good approximation, scattering in energy can be neglected, and the linearized, gyrophase-averaged Fokker-Planck operator reduces to a Lorentz-like operator of the form

$$C_j h_j = 2\hat{\nu}_j \left(\frac{T}{E}\right)_j^{3/2} \frac{(1-\lambda B)^{1/2}}{B} \frac{\partial}{\partial\lambda} \times \left(\lambda(1-\lambda B)^{1/2} \frac{\partial}{\partial\lambda}\right) h_j \tag{27}$$

where $\lambda \equiv \mu/E$ is the pitch-angle variable. This implies that in velocity space the equation for h now simplifies to a one-dimensional differential equation in λ with the energy variable becoming an explicit parameter. In the absence of impurities, the collision frequencies for ions and electrons are, respectively,

$$\hat{\nu}_i = \nu_i H(z)$$

and

$$\hat{\nu}_e = \nu_e[1 + H(z)] \tag{28}$$

Here,

$$\nu_j \equiv 4\pi n_j e^4 \ell n\Lambda / [M_j^{1/2}(2T_j)^{3/2}]$$

is the familiar Spitzer frequency, the function H(z) is defined as

$$H(z) \equiv \frac{1}{\pi^{1/2} z} \exp(-z^2) + \left(1 - \frac{1}{2z^2}\right) \frac{2}{\pi^{1/2}} \int_0^z dt \exp(-t^2) \tag{29}$$

with $z \equiv (E/T_j)^{1/2}$, and both electron-electron and electron-ion collisions are included in ν_e [29]. This form is employed in the more rigorous calculations of collisional effects on trapped-ion [29–32] and trapped-electron [69–72] instabilities. Since conservation of number, momentum, and energy in the collision operator is not essential to the derivation of the trapped-particle modes, Kadomtsev and Pogutse [2, 20] have introduced a much simpler model based on the BGK operator [73]. This modified "Krook operator", which has the form

$$C_j h_j = -\frac{\nu_j}{\varepsilon}\left(\frac{E}{T_j}\right)^{-3/2} h_j \tag{30}$$

is widely used because it yields collisional growth and damping estimates within roughly a factor of two of results using the more complicated Fokker-Planck form given in Eq.(27) [29, 69]. In the simplest derivation of dissipative trapped-ion modes, the energy dependence in Eq.(30) can also be ignored [2]. However, this energy dispersion in the effective collision frequency is a very important feature in the dissipative de-stabilization of trapped-electron modes [20].

As one passes into the highly collisional range (i.e. Pfirsch-Schlüter regime), the conservation properties of the collision operator become important. Specifically, with regard to the collisional drift mode, at least number conservation must be satisfied to derive the basic form of the instability [9]. For a proper inclusion of the additional dissipative de-stabilization associated with temperature gradients, energy conservation is also required [74]. These properties are, of course, automatically satisfied if one uses the Braginskii fluid equations [10]. For kinetic derivations of dissipative drift instabilities, appropriate forms of the BGK [73]

and Dougherty [75] collision models have been employed [76, 74]. In what follows, the formalism presented will focus on instabilities in the lower collisional regimes, i.e. the banana and plateau regimes.

At low collisionalities, C_j can be ignored in Eq.(25), and an exact solution for $\hat{h}_j$ can be readily obtained. To do this, Rutherford and Frieman [64] found it convenient to introduce an integrating factor of the form, $\exp(-i\hat{I}_a^b)$ with

$$\hat{I}_a^b \equiv \int_a^b d\theta_1 \left(Rq \frac{1}{v_{||}} (\omega + \omega_{D1}) - S^1 \right) \quad (31)$$

and $S^1 \equiv m - \ell q(r_1)$. In dealing with the untrapped particles, the periodicity requirements for θ given in Eq.(18) must be satisfied. Allowing for this constraint and using $\exp(-i\hat{I}_a^b)$ to integrate Eq.(25) from θ to $\theta + 2\pi$ then gives

$$(\hat{h}_U)_j = \frac{\exp(i\hat{I}_\theta^{\theta+2\pi}/2)}{2\sin(\hat{I}_\theta^{\theta+2\pi}/2)} \times \int_\theta^{\theta+2\pi} ds_1 \frac{1}{v_{||}} A_j \exp(-i\hat{I}_\theta^{\theta_1}) \quad (32)$$

with $ds_1 = Rqd\theta_1$ and $(\hat{h}_U)_j \equiv \hat{h}_j$ for untrapped particles.

For the trapped particles, the appropriate boundary conditions are given in Eq.(19). Since periodicity in θ is clearly not a constraint here, it is convenient to first multiply Eq.(25) by $\exp(iS^1\theta)$. The resultant equation for $\tilde{h}_j \equiv \hat{h}_j \exp(-iS^1\theta)$ can be solved as before, except that now $\hat{I}_a^b$ is replaced by $\tilde{I}_a^b$ with

$$\hat{I}_a^b \equiv \int_a^b ds_1 \frac{1}{v_{||}} (\omega + \omega_{D1}) \quad (33)$$

Using the conditions imposed by Eq.(19) and integrating Eq.(25) between the turning points, $\pm\theta_0$, then leads to the solution

$$(\hat{h}_T)_j = \frac{\exp(iS^1\theta)}{\sin(\hat{I}_{-\theta_0}^{\theta_0})} \times \int_{-\theta_0}^{\theta_0} ds_1 \frac{1}{v_{||}} A_j \exp(-iS^1\theta_1) \times \begin{cases} \cos(\hat{I}_{-\theta_0}^{\theta_1})\cos(\hat{I}_\theta^{\theta_0}) & \text{for } \theta_1 \le \theta \\ \cos(\hat{I}_{-\theta_0}^{\theta})\cos(\hat{I}_{\theta_1}^{\theta_0}) & \text{for } \theta_1 \ge \theta \end{cases} \quad (34)$$

with $(\hat{h}_T)_j \equiv \hat{h}_j$ for trapped particles.

If a sufficiently simple model for C_j is adopted, the preceding results can be easily generalized to include collisional effects. For example, the only modification in $(\hat{h}_T)_j$ resulting from the use of the Krook-type operator in Eq.(30) appears in the expression for $\hat{I}_a^b$. Here it is adequate to just replace ω by $\omega + i\nu_f$ in Eq.(33) with $\nu_f \equiv (\nu/\epsilon)(E/T)^{-3/2}$. The influence of collisions on untrapped particles in the banana regime is usually ignored because most of them are relatively insensitive to pitch-angle scattering. An exception, of course, are the ones close to the velocity-space boundary layer between trapped and circulating particles. However, a proper analysis of these effects requires the use of a more complicated operator such as the Fokker-Planck form given in Eq.(27).

At this point, it is possible, in principle, to substitute the results for h_j into Eq.(14), the quasi-neutrality condition, and to write down the basic mode equation. In practice, however, it is difficult to work directly with the forms given by Eqs (32) and (34). The most common approach is to consider the more tractable expressions obtained in the limits where either $\omega/\omega_{b,t}$ or $\omega_{b,t}/\omega$ is small. Here $\omega_{b,t}$ designates the bounce and transit frequencies with $\omega_b \equiv 2\pi/\tau_b$, $\omega_t \equiv 2\pi/\tau_t$, and the corresponding periods are given by

$$\tau_b \equiv \oint_T ds_1/v_{||} = 2\int_{-\theta_0}^{\theta_0} d\theta_1 \, Rq/|v_{||}|$$

and (35)

$$\tau_t \equiv \oint_U ds_1/v_{||} = \int_{-\pi}^{\pi} d\theta_1 \, Rq/v_{||}$$

Note that, at the boundary between trapped and untrapped particles, $2\omega_b = |\omega_t|$.

For the trapped particles, it is clear that the only relevant asymptotic limit is $|\omega/\omega_b| \ll 1$. This implies that factors of the form, $\hat{I}_a^b$, appearing in Eq.(34) are also small, so that the expression for $(\hat{h}_T)_j$ reduces to

$$(\hat{h}_T)_j = \left[\frac{Ze}{T} F_M \frac{(\omega - \omega_T^*)}{[\omega + i\nu_f + (\overline{\omega_{D1}})_T]} \right.$$

$$\times \left(\overline{\left\langle \Phi^{(0)} \right\rangle_{\phi'} \exp[-iS^{1}(\theta_1 - \theta)]} \right)_T \Big]_j \quad (36)$$

where

$$\left\langle \Phi^{(0)} \right\rangle_{\phi'} \equiv \left\langle \hat{\Phi}[r' + (1/\Omega) v_\perp \sin\phi', \theta] \times \exp(ik_\theta (1/\Omega) v_\perp \cos\phi') \right\rangle_{\phi'}$$

and the bar denoted the trapped-orbit-average, i.e.

$$(\bar{A})_T \equiv \frac{2}{\tau_b} \int_{-\theta_0}^{\theta_0} ds_1 \frac{1}{|v_{||}|} A \quad (37)$$

Since the parallel velocity of these particles is small (especially near the turning points, $\pm \theta_0$), the θ-dependence in $v_{||}$ is important here.

In dealing with the untrapped particles, both limits, $|\omega/\omega_t| \ll 1$ and $|\omega_t/\omega| \ll 1$, are of interest. For $|\omega/\omega_t| \ll 1$, the I_a^b factors are small, and the expression given by Eq.(32) correspondingly reduces to

$$(\hat{h}_U)_j = \left[\frac{Ze}{T} F_M \frac{(\omega - \omega_*^T)}{[\omega + (\overline{\omega_{D1}})_U - \omega_t S^1]} \times \left(\overline{\left\langle \Phi^{(0)} \right\rangle_{\phi'}} \right)_U \right]_j \quad (38)$$

with the bar denoting the untrapped-orbit-average, i.e.

$$(\bar{A})_U \equiv \frac{1}{\tau_t} \int_{-\pi}^{\pi} ds_1 \frac{1}{v_{||}} A \quad (39)$$

Unlike the trapped particles, most of these particles have relatively large parallel velocity. Hence, it is a reasonable approximation to ignore the θ-dependence in $v_{||}$ for circulating particles. This implies that $\tau_t \cong 2\pi Rq/v_{||}$. Since the θ-variation in $\Phi^{(0)}$ is also weak,

$$\left(\overline{\left\langle \Phi^{(0)} \right\rangle_{\phi'}} \right)_U \cong \left\langle \Phi^{(0)} \right\rangle_{\phi}$$

in Eq.(38).

Using $B \cong B_0(1 - \epsilon\cos\theta)$ and recalling the definition for the effective magnetic drift frequency in Eq.(26), the orbit averages can be readily performed to give [46]

$$\overline{\omega_{D1}} = \frac{k_\theta v^2}{\Omega R} [G_1(\kappa) + 2\hat{s} G_2(\kappa)] \quad (40)$$

where $\hat{s} \equiv rq'/q$ and the functions, $G_1(\kappa)$ and $G_2(\kappa)$, are expressed in terms of complete elliptic integrals. Here the velocity-space pitch-angle parameter, κ, is determined by

$$2\kappa^2 = 1 + \epsilon^{-1}(1 - \lambda)$$

with trapped particles falling in the range, $0 < \kappa < 1$, and circulating particles in the range

$$1 < \kappa < [(1 + \epsilon^{-1})/2]^{1/2}$$

The total function,

$$H(\kappa) \equiv G_1(\kappa) + 2\hat{s} G_2(\kappa)$$

is plotted in Fig.3, and indicates that, to a good approximation, $(\overline{\omega_{D1}})_U \cong 0$. Hence, the asymptotic expression for $(\hat{h}_U)_j$ given in Eq.(38) can be further simplified to the form

$$(\hat{h}_U)_j = \left(\frac{Ze}{T} F_M \frac{(\omega - \omega_T^*)}{\omega - (S^1/Rq) v_{||}} \right)_j \left\langle \Phi^{(0)} \right\rangle_{\phi'} \quad (41)$$

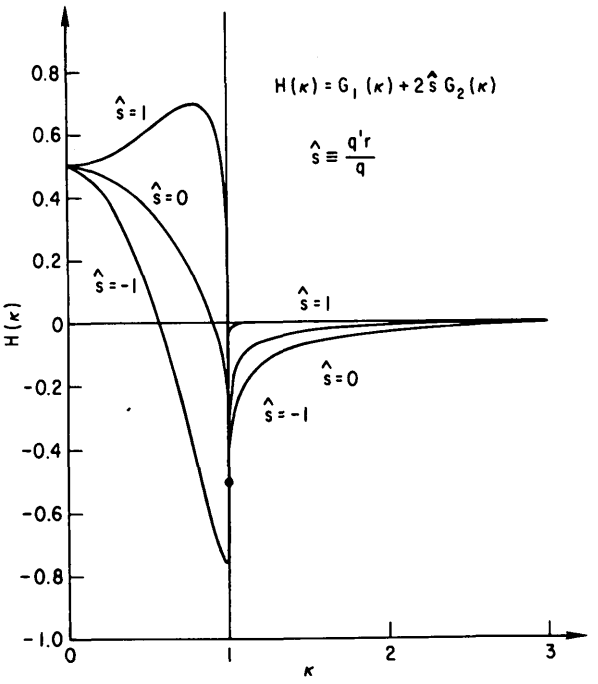

FIG.3. Velocity-space pitch-angle-dependent part of the orbit-averaged magnetic-drift frequency, $\overline{\omega_{D1}}$. Here $2\kappa^2 \equiv 1 + \epsilon^{-1}(1 - \lambda)$.

with $S^1 \equiv m - \ell q(r_1)$. For trapped particles,

$$\overline{\omega_{D1}} = 2\epsilon_n \omega_j^* (E/T_j) H(\kappa, \hat{s})$$

with $\epsilon_n \equiv r_n/R$ and $H \cong 0.6$ for $\hat{s} = 1$ [23].

Before considering the other asymptotic limit of interest for circulating particles (i.e. $|\omega_t/\omega| \gg 1$), it is useful to note that Eq.(32) can be expressed in a more convenient form. Making the usual approximation that the θ-dependence of $v_{\|}$ can be ignored (except in terms involving $[v_{\|} - (v_{\|})_1]$), this equation becomes

$$\left(\hat{h}_U\right)_j = \left(\frac{Ze}{T} F_M (\omega - \omega_T^*) \exp(i\Lambda \sin\theta) \right.$$

$$\times \sum_n \tilde{\Phi}_n(r_1) \exp(in\theta)$$

$$\left. \times \sum_p J_p(\Lambda) \frac{\exp(-ip\theta)}{\omega - (S + n - p)\hat{\omega}_t} \right)_j \qquad (42)$$

where

$$S \equiv m - \ell q(r'), \Lambda \equiv \hat{\omega}_D/\hat{\omega}_t$$

$\hat{\omega}_D$ is defined in Eq.(26), $\hat{\omega}_t \equiv v_{\|}/Rq$, and use has been made of the decomposition

$$\left\langle \phi^{(0)} \right\rangle_{\phi'} \equiv \sum_n \tilde{\Phi}_n(r_1) \exp(in\theta) \qquad (43)$$

and the Bessel function identity,

$$\exp(-i\Lambda \sin\theta) \equiv \sum_{p=-\infty}^{\infty} J_p(\Lambda) \exp(-ip\theta) \qquad (44)$$

In the limit $|\omega_t/\omega| \ll 1$, Eq.(42) can be simplified considerably. Using the definitions in Eqs (43) and (44), taking $|\hat{\omega}_D \cos\theta/\omega| \ll 1$, and noting that

$$\sum_p p J_p \exp(-ip\theta)$$

$$= \Lambda \cos\theta \exp(-i\Lambda \sin\theta) \qquad (45)$$

leads to the result

$$\left(\hat{h}_U\right)_j = \left\{ \frac{Ze}{T} F_M \frac{(\omega - \omega_T^*)}{\omega} \left[1 - \right.\right.$$

$$\frac{\hat{\omega}_D \cos\theta}{\omega} - i \frac{\hat{v}_D \sin\theta}{\omega} \frac{\partial}{\partial r} \qquad (46)$$

$$\left. \left. - \left(\frac{v_{\|}}{\omega Rq}\right)^2 \left(\frac{\partial}{\partial\theta} + iS\right)^2 \right] \left\langle \phi^{(0)}(r) \right\rangle_{\phi'} \right\}_j$$

where $\hat{v}_D \equiv -(\hat{\omega}_D/k_\theta)$. To arrive at this final form, use has been made of the fact that Eqs (21) and (22) imply

$$\frac{\partial}{\partial\theta_1} = \frac{\partial}{\partial\theta} + \frac{1}{v_{\|}} Rq \hat{v}_D \sin\theta \frac{\partial}{\partial r} \qquad (47)$$

Terms involving odd functions of $v_{\|}$ have been dropped from Eq.(46) since they do not contribute to the mode equation.

In the preceding analysis, the asymptotic forms for $\hat{h}_j$ have been obtained by passing to the appropriate limits of the exact solutions. These approximate forms can also be calculated directly by using $\omega/\omega_{b,t}$ or $\omega_{b,t}/\omega$ as a smallness ordering parameter in Eq.(25). This frequently used procedure is quite simple to implement and is given in detail, e.g. in Refs [64, 65].

A different but equivalent method for deriving the perturbed distribution function involves performing the total time integration along the unperturbed guiding-centre orbits [78, 46, 27]. For the Krook collision model of Eq.(30), Eq.(25) can be expressed as

$$\hat{h}_j = -i \int_{-\infty}^{t} dt_1 A \exp[-i(\omega + i\nu_f)(t_1 - t)]$$

$$\times \exp[i(m\theta_1 - \ell\zeta_1) - i(m\theta - \ell\zeta)] \qquad (48)$$

where $\theta_1 = \theta(t_1)$, $\zeta_1 = \zeta(t_1)$, A is the right side of Eq.(20), and

$$(m\theta_1 - \ell\zeta_1) - (m\theta - \ell\zeta)$$

$$= -\ell \int_t^{t_1} dt' \left(\frac{d\zeta}{dt'} - q(r_s) \frac{d\theta}{dt'} \right) \qquad (49)$$

with $q(r_s) \equiv m/\ell$ and

$$(v_D)_\theta = (d\zeta/dt) - q(r')(d\theta/dt)$$

The phase factor here can be expressed in the form, $\alpha(t_1 - t) + \beta(t_1)$, where $\beta(t_1)$ represents a periodic function of t_1. As noted by Coppi [78, 46], it is convenient to group the factor, $\exp[i\beta(t_1)]$ with the time-dependent part of A, and to then represent the resulting

expression as a sum over harmonics of $\omega_{b,t}$. Using such decompositions, the time integration in Eq.(48) can be easily performed to yield

$$\hat{h}_j = \left(\frac{Ze}{T} F_M (\omega - \omega_T^*) \right.$$

$$\left. \times \sum_p \frac{\tilde{\phi}(p) \exp[ip\omega_{b,t}\hat{t}(\theta)]}{\omega - i\nu_f + \overline{\omega_{Dl}} - [p + S^{-1}H(\lambda_c - \lambda)]\omega_{b,t}} \right) \tag{50}$$

where

$$\tilde{\phi}(p) = \frac{1}{\tau_{b,t}} \oint_{T,U} dt_1 \left\langle \phi^{(0)} \right\rangle_{\phi'}$$

$$\times \exp[i\beta_{b,t}(t_1)] \exp(-ip\omega_{b,t} t_1) \tag{51}$$

$$\hat{t}(\theta) = \int^{\theta} d\theta_1 qR/v_{||} \,, \quad \lambda_c = 1 - \varepsilon,$$

and $H(\lambda_c - \lambda) = 0$

for trapped particles and $H(\lambda_c - \lambda) = 1$ for untrapped particles. More detailed derivations of this result are clearly presented in Refs [46, 27].

2.2. Mode structure

With the forms for the perturbed distribution function determined, the quasi-neutrality condition can now be used to generate the basic mode equation. For most drift waves, the radial structure of such an equation is strongly affected by the gyrophase-averaged function, $\langle \Phi^{(0)} \rangle_{\phi'}$, appearing in $\hat{h}_j$. Recalling that

$$h_j \equiv \hat{h}_j \exp[-i\omega t + i(m\theta' - \ell\zeta')]$$

and that the velocity space integration involves the operation $\int_0^{2\pi} d\phi$, it is clear that one must evaluate the function,

$$\left\langle\!\left\langle \hat{\Phi}(r' + v_\perp \frac{1}{\Omega} \sin\phi', \theta) \right.\right.$$

$$\times \exp(ik_\theta v_\perp \frac{1}{\Omega} \cos\phi') \Big\rangle_{\phi'}$$

$$\left.\left. \times \exp(-ik_\theta v_\perp \frac{1}{\Omega} \cos\phi) \right\rangle\!\right\rangle_{\phi}$$

where $r = r' + (v_\perp/\Omega)\sin\phi'$. Without loss of generality, $\hat{\Phi}(r,\theta)$ can be expressed in terms of its Fourier transform, so that

$$\left\langle \phi^{(0)} \right\rangle_{\phi'} = \frac{1}{2\pi} \int_{-\infty}^{\infty}$$

$$\times dk_r A(k_r) \exp(ik_r r') J_0(k_\perp v_\perp/\Omega) \tag{52}$$

where $k_\perp^2 \equiv k_\theta^2 + k_r^2$ and

$$A(k_r) = \int_{-\infty}^{\infty} dr \exp(-ik_r r) \hat{\Phi}(r,\theta) \tag{53}$$

The second gyrophase average operation then gives

$$\left\langle\!\left\langle \phi^0 \right\rangle_{\phi'} \exp(-ik_\theta v_\perp \frac{1}{\Omega} \cos\theta) \right\rangle\!\right\rangle_{\phi} \equiv \left\langle\!\left\langle \left\langle\!\left\langle \right\rangle\!\right\rangle_{\phi'} \right\rangle\!\right\rangle_{\phi}$$

$$= \frac{1}{2\pi} \int_{-\infty}^{\infty} dk_r \exp(ik_r r) J_0^2 \left(\frac{k_\perp v_\perp}{\Omega} \right)$$

$$\times \int_{-\infty}^{\infty} dr \exp(-ik_r r) \hat{\Phi}(r,\theta) \tag{54}$$

Since finite-gyroradius terms are generally negligible for electrons (i.e. $J_0^2 \cong 1$), Eq.(54) just reduces to

$$\left\langle\!\left\langle \right\rangle_{\phi'} \right\rangle\!\right\rangle_{\phi} = \hat{\Phi}(r,\theta)$$

for the electron response. For the ions, the radial differential structure is easily obtained by expanding $J_0^2(k_\perp v_\perp/\Omega)$ for $k_r v_\perp/\Omega < 1$. Integrating twice by parts over r then gives

$$\left\langle\!\left\langle \right\rangle_{\phi'} \right\rangle\!\right\rangle_{\phi}$$

$$= \left[J_0^2 + \left(\frac{k_\theta v_\perp}{\Omega} \right) J_0 J_1 \frac{1}{k_\theta^2} \frac{\partial^2}{\partial r^2} \right] \hat{\Phi}(r,\theta) \tag{55}$$

where $k_\theta v_\perp/\Omega$ is the argument of the Bessel functions. For the usual long-wavelength limit, $k_\perp \rho_i < 1$ (i.e. $k_\theta \rho_i$ also small), this reduces to the familiar form

$$\left\langle\!\left\langle \right\rangle_{\phi'} \right\rangle\!\right\rangle_{\phi} = \left[1 - \frac{1}{2} \left(\frac{k_\theta v_\perp}{\Omega} \right)^2 \right.$$

$$\left. + \frac{1}{2} \left(\frac{v_\perp}{\Omega} \right)^2 \frac{\partial^2}{\partial r^2} \right] \hat{\Phi}(r,\theta) \tag{56}$$

In addition to the finite-ion-gyroradius effects, the geodesic or "banana" drifts can also influence the radial structure of drift waves. These excursions are particularly important for instabilities, such as the trapped-ion modes, which have characteristic frequencies below the ion-bounce frequency ($\omega < \omega_{bi}$). Here the radial mode structure is governed primarily by the average trapped-ion banana excursion, ρ_{Bi}, which is always greater than the average ion gyroradius, ρ_i. This point will be explained in more detail in Section 2.2.2.

For instabilities, such as the universal drift modes and trapped-electron modes, the effect of the geodesic drifts is weaker because complete ion banana excursions do not occur on the time-scale of interest, i.e. $\omega > \omega_{bi}$. This fact is evident upon examination of the basic mode equation obtained in the familiar limit, $(\omega_{b,t})_i < \omega < (\omega_{b,t})_e$. For $k_r \rho_i < 1$, Eqs (36), (41), (46) and (55), together with the quasi-neutrality condition, lead to the following two-dimensional (2D) integro-differential eigenmode equation:

$$\left\{ A\rho_i^2 \frac{\partial^2}{\partial r^2} + B + C\left(\frac{\partial}{\partial\theta} + iS\right)^2 + D\left[\cos\theta - i\left(\frac{\sin\theta}{k_\theta}\right)\frac{\partial}{\partial r}\right]\right\}\hat{\Phi}(r,\theta)$$
$$= \left\langle \frac{(\omega - \omega_T^*)}{(\omega + \overline{\omega_{Dl}} + i\nu_f)} \times \left(\overline{\hat{\Phi}(r,\theta_l)\exp[iS(\theta-\theta_l)]}\right)_T \right\rangle_{T,e} + \left\langle \frac{(\omega - \omega_T^*)}{[\omega - (S/Rq)v_{||}]} \right\rangle_{U,e} \hat{\Phi}(r,\theta) \quad (57)$$

where

$$A \equiv -\frac{1}{2}\left\{\left(\tau + \frac{\omega_*}{\omega}\right)\left(\Gamma_0 - \Gamma_1\right) + \eta_i \frac{\omega_*}{\omega}\left[\Gamma_0 + 2b\left(\Gamma_1 - \Gamma_0\right)\right]\right\}$$

$$B \equiv 1 + \tau - \left(\tau + \frac{\omega_*}{\omega}\right)\Gamma_0 - \eta_i \frac{\omega_*}{\omega} b\left(\Gamma_1 - \Gamma_0\right)$$

$$C \equiv \frac{1}{2}\left(\frac{v_i}{\omega q R}\right)^2 \left\{\left(\tau + \frac{\omega_*}{\omega}\right)\Gamma_0 + \eta_i \frac{\omega_*}{\omega}\left[\Gamma_0 + b\left(\Gamma_1 - \Gamma_0\right)\right]\right\}$$

$$D \equiv \frac{\varepsilon_n \omega}{\tau\omega_*}\left\{\left(\tau + \frac{\omega_*}{\omega}\right)\left[\left(2-b\right)\Gamma_0 + b\Gamma_1\right] + \eta_i \frac{\omega_*}{\omega}\left[\left(2 - 4b + 2b^2\right)\Gamma_0 + b\left(3-2b\right)\Gamma_1\right]\right\}$$

and

$$\left\langle \Lambda(v) \right\rangle_{T,U} \equiv \frac{1}{n}\int_{T,U} d^3v F_M \Lambda(v) \quad (58)$$

In this equation, $\Gamma_n \equiv I_n(b)\exp(-b)$ with I_n being modified Bessel functions

$$b \equiv k_\theta^2 \rho_i^2/2, \quad \tau \equiv T_e/T_i$$

$$\varepsilon_n \equiv r_n/R, \quad \omega_* \equiv \omega_e^*, \quad S \equiv m - \ell q(r)$$

and

$$\overline{(\omega_{Dl})}_e = -2\varepsilon_n \omega_* (E/T_e) H(\kappa, \hat{s})$$

with $H(\kappa,\hat{s})$ given in Fig.3. The contribution from ion-Landau resonances can be calculated from Eq.(32) and is given, e.g. in Ref. [27].

In dealing with trapped-ion modes, the appropriate forms for the density response of ions as well as electrons can be calculated from Eqs (36) and (41). Since the characteristic frequencies here lie in the range $\omega < (\omega_{b,t})_i \ll (\omega_{b,t})_e$, electron bounce and transit resonances can be safely ignored. The quasi-neutrality condition then yields the following 2D eigenmode equation for these typically long-wavelength ($k_\perp \rho_i < 1$) instabilities:

$$(1+\tau)\hat{\Phi}(r,\theta) = \sum_{j=i,e} \tau_j \left\langle \frac{(\omega - \omega_T^*)}{\omega + \overline{\omega_{Dl}} + i\nu_f} \times \left(\overline{\hat{\Phi}(r,\theta_l)\exp[iS(\theta-\theta_l)]}\right)_T \right\rangle_{T,j} + \tau\left\langle \frac{\omega - \omega_T^*}{[\omega - (S/Rq)v_{||}]} \right\rangle_{U,i} \hat{\Phi}(r,\theta) \quad (59)$$

with $\tau_e \equiv 1$ and $\tau_i \equiv \tau \equiv T_e/T_i$. Here the radial structure is determined primarily by the banana excursions in the trapped-ion response and by the effective parallel wavelength, $S/Rq = [m - \ell q(r)]/Rq$, of the circulating ions.

Before proceeding with the discussion of the local and non-local analysis of Eqs (57) and (59), it should be noted that forms for the potential different from the ansatz given in Eq.(17) can also be employed. One popular choice [29, 64] involves introducing the radially local perpendicular co-ordinate in the magnetic surface, $q(r)\theta - \zeta$, and considering

$$\Phi \propto \exp\{i\ell[q(r)\theta - \zeta]\}$$

Connor and Hastie [67], however, have emphasized that such a waveform is not periodic in θ away from a rational surface and can, therefore, only be employed in systems with very weak shear. To restore periodicity they introduce an additional phase factor which leads to the following ansatz for the potential:

$$\hat{\Phi} = \hat{\Phi}(r,\theta)\exp[-i\omega t - i\ell\zeta + i\ell q(r)\theta + iS(r)F(\theta)] \qquad (60)$$

where $\hat{\Phi}$ and S(r) are defined as before, and $F(\theta)$ is a general function determined by

$$F(\theta) = \int^{\theta} d\theta' \; G(\theta') \qquad (61)$$

with $G(\theta + 2\pi) = G(\theta)$. The ansatz of Eq.(17) corresponds to the choice $G = 1$ or $F(\theta) = \theta$. Other forms for $G(\theta)$ have been employed, e.g. by Coppi and Rewoldt in their radially non-local analysis of both odd and even modes [46].

As is evident from Eqs (57) and (59), obtaining general solutions to the 2D eigenmode equations is a formidable task. Until recently, the usual approach has been to make some simplifying assumptions which essentially reduce the problems to one-dimensional calculations. The simplest approximation, of course, is to consider the local limit where the mode structure in both r and θ is essentially ignored. This approach is frequently employed in calculations which seek to establish the existence of an instability and to emphasize the essential features of the mode rather than detailed stability criteria [2]. However, to determine the influence of non-local effects, such as magnetic shear, it is necessary to determine the mode structure. This problem is complicated by the fact that toroidal effects, which account for the slow poloidal variation in $\hat{\Phi}(r,\theta)$, effectively couple the radial dependence to different poloidal harmonics, i.e.

$$\Phi^{(0)} \propto \hat{\Phi}(r,\theta)\exp(im\theta) = \exp(im\theta)\sum_n \hat{\Phi}_n(r)\exp(in\theta)$$

If the toroidal coupling is very weak, the θ-variation can be ignored, and the problem reduces to a 1D calculation for the radial normal modes. In the opposite limit (i.e. strong coupling), the θ-variation is dominant, and the relevant 1D problem becomes one of calculating the mode structure along the magnetic field line. These standing modes, which are extended in radius and are relatively insensitive to variations in that direction, are analogous to the quasi-modes derived by Roberts and Taylor [79]. For the drift modes governed by Eq.(57), the degree of toroidal coupling is determined primarily by the magnitude of the trapped-electron driving term and the ion magnetic drift terms compared to the other terms in that equation. In general, these toroidal factors are neither dominant nor negligible, so that a fully 2D analysis is necessary.

2.2.1. Radially local analysis-1D

The general methods for dealing with the 1D radially local problem are best illustrated by considering the analysis of the dissipative trapped-ion and trapped-electron instabilities. For the trapped-ion modes, the usual frequency ordering invoked is $|\nu_i/\omega|$, $|\omega/\nu_e|$, $|\omega/(\omega_{b,t})_i| = O(\delta)$ with δ being a smallness parameter [2]. This implies that, to lowest order, Eq.(59) reduces to the following integral equation:

$$(1 + \tau^{-1})\hat{\Phi}(\theta)\exp(-iS\theta) = \left\langle \frac{(\omega - \omega^*_{Ti})}{(\omega - \overline{\omega_{Di}})} \left(\overline{\hat{\Phi}(\theta)\exp(-iS\theta)} \right)_T \right\rangle_T \qquad (62)$$

where $\overline{\omega_{Di}} \equiv \overline{(\omega_{D1})_i}$, and the radial dependence has been dropped. The solution to this equation determines the mode structure along the field line as well as ω_0, the lowest-order mode frequency. These results can then be used in a straightforward application of perturbation theory to calculate the first-order contributions accounting for electron collisional

growth, ion-collisional damping, and ion Landau resonance effects [29, 31, 32].

Following the variational procedure introduced by Rosenbluth, et al. [29], Eq.(62) can be expressed in a quadratic form:

$$\lambda_0 \equiv \frac{\tau + (\omega_*/\omega_0)}{1+\tau} = \frac{\oint Rq\, d\theta/B \left(\int_{1/B_{max}}^{1/B} d\lambda B [a_0(\lambda)/(1-\lambda B)^{1/2} L(\lambda)] \right)^2}{\int_{1/B_{max}}^{1/B_{min}} d\lambda\, a_0^2(\lambda)/L(\lambda)} \quad (63)$$

where

$$L(\lambda) \equiv 2Rq \int_{-\theta_0}^{\theta_0} d\theta/(1-\lambda B)^{1/2}$$

is the trapped-particle connection length, the magnetic drift term has been neglected for simplicity, and

$$a_0(\lambda) \equiv \left(\frac{e}{RT_i}\right)\left(2Rq\right) \times \int_{-\theta_0}^{\theta_0} d\theta\, \frac{\hat{\phi}(\theta)\exp(-iS\theta)}{(1-\lambda B)^{1/2}} \quad (64)$$

It is convenient here to choose a trial function of the form, $a_0(\lambda) = c_1 + c_2\lambda + c_3\lambda^2 + \ldots$, with c_n being adjustable coefficients. Since it is well known that the growth rate is roughly proportional to $\epsilon\omega_0^2/\nu_e$ [2], it is clear that the coefficients in the trial function must be chosen to minimize λ_0 in Eq.(63). This leads to a matrix equation which can be easily solved numerically to give ω_0 and the coefficients c_n. With $a_0(\lambda)$ thus determined, the mode structure along the field line can be obtained by inverting Eq.(64). The results of this procedure indicate a moderately ballooning-type structure centred around the magnetic field minimum with a functional dependence given roughly by

$$\Phi(\theta)\exp(-i\ell q\theta) \propto 1 + \cos\theta$$

Since the collisional and resonant contributions are first-order effects, they can be analysed individually within a perturbative framework. To lowest order, the perturbed distributions leading to Eqs (62) and (63) vanish for the electrons and the untrapped ions. For the trapped ions the appropriate form is given by

$$\hat{h}_T^{(0)} = (e/T) F_M [(\omega - \omega_T^*)/\omega] [\overline{\hat{\phi}\exp(-iS\theta)}]_T \quad (65)$$

In calculating the first-order collisional effects, these results together with the solutions to Eq.(63) can be used to reduce the basic equation for $\hat{h}_j$ [i.e. Eq.(25)] to the following form:

$$\left(\frac{R}{\tau_j}\right)\left(\omega_0 - \omega_{T_j}^*\right) a_0(\lambda) = \left[2i\nu \left(\frac{T}{E}\right)^{3/2} \frac{\partial}{\partial\lambda} \left(\oint \frac{1}{B} Rq d\theta \lambda (1 - \lambda B)^{1/2} \frac{\partial \hat{h}}{\partial \lambda} \right) \right]_j \quad (66)$$

with $\hat{h} = \hat{h}^{(0)} + \hat{h}_c^{(1)}$ and the right-hand side of this equation coming from the trapped-orbit average of the Fokker-Planck operator given in Eq.(27). Solutions here must satisfy the velocity-space boundary conditions: (i) $\hat{h}_j = 0$ at the turning points ($\lambda = 1/B_{max}$) to ensure that the function connects continuously to the untrapped region; and (ii) $\partial\hat{h}_j/\partial\lambda$ remains finite at $\lambda = 1/B_{max}$ (i.e. far from the turning points).

For the electrons, $\hat{h} = \hat{h}_c^{(1)}$ and Eq.(66) can be directly integrated subject to the boundary conditions described. We can then simply use the resulting form for $\hat{h}_e$ to show that the electron collisions lead to a growth rate proportional to $\epsilon\omega_0^2/\nu_e$ [30, 29]. For the ions the problem is complicated by the fact that the substitution of $\hat{h}_i^{(0)}$ into Eq.(66) leads to a logarithmic singularity. Specifically, the ion-bounce period appearing in $\hat{h}_i^{(0)}$ diverges logarithmically in the boundary layer where λ approaches $1/B_{max}$. To resolve this difficulty, Rosenbluth, et al. [29] introduced a trial function which approaches zero more rapidly than $1/\ln[\lambda - (1/B_{max})]$ in the boundary layer but reduces to the unperturbed solution, $a_0(\lambda)$, away from it. The function

$$a_0(\lambda)\left(1 + \exp\{-\alpha[\lambda - (1/B_{max})]\}\right)$$

satisfies these requirements, and, as shown in detail in Ref.[29], the coefficient α can be evaluated by a variational procedure. Results of this analysis lead to an ion-collisional damping rate proportional to $-(\nu_i/\epsilon)^{1/2}[\ln(\nu_i/\epsilon)^{1/2}]^{-3/2}$ instead of the more familiar $-(\nu_i/\epsilon)$ coming from the simple Krook model. instead of the more familiar $-(\nu_i/\epsilon)$ coming from the simple Krook model.

To calculate ion Landau resonance effects, it is convenient to employ the exact solutions for $\hat{h}_j$, given in Eqs (32) and (34). The resonant terms are first-order quantities which come from the imaginary part of these functions. This imaginary part, together with the lowest order $\hat{h}_j^{(0)}$, are then substituted into the quasi-neutrality condition. Operating on the resultant expression with

$$\oint Rqd\theta\hat{\Phi}^*/B$$

gives a quadratic form which can be perturbatively expanded to yield the appropriate Landau damping or growth. This procedure is explained in detail in Refs [31, 32]. In general, it is found that the Landau damping (or growth) rate for bounce [31] and transit [30] resonances is comparable in magnitude if $|S| = |m - \ell q| \cong 1/2$ in the circulating response. Both effects scale roughly as

$$\gamma_{LD} \propto -(1 - 1.5\eta_i)(\omega_0)^4(qR/\epsilon^{1/2}v_i)^3$$

[29–32].

For the trapped-electron modes, Eq.(57) in its simplest radially local form can be expressed as

$$\left[1 - \frac{\omega_*}{\omega} + b_\theta + \frac{1}{2}\left(\frac{c_s}{\omega qR}\right)^2 \frac{\partial^2}{\partial\theta^2}\right] \times \hat{\Phi}(\theta)\exp(-iS\theta) = \Gamma\left(\overline{\hat{\Phi}(\theta)\exp(-iS\theta)}\right)_T \tag{67}$$

where

$$\Gamma \equiv \epsilon^{1/2}\left(\frac{2}{\pi^{1/2}}\right)\int_0^\infty d\bar{E}\,\bar{E}^{1/2} \times \exp(-\bar{E})\,\frac{(\omega - \omega_{Te}^*)}{(\omega - \overline{\omega_{De}} + i\nu_{f,e})}$$

$$\bar{E} \equiv E/T_e$$

$$\overline{\omega_{De}} \simeq \epsilon_n\omega_*\bar{E} \text{ for } (rq'/q) \simeq 1$$

$$c_s^2 \equiv 2T_e/M_i,\ b_\theta = k_\theta^2\rho_s^2/2$$

and

$$\rho_s^2 \equiv (c_s/\Omega_i)^2$$

Here $\tau^{-1} \equiv T_i/T_e$ has been taken as very small, and ion-magnetic drifts and circulating electron resonances have been ignored. If the contribution of the ion-acoustic term,

$$(c_s/\omega qR)^2\partial^2/\partial\theta^2$$

is much less than the trapped-electron driving term, Γ, then Eq.(67) reduces to the same general form as the integral equation for the trapped-ion instability given in Eq.(62). The same variational procedure can thus be applied, and the result is again a ballooning-type mode structure centred around the magnetic field minimum, i.e. for $S = 0$, $\hat{\Phi}(\theta) \propto 1 + \cos\theta$. For this ballooning or "strong-coupling" limit, the de-stabilizing driving term, Γ, can be moderately enhanced (less than a factor of 2) over its simple local value.

As the magnitude of the ion acoustic term becomes comparable to or larger than Γ, it is necessary to deal with Eq.(67) in its complete integro-differential form. A common approach to this type of problem is to use the Fourier decomposition,

$$\hat{\Phi}(\theta) = \sum_n \Phi_n \exp(in\theta)$$

to generate a matrix equation which is then solved numerically. Following this procedure, Liewer, et al. [80] found that in the weak ion-acoustic limit the trapped-electron term generates a strong coupling of the Fourier components which leads to the ballooning result of the variational calculation. However, as the ion acoustic term becomes dominant (i.e. "weak-coupling" limit), the ballooning effect is correspondingly eliminated. In earlier work, Kadomtsev and Pogutse used this same numerical technique to calculate the ballooning mode structure of the collisionless (inter-change) trapped-particle instability in the radially local limit [3]. As a final point, it should be noted that a more rigorous treatment of collisional effects for the trapped-electron modes can be readily carried out by using the procedures just described in the dissipative trapped-ion mode calculations [29, 81].

2.2.2. Radial analysis-1D

If the toroidal coupling of the poloidal Fourier components is not taken into account and the θ-dependence in $\hat{\Phi}\exp(-iS\theta)$ is ignored, the drift-wave mode structure problem effectively reduces to a 1D radial eigenmode calculation. Since $\hat{\Phi}$ is no longer a function of θ in this limit, the parallel wavenumber is given by $k_\parallel = S/Rq = [m - \ell q(r)]/Rq$. For the collisionless drift and trapped-electron instabilities, the ion acoustic term ($\propto k_\parallel^2 c_s^2$) affects the mode structure very strongly. The usual approach is to expand around a reference mode rational surface, r_s, and then to express Eq.(57) in terms of the dimensionless radial variable,

$$x \equiv (r - r_s)/\rho_s, \text{ with } \rho_s \equiv c_s/\Omega_i$$

The radial factor in $k_\parallel$ is now given by

$$S \simeq -\ell q'(r-r_s) \simeq -k_\theta \rho_s \hat{s} x$$

with $\hat{s} \equiv rq'/q$. In terms of the shear length,

$$L_s \equiv [(\varepsilon/q)\, d\ell nq/dr]^{-1}$$

this leads to the familiar form

$$k_\parallel = -k_\theta \rho_s x/L_s$$

Hence, Eq.(57) reduces approximately to

$$\left[\frac{1}{\tau} A \frac{\partial^2}{\partial x^2} + \hat{B} - \left(k_\theta \rho_s \hat{s}\right)^2 C x^2\right] \hat{\phi}(x) = -R(x)\hat{\psi}(x) \quad (68)$$

where $\hat{B} \equiv B - \Gamma$, A, B, and C are defined in Eq.(57), $-R(x)$ is the untrapped-electron response on the right-hand side of that equation, Γ is defined in Eq.(67) and ion magnetic drifts are ignored.

The derivation of normal-mode solutions to Eq.(68) have, in general, followed the procedure introduced by Pearlstein and Berk [15] for collisionless drift instabilities. In their analysis as well as in analogous studies of trapped-electron modes [82, 83], the circulating electron term, R(x), is taken to be a first-order quantity. Hence, to lowest order, the radial equation reduces to the Weber equation which has solutions of the form

$$\hat{\phi}(x) = H_n(\sigma^{1/2} x)\exp(-\sigma x^2/2) \quad (69)$$

where H_n are Hermite polynomials,

$$\sigma = \pm k_\theta \rho_s \hat{s} (C\tau/A)^{1/2} \quad (70)$$

and the following eigenvalue condition must be satisfied:

$$B - \Gamma = \sigma (A/\tau)(2n + 1) \quad (71)$$

To better understand the preceding results, it is useful to note that the left-hand side of Eq.(68) is similar in structure to the familiar harmonic-oscillator equation. Since $C\tau/A$ is usually negative, the propagation potential has the form of an antiwell. Accordingly, the solutions are primarily oscillatory in character with the oscillations becoming very rapid as the distance from the reference rational surface becomes large, i.e. the factor σ in Eq.(69) is primarily imaginary. The usual local dispersion relation for trapped-electron modes [20, 23] can be easily recovered by setting the left-hand side of Eq.(71) equal to zero.

In Eq.(70) the sign of σ is determined by the proper radial boundary conditions. As pointed our by Pearlstein and Berk, the relevant physical picture is one of waves carrying energy away from the radial location, where the mode is unstable, out to a region where the energy can be absorbed by ion-Landau damping. Although it is necessary to specify this energy sink in the physical picture, it need not be included in the actual equation analysed. This is because the important shear damping effects result entirely from the outward propagation of the drift wave. Comparison of the solution given in Eq.(69) with the eikonal form yields, for $n = 0$,

$$\hat{\phi}(x) = \exp(-\sigma x^2/2) = \exp\left(i\rho_s \int dx\, k_x\right)$$

which in turn implies that

$$ik_x = -\sigma x \simeq \mp i(k_\theta c_s x/\omega L_s)$$

Hence, the choice of outgoing wave boundary conditions (i.e. $v_g = d\omega/dk_x > 0$ with $x > 0$) indicates that the upper sign must be taken in Eq.(70). With σ thus determined, the right-hand side of Eq.(71) gives the shear-stabilizing contribution, which can be approximated by

$$-i(r_n/L_s)(\omega_*/\omega)(2n + 1)$$

Hence, the eigenvalue equation becomes

$$B - \Gamma = -i(r_n/L_s)(\omega_*/\omega)(2n+1) \qquad (72)$$

However, to treat the magnetic drift effects in Γ properly, Eq.(71) cannot be reduced from its transcendental form, i.e. the eigenvalues must be calculated numerically [22, 23].

The untrapped-electron response, R(x), can be expressed in terms of $Z(\zeta_e)$, the plasma dispersion function [84], with

$$\zeta_e \equiv \omega/k_{||} v_e = (\omega L_s)/(k_\theta \rho_s v_e x)$$

This term accounts for the de-stabilization of collisionless drift waves and has the form

$$R(x) = (1 - \frac{\omega_*}{\omega})\,\zeta\, Z(\zeta)$$

$$- \frac{\omega_*}{\omega}\,\eta_e \zeta\left(\zeta + (\zeta^2 - \tfrac{1}{2})\,Z(\zeta)\right) \qquad (73)$$

with $\zeta \equiv \zeta_e$ here. Note that for the usual limit of interest, $|\zeta_e| \ll 1$, the Z-function can be approximated by $i\pi^{1/2}$ [84]. For trapped-electron modes this resonant effect can be stabilizing [28]. However, in the absence of collisional broadening [70–72], the velocity space of the resonant electrons is greatly reduced when trapping is taken into account. Allowing for the trapped-particle boundaries in velocity space, we can perform the appropriate integrations to obtain the result [28]:

$$R(x) = \left(1 - \frac{\omega_*}{\omega}\right)\zeta\left[Z(\zeta) - Z(\hat{\zeta})\right]$$

$$- \frac{\omega_*}{\omega}\,\eta_e \zeta\left[\zeta - \hat{\zeta} + \left(\zeta^2 - \tfrac{1}{2}\right)Z(\zeta)\right.$$

$$\left. - \left(\hat{\zeta}^2 - \tfrac{1}{2}\right)Z(\hat{\zeta})\right] \qquad (74)$$

with $\hat{\zeta} \equiv \zeta/(\epsilon)^{1/2}$. In arriving at this approximate form, it is assumed that $(1 - B/B_{max}) \cong (\epsilon)^{1/2}$. As shown, e.g. in Ref.[16] for collisionless drift modes and in Ref.[72] for trapped-electron modes, the contribution from R(x) has usually been calculated using standard perturbation theory. Rosenbluth and Catto [85] have analysed the collisionless drift mode problem with a more rigorous, non-perturbative approach. They concluded that the perturbative calculation is really quite accurate. Numerical solutions obtained by Gladd and Horton [16] also support this conclusion. However, it has very recently been found that these results [85, 16] are applicable only if one retains just the imaginary part of the Z-function. In fact, if the complete Z-function response is used, numerical results have indicated that the universal eigenmodes cannot be de-stabilized in the slab limit [19a]. Finally, as a general comment on all of the preceding 1D radial calculations, it should be emphasized that, in a strict sense, the 1D radial model used is valid for toroidal systems only if the mode rational surfaces are well-separated and if ∇B-drift effects are negligible. Specifically, the effective turning point,

$$x_T \simeq [(L_s/r_n)(\omega_*/\omega)]^{1/2}$$

cannot exceed the spacing between rational surfaces,

$$\Delta r_s \simeq L_s/(k_\theta R q)$$

i.e.

$$k_\theta \rho_s < (r_n/qR)(L_s/r_n)^{1/2}$$

For trapped-ion modes, Eq.(59) in the 1D radial limit reduces to

$$(1 + \tau - \Gamma)\hat{\Phi}(r)$$

$$- \tau\left\langle \frac{(\omega - \omega_T^*)}{\omega + \overline{\omega_{Dl}} + i\nu_f}\left(\overline{\hat{\Phi}(r)}\right)_T \right\rangle_{T,i}$$

$$= -\tau R_i(r)\hat{\Phi}(r) \qquad (75)$$

where

$$R_i(r) = 1 - \left(\frac{\omega_{*i}}{\omega}\right)\zeta\left[Z(\zeta) - Z(\hat{\zeta})\right]$$

$$- \frac{\omega_{*i}}{\omega}\,\eta_i \zeta\left[\zeta - \hat{\zeta} + \left(\zeta^2 - \tfrac{1}{2}\right)Z(\zeta)\right.$$

$$\left. - \left(\hat{\zeta}^2 - \tfrac{1}{2}\right)Z(\hat{\zeta})\right] \qquad (76)$$

Here

$$\zeta \equiv \omega/k_{||} v_i, \quad \hat{\zeta} \equiv \zeta/(\epsilon)^{1/2}$$

$$k_{||} = [m - \ell q(r)]/Rq$$

and untrapped-ion banana excursions have been neglected. As noted earlier, the dominant radial excursion here comes from the average trapped-ion banana drifts. The fact that the orbit average on $\hat{\Phi}(r)$ is to be performed at constant r_1, implies that

$$\overline{\left(\hat{\Phi}(r)\right)} \simeq \left(1 + \overline{(r - r_1)} \frac{\partial}{\partial r_1} + \frac{1}{2}\overline{(r - r_1)^2} \frac{\partial^2}{\partial r_1^2}\right) \hat{\Phi}(r_1) \qquad (77)$$

where $(r - r_1)$ represents the banana excursion and $|k_r(r - r_1)|$ is taken to be small. Transforming back to the r-frame, and operating on Eq.(75) with

$$\oint d\theta/B$$

then leads approximately to the result

$$\left(\rho_{Bi}^2 \frac{\partial^2}{\partial r^2} + Q(r,\omega)\right) \hat{\Phi}(r) = 0 \qquad (78)$$

where

$$Q(r,\omega) \equiv -\frac{1}{\Gamma_i}\left(1 + \tau^{-1} - \tau^{-1}\Gamma - \Gamma_i + R_i\right)$$

$$\Gamma_i \equiv \epsilon^{1/2}\left(\frac{2}{\pi^{1/2}}\right)\int_0^\infty d\bar{E}\, \bar{E}^{1/2} \times \exp(-\bar{E}) \frac{(\omega - \omega_{Ti}^*)}{(\omega - \overline{\omega_{Di}} + i\nu_{f,i})}$$

$$\bar{E} \equiv E/T_i, \quad \overline{\omega_{Di}} \simeq -\epsilon_n \tau^{-1} \omega_* \bar{E}$$

for $(rq'/q) \cong 1$, Γ is defined in Eq.(67), and

$$\rho_{Bi} \simeq \rho_i q/\epsilon^{1/2}$$

is the average banana width. The local dispersion relation just corresponds to $Q(r,\omega) = 0$.

At this point it is useful to recall that the ordering,

$$|\omega/(\omega_{b,t})_i| << 1$$

impliies that ion transit resonances are strong close to a reference mode rational surface but become negligible away from it. This, of course, is just opposite to the situation for collisionless drift and trapped-electron modes. For the trapped-ion modes, there is no term in the effective radial potential, $Q(r,\omega)$, analogous to the ion sound term. In fact, in the absence of untrapped-ion resonances [i.e. neglecting $R_i(r)$], Eq.(78) exhibits only one turning point. By postulating appropriate boundary conditions at large r to provide a second turning point, Jablon, et al. [86] and Ross and Horton [87] have obtained radially non-local modes using the familiar WKB method. However, as noted in Ref.[87], the presence of magnetic shear implies that the ion transit resonances, which are strongly dependent on $k_{||}(r)$, must be taken into account.

For finite values of shear, the non-local modes can now extend over a number of rational surfaces (r_s). Close to such surfaces, the strong ion-Landau damping forces narrow peaks in the effective radial potential, $Q(r,\omega)$. Gladd and Ross [34] have solved this more realistic problem by applying standard numerical procedures. They found that the peaks in $Q(r,\omega)$ cause strong reflection, which produce standing waves with nodes close to the rational surfaces. These are spaced at intervals roughly given by $(\ell q')^{-1}$. It is also emphasized that since the parallel phase velocity exceeds the thermal velocity close to r_s, the resultant ion-Landau damping can remain a stabilizing effect even in the presence of large temperature gradients. This, of course, differs from the usual transit resonances away from r_s, which require $\eta_i < 2/3$ to be stabilizing [29, 30]. It is also noted that, in contrast to earlier work [87], the eigenvalues are found to be nearly independent of the outer boundary conditions. A typical picture of the effective radial potential, $Q(r,\omega)$, and the corresponding eigenfunction are given in Fig.4.

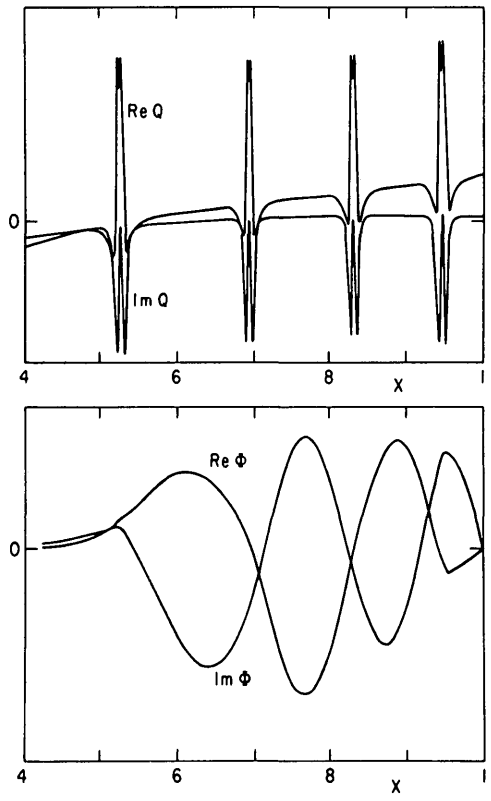

FIG.4. Typical radial potential, $Q(r,\omega)$, and corresponding eigenfunction, $\phi(r)$, for the dissipative trapped-ion instability. Here $x \equiv r/a$ with a being the total plasma radius (or radius at the limiter).

2.2.3. *Two-dimensional problem*

As noted earlier, the 1D calculations described in Sections 2.2.1 and 2.2.2 have limited applicability because the mode structure of drift waves in a torus is essentially two-dimensional. Up to the present time, owing to the obvious complexity of the problem, there have been no fully 2D calculations of the trapped-ion instability. However, significant progress in analysing collisionless drift modes [88] and trapped-electron modes [27, 89] within a 2D framework has recently been reported. For the remainder of this section, attention will, accordingly, be focused on Eq.(57).

Using a simplified model equation in which resonance effects are ignored, Taylor [88] addressed the question of how much non-uniformity (i.e. θ-variation) in the magnetic field strength and shear are required to nullify the stabilizing influence of shear on collisionless drift waves. The equation analysed is similar in structure to the left-hand side of Eq.(57).

Although the modulation in shear strength over the magnetic surface can be large in a device like the Levitron, it is generally a small effect in tokamaks and will not be considered in what follows.

If the toroidal coupling effect associated with the trapped-electron term is ignored along with all transit resonances, the 2D mode equation can be expressed as

$$\left[\frac{1}{\tau} A \frac{\partial^2}{\partial x^2} + \hat{B} - C\left(j - \alpha x\right)^2\right]\hat{\Phi}_j(x) + \frac{1}{2} D\left[\hat{\Phi}_{j+1}(x) + \hat{\Phi}_{j-1}(x) + \frac{1}{k_\theta \rho_s}\frac{\partial}{\partial x}\left(\hat{\Phi}_{j+1}(x) - \hat{\Phi}_{j-1}(x)\right)\right] = 0 \tag{79}$$

where the various factors are defined in Eqs (57) and (68), $\alpha \equiv k_\theta \rho_s \hat{s}$, and use has been made of the decomposition

$$\hat{\Phi}(x,\theta) = \sum_j \hat{\Phi}_j(x)\exp(ij\theta)$$

For cases where the toroidal coupling is strong, one can follow Taylor's procedure of considering the limit in which $\hat{\Phi}_j(x)$ varies slowly with j. By replacing $\hat{\Phi}_j(x)$ with the continuous function, $\hat{\Phi}(x,j)$, the difference terms, $\hat{\Phi}_{j+1} \pm \hat{\Phi}_{j-1}$, in Eq.(79) can be approximated as derivatives with respect to j [e.g. $\hat{\Phi}_{j+1} - \hat{\Phi}_{j-1} = 2\partial\hat{\Phi}(j)/\partial j$]. Making the change of variables $y = x - (j/\alpha)$, in the resultant expression then leads to the result

$$\left(\hat{A}\frac{\partial^2}{\partial y^2} + \hat{B} + D - C\alpha^2 y^2\right)\hat{\Phi}(y) = 0 \tag{80}$$

where

$$\hat{A} \equiv (A/\tau) + (D/2\alpha^2)(1 - 2\hat{s})$$

This again is just the Weber equation with solutions of the form given in Eq.(69). The corresponding expression for σ and the eigenvalue equation now become

$$\sigma = \alpha(C/\hat{A})^{1/2} \tag{81}$$

and

$$B + D - \Gamma = \sigma\hat{A}(2n + 1) \tag{82}$$

Clearly, if $D = 0$, then $\hat{A} = A/\tau$, and the previous one-dimensional results are recovered exactly.

As noted in the earlier discussion, the outward radiation of energy by waves, which are primarily oscillatory, accounts for the shear damping effects. With the inclusion of the ion magnetic drift terms, this general picture remains qualitatively correct provided $\hat{A}$ also remains negative. However, if

$$\hat{A} \equiv (A/\tau) + (D/2\alpha^2)(1 - 2\hat{s}) > 0 \tag{83}$$

the form of the effective potential in Eq.(80) changes from an anti-well to a well, and the resultant modes become non-propagating. As a consequence, the shear damping effects are accordingly suppressed. The basic structure now resembles a "quasi-mode" [79], i.e. the mode can be represented as a sum of degenerate radially localized normal modes. Each of these component normal modes is centred on a different rational surface (i.e. at $x = x_m$, $x_{m\pm1}$, etc.) and each has comparable amplitude (i.e. $|\hat{\Phi}_m| \cong |\hat{\Phi}_{m\pm1}|$, etc.). In the present calculation, the fact that $A < 0$ and $D/\alpha^2 > 0$ in Eq.(83) indicates that this onset condition for a mode, which is insensitive to shear and which is localized at the magnetic field minimum, implies the requirement that the shear be sufficiently weak, i.e. $\hat{s} < 1/2$. For this result to be valid, it is additionally required that the strong coupling approximation be satisfied. Specifically, from Eqs (69) and (81), the condition that more than the principal poloidal harmonic is important implies that $|\sigma/\alpha^2| < 1$ with σ being positive and predominantly real. It should also be noted that in this analysis allowance has not been made for variations in the equilibrium density gradients. As pointed out by Taylor, such variations determine the actual location and radial profile of these "global" modes [88]. Moreover, if the "global" boundary conditions are chosen to reflect rather than outwardly convect energy, the shear stabilization (associated with the outward propagation) can be eliminated even when Eq.(83) is not satisfied.

As noted earlier, the trapped-electron term on the right-hand side of Eq.(57) can also introduce significant toroidal coupling. Rewoldt, et al. [27] have included such effects along with the transit resonances of both ions and electrons in a fully 2D analysis of the trapped-electron instability. In their calculation, the resonant contributions are treated exactly rather than perturbatively, and allowance is made for the eigenmodes to extend over several rational surfaces. The equation analysed is similar in form to Eq.(57) except that ion transit resonances and higher-order finite-ion-gyroradius connections

$$(\propto \rho_i^4 \partial^4/\partial r^4)$$

have also been added.

Recalling that the spacing between rational surfaces is $\Delta r_s \cong (\ell q')^{-1}$, Rewoldt, et al. expressed the radial variable in terms of

$$S(r) = \ell[q(r) - q(r_s)] \simeq (r - r_s)/\Delta r_s$$

Since Δr_s is generally much smaller than typical equilibrium scale lengths for realistic tokamak conditions (e.g. $\hat{s} \equiv rq'/q \cong 1$), the radial equilibrium gradients can be taken as constant to a good approximation. The perturbed potential is then represented in terms of complete sets of poloidal and radial basis functions given by

$$\hat{\Phi}(\theta, S) = \sum_{n=0}^{\infty} \sum_{j=-\infty}^{\infty} \hat{\Phi}_{j,n} g_j(\theta) h_n(S) \tag{84}$$

where

$$g_j(\theta) = (2\pi)^{-1/2} \exp(ij\theta)$$

$$h_n(S) = M_n^{-1/2} H_n(\sigma^{1/2} S) \exp(-\sigma S^2/2)$$

$$M_n \equiv (\pi/\sigma)^{1/2} 2^n n!$$

and σ is a parameter (with its real part greater than zero) which is adjusted to optimize the convergence of the radial series. This form clearly satisfies the periodicity requirements as well as the radial boundary condition, $\hat{\Phi} \to 0$ as $S \to \pm\infty$. The latter corresponds to outgoing energy and also allows for localized modes that spread over a number of rational surfaces. Substituting Eq.(84) into the mode equation, multiplying by $g_{j'}^*(\theta) h_{n'}(S)$, and integrating over θ and S then gives the basic matrix equation, which is solved by standard numerical procedures [27].

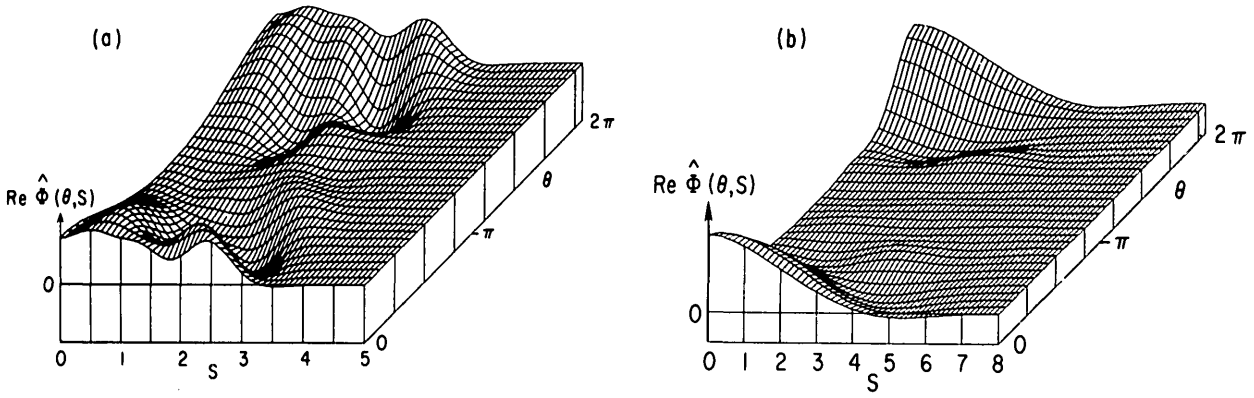

FIG.5. Real part of the 2D eigenfunction for trapped-electron modes with $k_\theta \rho_i = 0.2$ (a) and $k_\theta \rho_i = 1.4$ (b). The poloidal angle, θ, is zero at the outside of the torus (magnetic-field minimum) and the radial variable is $S = (r - r_s)/\Delta r_s$ with r_s being the radius of the reference rational surface around which the mode is centred, and Δr_s being the distance between mode rational surfaces.

Comparison of the results of the 2D analysis with those from the 1D radial calculations for representative cases indicate relatively small variations in the eigenvalues. However, the actual mode structure, as shown in Fig.5(a), is quite different from the simple 1D result, i.e. in contrast to the usual 1D analysis involving only a single rational surface, the eigenfunction is seen to extend over a number of such surfaces. It should also be noted here that as an alternative approach to expanding in radial basis functions, one can also apply numerical techniques to solve the linearly coupled radial differential equations directly. This procedure, which allows the introduction of variations in the equilibrium gradients, is currently being developed by Ross and Miner [90].

The radial differential form of the mode equation treated in the preceding calculations is valid provided the radial wavelengths are sufficiently long, i.e., $k_r \rho_i < 1$. Rewoldt, et al. [27] have found that as $k_\theta \rho_i$ approaches unity, the calculated 2D mode structure indicates that this constraint is not satisfied. Since the simplest local calculations [22–24] show that the maximum growth rates typically appear in the range $k_\theta \rho_i \gtrsim 1$, a reformulation of the analysis of the radial dependence in the 2D equation becomes necessary. Working with the unexpanded form of the ion gyroradius factor given in Eq.(54), Tang, et al. [89] have recently obtained solutions to the resultant 2D integral equation. They noted that for the general case of arbitrary k_r, the r-integration in Eq.(54) can be analytically calculated as before, but the k_r-integration must now be numerically evaluated. Using the basis functions given in Eq.(84), a matrix equation, similar in structure to the one obtained for the long-radial-wavelength (differential) problem [27], is generated. Hence, the same numerical procedures can again be applied. The 2D results have indicated that, in general, the growth rates are smaller than those from 1D calculations and that this difference becomes more pronounced as $k_\theta \rho_i$ increases. In addition, it is found that, in contrast to the long-wavelength cases, the 2D mode structure at shorter wavelengths exhibits a strong ballooning around the magnetic field minimum. This effect is illustrated for a typical case in Fig.5b. Tang, et al. [89] have noted that the differences with the 1D eigenvalues and especially the pronounced ballooning effect are likely related to the enhanced phase oscillations in the trapped-electron driving term. In particular, since S is proportional to $k_\theta(r - r_s)$, the phase $iS(\theta - \theta_1)$, which appears in the orbit-averaged potential there can become large if either k_θ increases (i.e. shorter wavelengths) or the distance from the reference rational surface, $(r - r_s)$, increases.

As a final point, it should be noted that the type of eigenfunction calculated in Refs [27] and [89] is degenerate in m, the poloidal mode number at the reference rational surface around which the mode is centred. The truncation in the series of basis functions given in Eq.(84) is dictated by the convergence to a unique eigenvalue. Although the addition of more terms in the series of basis functions can lead to a wider radial extent than shown in Fig.(5), the eigenvalue (and hence the growth rate) is found to be unchanged to a good approximation. In fact, in the absence of equilibrium variations, one can construct a very broad mode extending over the entire plasma [90].

However, in practice, the radial extent will be limited by the equilibrium gradients. It should also be pointed out that the eigenvalue can be modified by a different choice of radial boundary conditions. For example, the stabilizing influence of shear, associated with the outward convection of energy, could be entirely eliminated by choosing perfectly reflecting conditions.

2.3. Finite-beta (non-electrostatic) modifications

Although tokamaks are basically low-β ($\beta \equiv$ plasma pressure/magnetic pressure) systems, the influence of related electromagnetic effects on microinstabilities can nevertheless be significant. For the low-frequency drift and trapped-particle modes, it has generally been found that such finite-beta effects tend to be stabilizing. In particular, attention has been focused on three separate physical mechanisms, namely: (i) the diamagnetic or "self-dug" well generated by the plasma pressure; (ii) the finite-β enhancement of the non-concentric shift of the magnetic surfaces; and (iii) the coupling between drift waves and shear-Alfvén waves.

It has been emphasized in many papers that if the orbit-averaged magnetic drift of the trapped particles is unfavourable, the de-stabilization of trapped-electron [22–25] and trapped-ion [33] modes can be strongly enhanced. Moreover, the collisionless (interchange) trapped-particle instability is entirely driven by these drifts [2]. The primary influence of the first two finite-β mechanisms listed above is to reduce this effect. To analyse such processes, it becomes necessary to replace the simple circular concentric magnetic surface model, used in most electrostatic calculations, with a model which is appropriate for a finite-β equilibrium. For a given pressure distribution, this is determined by the familiar equilibrium equations,

$$\nabla \vec{P} = \frac{1}{c} \vec{J} \times \vec{B}$$
$$\nabla \times \vec{B} = \frac{4\pi}{c} \vec{J} \qquad (85)$$

and

$$\nabla \cdot \vec{B} = 0$$

where $\vec{P}$ is the pressure and $\vec{J}$ is the current density. By making simplifying assumptions, such as scalar pressure and constant current profile, these equations can be solved analytically [91].

Analysing an appropriate finite-β equilibrium, Rosenbluth and Sloan [40] found that if β is sufficiently large, the resulting favourable magnetic field gradient induced by the pressure of the plasma can nullify the de-stabilizing unfavourable field gradients associated with the vacuum magnetic field. However, this would require values of $\beta > a/R$, which is unlikely to be reached. Specifically, since β_p (plasma pressure/poloidal magnetic field pressure) in standard tokamaks must be kept below the aspect ratio (R/a) to maintain equilibrium [91], $\beta \cong \beta_p (a/Rq)^2 \ll 1$. In studying the achievable range, $\beta \cong O[(a/R)^2]$, Glasser, et al. [41] and Dobrott and Greene [92] have shown that the combined influence of finite β and finite vertical ellipticity in the plasma cross-section can generate the desired favourable gradient effect.

As noted by Shafranov [93], the equilibrium solutions to Eq.(85) generally exhibit a non-concentric outward shift of the magnetic surfaces (away from the magnetic axis). Although this effect is weak for low β, Newberger [94] has pointed out that such shifts can become significant if β exceeds a few percent. Considering a poloidal field of the form

$$B_p \simeq B_p^{(0)} (1 + \Lambda \varepsilon \cos\theta)$$

with Λ being the shift parameter, and the usual form for the toroidal field,

$$B_T \simeq B_T^{(0)} (1 - \varepsilon \cos\theta)$$

the orbit-averaged ∇B-drift frequency of the trapped particles, $\overline{(\omega_{D1})_T}$, can be calculated as in the electrostatic case. Here the shift effect is stabilizing in that it increases the range in velocity space (i.e. in λ) where the drifts are favourable.

In general, one can obtain a reasonable picture of the stabilizing influence of the finite beta effects just discussed by simply analysing the expression for $\overline{(\omega_{D1})_{Tj}}$. However, to study the coupling between the drift and shear-Alfvén branches, it becomes necessary to simultaneously deal with the quasi-neutrality condition and the parallel-current equation obtained from Ampère's law. Effects associated with compressional Alfvén waves are usually ignored since $\beta \ll 1$ for standard tokamaks. In the simplest local limit, the finite-β analysis leads to the well-known dispersion relation [8]

$$\left(1 - \frac{\omega_*}{\omega}\right)\left[1 - \left(\frac{\omega}{k_{||} v_A}\right)^2 \left(1 + \frac{\omega_*}{\omega\tau}\right)\right]$$

$$= - \frac{k_\theta^2 \rho_s^2}{2} \left(1 + \frac{\omega_*}{\omega\tau}\right) \qquad (86)$$

with the de-stabilizing driving term (from either electron resonances or collisions) treated perturbatively. For

$$\omega \simeq \omega_* << k_{||} v_A$$

the coupling between the drift and shear-Alfvén branches is negligible, and the usual de-stabilizing downward shift in ω by the finite gyroradius term persists. If, however,

$$\omega \simeq \omega_* > k_{||} v_A$$

the shift can be reversed and the drift modes accordingly stabilized [95]. In terms of β, this condition

$$(\text{for } k_{||} \simeq 1/qR)$$

can be roughly approximated by

$$\beta > (r_n/qR)/(k_\theta \rho_i)$$

Effects due to trapped particles can be easily introduced in this local model and lead, of course, to a modification of the drift branch. Although the finite-β coupling can be effective in eliminating the analogous finite-gyroradius de-stabilization of the trapped-electron modes, it cannot strongly affect the de-stabilization associated with the temperature gradient-driven dissipative effects [28]. For trapped-ion modes, the phase velocity typically falls far below v_A, and the coupling process is correspondingly negligible.

Since the degree of coupling between the drift and shear-Alfvén branches is strongly dependent on $k_{||}$, a realistic evaluation of this effect requires a radially non-local treatment. The usual approach has been to follow the 1D radial analysis outlined in Section 2.2.2. Taking

$$k_{||} = k_\theta \rho_s x/L_s$$

as before, the effective unstable range for drift waves is now given by

$$v_i < (\omega_* L_s)/(k_\theta \rho_s x) < v_A, v_e$$

or

$$x_e, x_A < x < x_i$$

with

$$x_i \simeq L_s/r_n, \quad x_e \simeq (m_e/M_i)^{1/2} L_s/r_n$$

and

$$x_A \simeq \beta^{1/2} L_s/r_n$$

Here x_i and x_e represent respectively the estimates for the radial position where ion transit resonances (x_i) and electron transit resonances (x_e) become effective. The position x_A is where the coupling between the drift and shear-Alfvén branches becomes strong and can lead to stabilization of the drift modes [95]. If $v_A \cong v_e$, then $x_A \gtrsim x_e$, and the unstable range is reduced, i.e. x_A replaces x_e as the lower cut-off in the radial variable [16, 96, 48]. As pointed out by Catto, et al. [48], the upper cut-off for the actual interaction range is determined by the effective radial turning point, $x_T \cong (L_s/r_n)^{1/2}$, rather than by the ion-Landau damping point, $x_i \cong L_s/r_n$.

To obtain the radial normal modes for the finite-β-modified drift waves requires solving the two coupled differential equations, which correspond to the quasi-neutrality condition and the parallel-current equation. In the limits $k_\theta^2 \gg k_x^2$ and $k_x^2 \gg k_\theta^2$ (with $k_x^2 \rho_s^2 \ll 1$), these equations can be combined into a single second-order differential equation. Catto, et al. [48] have obtained solutions to such equations and have found that the resulting eigenvalue conditions indicate the finite-β terms are usually stabilizing. This favourable effect can be attributed in part to the effect mentioned above, namely, the reduction in the width of the region of interaction of the drift wave with the resonant electrons from $x_e < x < x_T$ to $x_A < x < x_T$. If poloidal ballooning effects are ignored, a similar analysis can be carried out for the trapped-electron modes [28].

As discussed earlier in this section, finite-β effects can significantly alter the simple equilibrium configurations considered in the electrostatic limit. For the remainder of this section, attention will be focused on finite-β modifications to the electrostatic formalism for perturbations. The perturbed electric and magnetic fields can be expressed as

$$\vec{\varepsilon} = - \nabla\Phi - \frac{1}{c} \frac{\partial}{\partial t} \vec{A}$$

and (87)

$$\vec{B}_1 = \nabla \times \vec{A}$$

with $\vec{A}$ being the magnetic vector potential. Following the same procedure as in the electrostatic case, the basic equation for the perturbed distribution function can be expressed in the same form as Eq.(12), except that $\Phi - (\vec{A} \cdot \vec{v}/c)$ now replaces Φ [94]. Solutions for h can also be obtained by applying the methods introduced in the electrostatic calculation. The results are then used in the quasi-neutrality condition, Eq.(14), and the parallel current equation,

$$-\nabla^2 A_{||} = \frac{4\pi}{c} j_{||}$$

$$= \frac{4\pi}{c} \sum_j Z_j e_j \int d^3v f_j^{(0)} v_{||} \qquad (88)$$

to generate the coupled mode equations.

For $\beta \ll 1$, the perpendicular components of $\vec{A}$, which give rise to compressional Alfvén waves, can be ignored to a good approximation. Hence, in Eq.(12) it is sufficient to replace Φ by $\Phi - (A_{||} v_{||}/c)$. Using the ansatz of Eq.(17) for $A_{||}$ and ignoring magnetic drifts for simplicity then gives

$$\left(\omega - iC_j - k_{||} v_{||} + i \frac{v_{||}}{Rq} \frac{\partial}{\partial \theta} \right) \hat{h}_j$$

$$= \left(\frac{e}{T} F_M \right)_j \left(\omega - \omega_{Tj}^* \right) \left\langle \Phi^{(0)} - A_{||}^{(0)} \frac{v_{||}}{c} \right\rangle_{\phi'} \qquad (89)$$

where

$$A_{||}^{(0)} \equiv \left\langle \hat{A}_{||} [r' + (1/\Omega) v_\perp \sin\phi', \theta] \right.$$

$$\left. \times \exp [ik_\theta (1/\Omega) v_\perp \cos\phi'] \right\rangle_{\phi'}$$

$\Phi^{(0)}$ has a similar form, and

$$k_{||} \equiv S/Rq \equiv [m - \ell q(r)]/Rq$$

The procedures described earlier in the electrostatic analysis can be similarly applied here to obtain $\hat{h}_j$ and the corresponding perturbed density responses. In the spirit of the 1D electrostatic radial calculations, the slow poloidal variation in $(\hat{\Phi}, \hat{A}_{||}) \exp(-iS\theta)$ will be ignored in the following derivation of the coupled radial mode equations for the collisionless drift and trapped-electron instabilities.

Recalling the definitions given in Eqs (57) and (68), the quasi-neutrality condition with the additional electromagnetic terms can be expressed in the form

$$\left(\frac{1}{\tau} A \frac{\partial^2}{\partial x^2} + \hat{B} + R(x) - (k_\theta \rho_s \hat{s})^2 C x^2 \right) \Phi(x)$$

$$= \left(1 - \frac{\omega_*}{\omega} - \Gamma + R(x) \right.$$

$$\left. - (k_\theta \rho_s \hat{s})^2 C x^2 \right) \left(\frac{\omega L_s}{k_\theta \rho_s c} \right) \frac{1}{x} A_{||}(x) \qquad (90)$$

As noted in Ref.[28], the total parallel current response can be obtained by operating on Eq.(89) with

$$\sum_j e_j \int d^3v$$

This leads to the result

$$\frac{k_{||}}{\omega} j_{||}(x)$$

$$= \frac{n_0 e^2}{T_e} \left(B - 1 + \frac{\omega_*}{\omega} + A\rho_i^2 \frac{\partial^2}{\partial r^2} \right) \Phi(x) \qquad (91)$$

with $j_{||}$ being the total parallel current density. The magnetic vector potential is, of course, related to this quantity by Ampère's law, i.e.

$$\left((\rho_s)^{-2} \frac{\partial^2}{\partial x^2} - k_\theta^2 \right) A_{||}(x) = \frac{4\pi}{c} j_{||}(x) \qquad (92)$$

Equations (91) and (92) can then be combined to give

$$\left(\frac{1}{2} \frac{\partial^2}{\partial x^2} - b_\theta^2 \right) A_{||}(x)$$

$$= \left(\frac{\omega}{v_A}\right)^2 \left(\frac{cL_s}{\omega k_\theta \rho_s}\right)\left(\frac{1}{x}\right)\left(B - 1\right.$$

$$\left. + \frac{\omega_*}{\omega} + \frac{1}{\tau} A \frac{\partial^2}{\partial x^2}\right) \Phi(x) \qquad (93)$$

with

$$v_A^2 \equiv B^2/(4\pi n_0 M_i)$$

This result, together with Eq.(90), determines the 1D radial mode structure of the collisionless drift and trapped-electron instabilities for a finite-β plasma.

3. REVIEW OF LINEAR EFFECTS ON LOW-FREQUENCY ELECTROSTATIC INSTABILITIES

Many of the important papers analysing specific linear effects on low-frequency microinstabilities have already been discussed in some detail in the preceding section. The purpose of the present section is to give a more comprehensive review of the work in this area covering the period from 1970 through 1977. Here the emphasis will be placed on the main features and conclusions of the papers rather than on the details of the calculations. Hence, some of the previously discussed papers will again be mentioned within the context of this general survey. Before proceeding, it should again be noted that alternative approaches to the basic formalism presented in Section 2 have frequently appeared in the literature [3, 9, 46, 66, 67]. For example, in dealing with long-wavelength modes ($k_\perp \rho_j \ll 1$), it is convenient to directly perform the gyro-phase average on Eq.(1) and to then work with the resulting drift-kinetic equation governing the distribution of guiding centres [97, 98].

3.1. Collisional and collisionless drift modes

The linear theory of collisional (dissipative) drift instabilities has undergone very little change since 1970. Most of the relevant work on this subject has already been covered in text-book format by Mikhailovskii [9], in the general review by Kadomtsev and Pogutse [3], and in a long survey-type article by Rukhadze and Silin [99]. A particularly useful result from Ref. [99] is the following expression giving the ion-ion collisional contribution at short wavelengths ($k_\perp \rho_i \gg 1$) when $|\nu_i/\omega| \ll 1$:

$$\Gamma_{ii} \simeq -i\left(\frac{1.25\nu_i}{\omega}\right)\left(k_\theta \rho_i \tau\right) \times \left(1 + \frac{\omega_*}{\omega\tau}\left(1 - 0.7\eta_i\right)\right) \qquad (94)$$

This viscous damping effect can be important in limiting the unstable spectrum of the drift modes at short wavelengths. Since $|\nu_i/\omega| \ll 1$ is usually satisfied in cases of interest, Eq. (94) can be readily incorporated in the calculations described in Section 2. Specifically, for the collisionless drift and trapped-electron instabilities, one can simply replace B by $B + \Gamma_{ii}$ in Eq. (57). The result given in Eq. (94) can also be reproduced from the formalism recently introduced by Catto and Tsang [66] for dealing with ion-collisional effects on drift modes.

In other recent work, Rogister and Hasselberg [74] have called attention to the possibility that the temperature-gradient-driven form of collisional drift instabilities could appear as precursors of the internal disruptions presently observed in tokamak experiments. The basic features of such instabilities have been well documented, e.g. by Rukhadze and Silin [99]. Also, shear stabilization criteria for current-driven forms of such modes have been discussed by Callen, et al. [12]. In the present paper, the authors consider very-long-wavelength modes ($m \sim 1$) which require an ordering different from the usual drift-wave ordering. Using the familiar single-rational-surface, 1D-radial model [15], they obtained a shear-dependent instability threshold which leads to results in apparent agreement with the onset of disruptions in the experiments. However, more recent work by Chen, et al. [19b] has emphasized that for such slab model calculations the dissipative drift waves are actually always stable. This analysis involves a careful non-perturbative treatment of the de-stabilizing dissipative electron term.

The collisionless or "universal" drift modes [15] have remained a popular subject of research over the past several years. In the early work on these instabilities, Krall and Rosenbluth [14] considered equilibrium variations in the density profile and generated a 1D radial equation by expanding around the maximum for ω_*. They found that a restricted class of unstable exponentially-decaying (i.e. non-propagating) radial normal modes can exist if the profile is sufficiently peaked around ω_*, and/or the

shear is sufficiently weak. Rutherford and Frieman [100] subsequently found that the collisionless drift waves can take the form of convectively unstable wave packets which are susceptible to shear stabilization. In 1969, Pearlstein and Berk [15] introduced outgoing wave boundary conditions into the radial analysis and discovered a general class of propagating normal modes. This calculation, which was discussed in detail in Section 2, stimulated a large number of subsequent papers incorporating their basic approach. It has been noted by Manheimer [101] that the time domain wave packet analysis of Lau and Briggs [102] leads to qualitatively equivalent results.

To obtain the shear stabilization criterion for universal modes, Pearlstein and Berk estimated the de-stabilizing (radially dependent) resonant electron contribution by taking its local value at the turning point, $x_T \simeq \rho_s (L_s/r_n)^{1/2}$, and then balancing it with the shear damping term. In the presence of electron temperature gradients, this is given approximately by

$$\frac{1}{4}\left|\frac{m_e L_s}{M_i r_n}\right|^{1/2}\left((k_\theta \rho_s)^2 - \eta_e\right) = \left|\frac{r_n}{L_s}\right| \tag{95}$$

which in turn leads to the familiar scaling, $|r_n/L_s|_{crit} \propto (m_e/M_i)^{1/3}$, for the critical shear. The evaluation of the resonant electron response was refined in later work by Mishin [96] and by Gladd and Horton [16], who applied standard perturbation theory. This essentially involves an integration of the non-local resonance over the radial range of interaction and leads to a moderate reduction in the shear-stabilizing effect, i.e. the de-stabilizing term on the left-hand side of Eq. (95) is now multiplied by the factor $\ell n\,|M_i r_n/m_e L_s|$. Mishin pointed out that the lower radial cut-off here should be determined by the condition, $k_{||}(x_A) v_A = \omega$, since local analysis [95] indicates that finite-β effects stabilize the drift waves for $x < x_A$. Gladd and Horton numerically evaluated the radial eigenmodes including both resonant electron and resonant ion effects and found the eigenvalues to be in good agreement with the results of the analytic perturbation analysis. With regard to the finite-β modifications, Catto, et al. [48] carried out a comprehensive analysis of the coupled radial equations obtained from the quasi-neutrality condition and the parallel-current equation. As discussed in Section 2.3, the finite-β effects on the drift waves generally tend to favour stability.

The Pearlstein-Berk-type analysis has also been used to obtain shear stabilization criteria for current-driven [103, 104] and temperature-gradient-driven [17] forms of the universal mode [8, 14]. The effects associated with the presence of a parallel current (along the magnetic field) can be readily estimated by considering a shifted Maxwellian distribution for the electrons, i.e. $F_e^{(0)} \propto \exp\{-[v_\perp^2 + (v_{||} - u_0)^2]/v_e^2\}$. Coppi [103] and Rosenbluth and Liu [104] found that such effects can lead to more restrictive requirements for shear stabilization. However, the influence here is relatively weak since the ratio, u_0/v_e, is usually very small in tokamaks. Liu [105] and Horton [106] have also noted that strongly sheared current profiles ($\propto du_0/dx$) can drive instabilities which could account for the anomalous skin effect observed in tokamak experiments. Because of the large current gradient required here, Liu, et al. [17] concluded in subsequent work that a more likely mechanism is the one associated with drift modes driven by reversed temperature gradients ($\eta_e < 0$). Specifically, in Ohmically heating the plasma, the temperature is expected to be peaked near the plasma boundary. Since $\eta_e < 0$ here, the resulting enhanced de-stabilization of the universal mode could contribute to the observed rapid disappearance of this temperature maximum.

The question of the reliability of the perturbative approach and of considering only the resonant part of the electron response was first investigated by Rosenbluth and Catto [85]. Considering the usual slab model with shear, they retained the full Z-function electron response. Their approach involved solving the resultant radial equation in the limit, $|\omega/k_{||}(x) v_e| >> 1$, (appropriate to the region near the rational surface, $x = 0$) and in the limit, $|\omega/k_{||}(x) v_e| << 1$ (where the usual outgoing wave boundary condition, $\Phi \to 0$ as $|x| \to \infty$, was invoked). A complicated eigenvalue equation was then obtained by asymptotically matching these solutions. The authors made rough analytic estimates of the eigenvalues and reported that the earlier calculations appeared to be accurate. However, it has been reported in very recent studies that this conclusion is in error. Specifically, Ross and Mahajan and Tsang, et al. [19a], in independent numerical calculations, found that the universal eigenmodes are always stable in a sheared slab geometry if the complete electron response (full Z-function) is retained. Of course, for strongly peaked radial density profiles [14], unstable eigenmodes can again appear. It should also be remembered that although they are generally less dangerous than the absolute type, the

convectively unstable form of collisionless drift waves [100] are likely to persist.

In toroidal systems, the collisionless drift instabilities can be present even in the absence of peaked profiles. As discussed in some detail in Section 2.3.3, the favourable influence of shear can be effectively nullified if the non-uniformity in either the shear or the magnetic field strength along the field lines is sufficiently great. These effects have been emphasized by Taylor [88] and also by Cordey and Hastie [107]. Introduction of the complete electron response in the analysis here does not alter the basic conclusions.

Universal modes have also been studied by means of particle codes. In a so-called "$2\frac{1}{2}$-D" (x, y, v_x, v_y, v_z) simulation, Lee and Okuda [108] considered a slab-type plasma model, which is uniform and periodic in y and non-uniform and bounded by conducting walls in x. The magnetic field is perpendicular to x with a small x-dependent y-component to introduce shear. In the shearless limit, the simulation results were found to be in very good agreement with analytically calculated growth rates. For the sheared cases, the shear stabilization thresholds appeared to roughly correspond to the $(m_e/M_i)^{1/3}$ scaling given following Eq. (95). However, the simulation has not yet resolved the question of whether such modes are absolute or convective in character. It should also be noted that the radial boundary condition ($\Phi = 0$ at plasma edge) imposed here implies a certain amount of reflection. Even if the reflection is infinitesimally small, it is still qualitatively different from the outgoing-wave boundary condition invoked in recent theoretical studies [19a]. Finally, it should be remembered that the particle simulations describe transient phenomena, while conventional theories generally deal with steady-state situations.

In early investigations of impurity effects on collisionless drift modes, Coppi, et al. [18] found that instabilities can occur if the impurity density gradient and the density gradient of the main plasma are oppositely directed. Using a BGK model, which conserves number, momentum, and energy, to calculate the impurity response, Wong [109] re-derived these results with a kinetic theory which was applied over the collisional as well as collisionless regimes. At low collisionalities, the de-stabilization comes from wave-particle resonances. In the opposite limit, where a fluid description of the impurity response is appropriate, the instabilities are driven by collisional dissipation. This is analogous to the usual qualitative picture of the drift wave transition between the collisional and collisionless regimes [9]. In a more quantitative sense, it has been pointed out by several authors that the actual values of the growth and damping rates for ordinary drift waves can be significantly modified by using the more accurate Dougherty [110] and Lorentz [111, 112] collision models. The effects treated by Wong, as well as the influence of impurities on a large variety of trapped-particle modes, have recently been summarized in a comprehensive article on impurity-driven modes by Coppi, et al. [113].

3.2. Trapped-particle instabilities

The importance of low-frequency microinstabilities associated with the magnetic trapping of particles in toroidal geometries was first emphasized by Kadomtsev and Pogutse in 1966 [2]. Since that time the investigation of trapped-particle modes has been a very very active area of theoretical research. As noted in Section 1.3, these instabilities can be classified very broadly as (i) trapped-electron modes which require $\nu_e^* \equiv \nu_{eff,e}/\omega_{be} < 1$ and fall in the usual drift wave range, $(\omega_{b,t})_i < \omega < (\omega_{b,t})_e$; and (ii) trapped-ion modes which require both $\nu_e^* < 1$ and $\nu_i^* < 1$ and fall in the range $\omega < (\omega_{b,t})_i$. At very high temperatures, where the collisional effects are entirely negligible, the trapped-ion modes evolve into the so-called collisionless or "interchange" trapped-particle modes. Coppi and co-workers have found that in this very collisionless regime, instabilities with odd symmetry around the magnetic field minimum can also appear. Unlike the usual trapped-ion and trapped-electron instabilities, the basic characteristics of these odd modes do not appear to be strongly affected by changes in the collisionality.

3.2.1. Trapped-electron modes

In the original derivation of the trapped-electron instability, Kadomtsev and Pogutse [20] showed that by introducing energy dispersion in a simple Krook-type collision operator [see Eq. (30)], drift waves in the presence of trapped electrons could be de-stabilized by electron temperature gradients together with collisional dissipation. For the usual case of positive temperature gradients ($\eta_e > 0$), they found that the onset of these instabilities requires $\nu_{eff,e} > \omega \sim \omega_*$. Employing the Pearlstein-Berk-type 1D radial analysis, Galeev and Sagdeev [82] obtained a shear stabilization criterion for such modés. In subsequent work, Liu, et al. [21] and Deschamps, et al. [114] found that even in the absence of

temperature gradients, the finite-ion-gyroradius shift of the mode frequency below ω_* could lead to dissipative trapped-electron modes analogous to the universal modes. Galeev and Sagdeev's radial calculations were extended to include this effect by Liu, et al. [21] and by Horton, et al. [83]. However, Sauthoff, et al. [115] have noted that the stabilizing influence of shear could be ineffective if the diamagnetic frequency profile is sufficiently peaked. Just as in the case of universal modes [14], strong peaking acts to change the effective radial potential from an anti-well to a well. The radial propagation of wave energy, essential for shear damping, is accordingly suppressed by reflections. For general conditions (where the profile is not so sharply peaked), the toroidal coupling, studied by Taylor [88] in connection with collisionless drift modes, can also lead to a suppression of shear damping. This effect, which requires strong toroidal coupling, is analysed for the trapped-electron modes in Section 2.2.3. Using a fluid-type response for the ions, Horton, et al. [116] have very recently performed a similar calculation with results in basic agreement with those given in Section 2.2.3.

In other investigations of toroidal coupling effects, Tang, et al. [117, 83] used a variational procedure to determine the ballooning-type mode structure along the field line. These results were reproduced in numerical calculations by Liewer, et al. [80], who added ion acoustic and ion-Landau-damping terms to the analysis. As discussed in Section 2.2.1, the extent of the ballooning is dependent on the relative strength of the trapped-electron driving (coupling) term compared to the ion acoustic (de-coupling)term. In general, however, the calculation of toroidal coupling together with shear effects requires a two-dimensional analysis. Rewoldt, et al. [27] have investigated this problem and have obtained 2D eigenmodes which are centred on a reference rational surface and typically spread over several neighbouring rational surfaces. Electron and ion resonances as well as important magnetic drift effects (which will be discussed later in this section) have been included in their calculation. To extend the regime of validity of this analysis to shorter radial wavelengths, Tang et al. [89] have introduced an integral equation formulation of the radial dependence. Details of these calculations and a summary of the principal results are given in Section 2.2.3. As noted in the discussion there, the eigenfunctions obtained in Refs [27, 89] are degenerate in the poloidal mode number, m. To determine the "global" radial mode structure, it is necessary to consider variations in the equilibrium gradients. A numerical procedure, which, in principle, allows the introduction of such variations for the longer-wavelength ($k_r \rho_i < 1$) modes, is currently being developed by Ross and Miner [90]. This essentially involves solving a large system of poloidally coupled radial differential equations.

The influence of finite-β modifications on trapped-electron modes has been investigated by Tang, et al. [28]. As indicated by the formalism presented in Section 2.3, the usual 1D radial analysis leads to a coupled pair of radial differential equations corresponding to the quasi-neutrality condition and the parallel-current equation. Since these are similar in structure to the equation encountered in the collisionless drift problem, the mathematical procedures introduced by Catto, et al. [48] were also applied here. The authors concluded that the finite-β coupling between the drift and shear Alfvén branches can be effective in eliminating the finite-ion-gyroradius de-stabilization [21] but cannot strongly influence the usual ∇T-driven effects.

In Ref. [28] the authors have also emphasized that since $\eta_e > 0$, the ∇T-related resonant electron term can provide a significant stabilizing contribution. For the familiar slab limit, this stabilizing factor would be roughly proportional to

$$\eta_e \omega_* \left| m_e L_s / M_i r_n \right|^{1/2} \ell n \left| M_i r_n / m_e L_s \right|$$

However, in the low-collision limit, trapping effects reduce the velocity space of the resonant electrons. The argument of the logarithmic term in the stability factor is accordingly reduced to $1/2\epsilon$. In subsequent work, Hinton and Ross [70] and Horton [71] pointed out that, at higher collisionalities, the resonance can be collisionally broadened. Using the Lorentz collision operator of Eq. (27) and dividing the electron velocity space into regions of collisionality bounded by surfaces of constant energy, these authors found that the enhanced resonant contribution can approach the slab result given above, even for $\nu_{*e} < 1$. More recently, Catto, et al. [72] and Tsang, et al. [118] have carried out similar calculations, but have emphasized the importance of distinguishing between perpendicular and parallel components in specifying the collisionality boundaries in velocity space (see Fig. 6). Unlike the earlier work [70], they found that for $\nu_{*e} \lesssim 1$, the reduction in the resonant electron response, caused by the presence of trapped electrons, remains a strong effect, i.e. resonance-broadening effects are weak. As a final point, it is useful to note

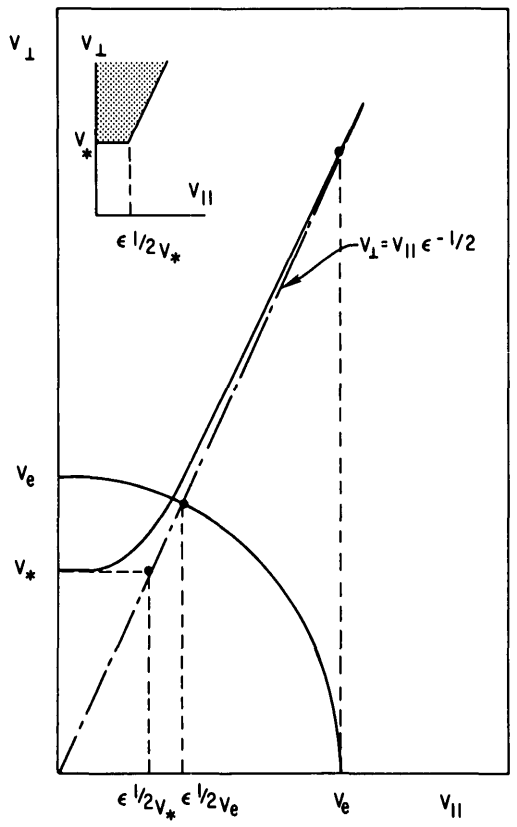

FIG. 6. Schematic diagram of electron velocity space with the trapped electrons falling in the shaded region. Here $v_* = (\nu_{*_e})^{1/4} v_e$ *is just the average velocity at which* $\nu_{*_e} = 1$, *and* $\nu_{*_e} = (\nu_{eff}/\omega_b)_e$ *is the usual banana regime parameter.*

that the basic approach in all the resonance-broadening calculations cited [70–72, 118] involves working with the Lorentz collision operator in the drift-kinetic equation (since electron gyroradius effects are negligible). A solution for the untrapped-electron distribution can be obtained by a Fourier transform method which leads approximately to the following response:

$$\left(\frac{n_U}{n_o}\right)_e \propto \int_U d^3v \, \frac{(\omega - \omega_T^*)}{|k_{||}|} \exp\left(-v^2/v_e^2\right)$$

$$\times \int_0^\infty dp \exp\left[-ip\left(v_{||} - \frac{\omega}{|k_{||}|}\right) - \frac{\nu_e p^3 v^2}{3|k_{||}|}\right] \qquad (96)$$

where p is the transform variable associated with $v_{||}$. This type of calculation has been carried out to trace the transition between the trapped-electron and collisionless drift instabilities.

A number of papers [22–25, 42] in recent years have emphasized the importance of including magnetic drifts in the analysis of trapped-electron instabilities. In earlier studies of collisionless drift modes, it was noted, e.g. by Coppi, et al. [119], that ∇B drifts could lead to instabilities localized in regions of bad curvature. Yoshikawa and Okabayashi [25] considered these effects in connection with the FM-1 spherator experiment and concluded that localization in unfavourable regions enhances the de-stabilization of the trapped-electron modes. In a more detailed radially local calculation, Adam, et al. [42] found that the ion ∇B-drift term (i.e. the $\omega_{Di} \cos\theta$-term) can lead to a form of the trapped-electron instability which is strongly localized along the field line. Unlike the usual modes, which balloon at the magnetic field minimum, these modes are localized away from B_{min} and have odd symmetry around their point of localization. The authors argued that although such modes have smaller local growth rates, they are also far less susceptible to the stabilizing influences of shear and circulating electron resonances (for $\eta_e \sim 1$). In addition to the usual dissipative de-stabilization associated with the ∇T and finite-ion-gyroradius effects, these modes can be further de-stabilized by ∇B-drift resonances in the trapped-electron response. This important driving mechanism was subsequently incorporated into the analysis of the conventional form of the trapped-electron modes by Tang, et al. [22] and Adam, et al. [23].

In the simplest local limit (i.e. ignoring radial effects, poloidal ballooning, ion ∇B drifts, and untrapped-electron resonances) Eq. (57) reduces to

$$1 + \tau - \left(\tau + \frac{\omega_*}{\omega}\right) \Gamma_0 - \eta_i \frac{\omega_*}{\omega} b(\Gamma_1 - \Gamma_0)$$

$$= \epsilon^{1/2} \left(\frac{2}{\pi^{1/2}}\right) \int_0^\infty d\bar{E}\, \bar{E}^{1/2}$$

$$\times \exp(-\bar{E}) \, \frac{(\omega - \omega_{Te}^*)}{(\omega - \overline{\omega_{De}} + i\nu_{f,e})} \qquad (97)$$

with $\bar{E} \equiv E/T_e$ and $\overline{\omega_{De}} \cong \epsilon_n \omega_* \bar{E}$ for $rq'/q \cong 1$. This has the essential features of the dispersion relation studied by Coppi and Rewoldt [24] and by Adam, et al. [22, 23], These authors have emphasized the fact that

the magnetic drifts can greatly enhance the instabilities at low collisionalities. The unstable frequency range, $\omega \gtrsim \nu_{\mathrm{eff,e}}$, noted by Kadomtsev and Pogutse [20], is now effectively extended to zero collisionality. Finding that the ∇B-drift-enhanced growth rate could be comparable in magnitude to the real part of the mode frequency, Adam, et al. noted that the usual perturbative approach [42, 83] for determining the eigenvalue is not applicable. They then proceeded to solve Eq. (97) numerically over a wide range of collisionality (ν_{*e}) and wave numbers (b) taking as typical parameters $\epsilon = \epsilon_n = 1/4$ and $\eta_e = \eta_i = 1$. The resultant growth rates were found to be substantially enhanced (e.g. by roughly a factor of 4 and larger for $\nu_{*e} \lesssim 0.1$). Shear stabilization criteria, obtained by applying the usual 1D radial analysis, were likewise found to be more severe and unlikely to be satisfied.

Using ϵ as an expansion parameter in Eq. (97), Coppi and Rewoldt [24] generated the following approximate quadratic form

$$\tau(1 - \Gamma_0) + 1 - \epsilon^{1/2} + \frac{\omega_*}{\omega}(\epsilon^{1/2} - \Gamma_0) + \frac{\epsilon^{1/2}\omega_*\omega_D}{\omega^2} = 0 \quad (98)$$

where η_i and $\nu_{f,e}$ are neglected for simplicity and $\omega_D = \epsilon_n\omega_*$. They pointed out that for $\Gamma_0 \cong \epsilon^{1/2}$, this equation indicates the existence of purely growing (non-resonant) fluid-like instabilites. The authors further noted that at long wavelengths (i.e. $b < 1$) one recovers the usual electron diamagnetic drift modes, but that at short wavelengths (i.e. $b > 1$) ion diamagnetic or "ubiquitous" drift modes can appear. Such modes are susceptible to de-stabilization by bounce resonances and electron collisional dissipation in the presence of temperature gradients. In Refs [24, 46] these effects were estimated by expanding the electron response to third order in ω/ω_{be}. A more detailed calculation of the electron collisional de-stabilization has recently been reported by Mikhailovskii [81]. Following the procedures introduced by Rosenbluth, et al. in the trapped-ion mode studies [29], he found the criterion for dissipative de-stabilization is given by $\eta_e > 1.5$, instead of the condition, $\eta_e > 2/3$, derived in the earlier work [24, 46]. Mikhailovskii has also estimated the finite-β influence on short-wavelength drift instabilities in the radially local limit [120]. Taking $k_\parallel \cong 1/qR$, he concluded that for $\beta_p \gtrsim 1/\epsilon^{1/2}$, the coupling between the drift and shear-Alfvén branches can readily stabilize these modes.

In recent work, Ross, et al. [121] have carried out a more detailed analysis of the relationship between the short-wavelength "ubiquitous" and fluid-like instabilities and the usual trapped-electron drift modes. Considering the short-wavelength ($b \gtrsim 1$) regime, they found that the non-resonant interaction with the magnetic drifts can become the dominant de-stabilizing mechanism for the electron drift modes. However, with regard to the ion diamagnetic ("ubiquitous") mode, particular relations between equilibrium parameters (ϵ, ϵ_n, η_j, etc.) must be satisfied before the phase velocity of the electron mode can change its sign to correspond to the ion diamagnetic direction. It is also pointed out that although the ∇B-driven growth terms tend to increase with b, ion-ion collisions [see Eq. (94)] can be very effective in damping these short-wavelength modes at sufficiently high collisionalities [121, 122]. The various electrostatic effects covered in the preceding discussion, as well as non-local ion ∇B drifts, have been included in the 2D calculations of Rewoldt, et al. [27, 89].

As pointed out by Tang, et al. [22, 23], the dangerous influence of the magnetic drifts can be reduced to a great extent in the presence of reversed-gradient density profiles. Such configurations can be generated, e.g. by surrounding the hot plasma with a "cold" transient blanket of neutral particles (see Fig. 7). Time-dependent radial-transport code calculations [123] have indicated that the resultant influx of neutrals can produce inverted density profiles falling in the banana regime ($\nu_{*e} < 1$) and persisting on a

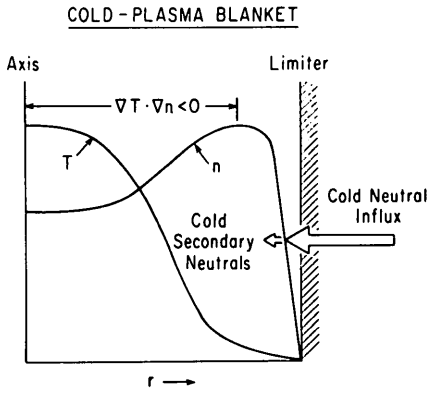

FIG. 7. Schematic density and temperature profiles with outward plasma density-peak generated by neutral-gas influx.

relevant time scale. The stabilizing influence on the unfavourable ∇B-drift resonances is obvious since the inverted density gradient reverses the sign of $\omega(\propto \omega_*)$ but leaves the sign of $\overline{\omega_{De}}$ unchanged. Detailed calculations here [22, 23], as well as in subsequent work [71], have generally indicated a substantial gain in stability over normal profiles for $\nu_{*e} < 1$. However, in extending the analysis to the higher-collisionality regimes, appropriate for the universal and dissipative drift instabilities, Horton [71] has noted that the inverted configuration can be less stable than the normal case for $\nu_{*e} > 1$. This is primarily due to the fact that the negative values of η_e, produced by the reversed density gradient, enhances the de-stabilization of the universal and dissipative drift modes.

Finally, it should be mentioned that in the past several years the elementary form of the trapped-electron instability (i.e. ignoring magnetic drift and all non-local effects) has also been analysed with respect to the presence of impurities [124, 125], current-driven effects [126, 127], particle simulation [128], and feedback stabilization [129]. Treating the impurities in the fluid limit, $v_I < v_i < \omega/k_\parallel$, Ross [124] and Bhadra [125] have concluded that such effects are relatively minor. Bussac, et al. [126] and Coppi and Rem [127] have considered the effect of a parallel current. Just as in the case of collisionless drift modes, the associated effect is generally weak because the current-driven contribution is proportional to the small quantity, u_0/v_e. A particle simulation of trapped-electron modes in a straight (rather than toroidal) geometry has recently been reported by Matsuda and Okuda [128]. These instabilities are analogous to those experimentally detected in linear systems by Deschamps, et al. [114] and by Prager, et al. [130]. It is noted that by varying the temperature gradient between zero and finite values, it is possible to observe both the ∇T-driven and the ion-gyroradius-driven forms of the dissipative trapped-electron instability. The possibility of feedback stabilization of low-frequency drift waves has been investigated by Chen and Furth, who proposed using modulated neutral-beam injection [131], and by Furth and Rutherford, who considered the use of modulated electron sources within the plasma [132]. In a more quantitative calculation, Sen and Sundaram [129] have recently confirmed that the neutral-beam feedback scheme suggested by Chen and Furth can provide an effective stabilizing mechanism for both trapped-electron and trapped-ion modes. The basic processes involve a de-energization of the wave and density smoothing.

3.2.2. *Trapped-ion modes*

In deriving the trapped-ion instability, Kadomtsev and Pogutse [2, 3] considered the local limit (ignoring mode structure modifications) and used a simple form of the Krook collision operator which excludes energy dispersion, i.e. $C_j = -\nu_j/\epsilon$. Subsequently, Sagdeev and Galeev [30] calculated the de-stabilizing electron collisions more carefully with a Lorentz model. They also considered the influence of ion transit resonances and found the resultant Landau damping to scale approximately as $\gamma_{LD} \propto -\omega^4/(\epsilon^{1/2} k_\parallel v_i)^3$. These effects, together with temperature gradients and a Lorentz model treatment of ion collisions, were incorporated by Rosenbluth, et al. [29] in a comprehensive radially local analysis. As described in some detail in Section 2.2.1, a variational procedure was introduced by these authors to determine the mode structure along the field line and to resolve the boundary layer problem associated with ion collisional effects. It was found that the presence of temperature gradients is generally de-stabilizing and can change the effective resonant response of the untrapped ions from damping to growth if $\eta_i > 2/3$. In addition, ion-collisional damping is moderately reduced from $\nu_i/\epsilon\omega$ to $(\nu_i/\epsilon\omega)^{1/2}[\ln(\epsilon\omega/\nu_i)]^{-3/2}$ and can also become de-stabilizing if $\eta_i > 1.75$.

In further studies of the trapped-ion modes, Tang has analysed the influence of ion bounce resonances [31], magnetic drifts [32], and ellipticity of the magnetic surfaces [31, 32]. Following the procedures discussed in Section 2.2.1, it was found that like the ion transit resonances, the bounce resonances are stabilizing for $\eta_i < 2/3$. The magnitudes of these effects are also comparable if $k_\parallel \cong 1/2qR$. With regard to the magnetic drifts, it was noted that ions, trapped in regions of good gradient ($dB/dr > 0$), can generate drift resonances leading to favourable Landau damping. Since vertical ellipticity in the cross-section of the torus increases the region of positive gradient [41], the stabilizing drift resonances are accordingly enhanced [32]. Defining the ellipticity parameter as $A \equiv \epsilon(\kappa_e^2 - 1)/q^2$, with κ_e being the ratio of the major to minor axes of the cross-section, it was found that stability can be significantly improved for $0 < A \lesssim 1.25$ with A = 0 corresponding to the circular case and A = 1.25 corresponding to $\kappa_e \sim 5$. This was attributed to the fact that, in addition to the increased drift damping, the elliptic configuration gives rise to enhanced ion collisions in the boundary layer and also enhances the bounce damping (for $\eta_i < 2/3$) by

increasing the average connection length of the trapped ions [31, 32]. As noted in Section 2.3, Newberger [94] has pointed out that the finite-β-related outward shift of the magnetic surfaces also enhances this effect.

In the preceding calculations, a constant-current profile ($q' = 0$) was assumed in order to facilitate the derivation of the appropriate equilibrium for an elliptical tokamak [31, 41]. However, as noted in Eq. (40) and Fig. 3, the region of favourable gradient drifts for the usual circular cross-section is effectively eliminated if $rq'/q \cong 1$. Hence, for typical radially varying current profiles, the Landau damping from the drift resonances can be negligibly small. On the other hand, for the inverted density profiles discussed earlier, this damping is restored and enhanced since the resonances now involve the trapped ions with average bad ∇B drifts, i.e. $\overline{\omega_{Di}} < 0$ [22]. As pointed out in Ref. [22], the reversed density gradients lead to a strong reduction of the electron collisional growth term together with a pronounced enhancement of the various damping mechanisms. The usual form of the trapped-ion instability should, therefore, be easily stabilized by inverted density profiles. However, in subsequent work, it was discovered by Tang, et al. [33] that a residual instability propagating in the ion diamagnetic direction can appear for density profiles which are either reversed or flat. Moreover, the authors emphasized that for sufficiently large ion temperature gradients ($\eta_i > 2/3$), the usual picture of the trapped-ion mode changes even for normal density profiles. Analytic as well as numerical solutions to the local dispersion relation,

$$1 + \tau = \Gamma + \Gamma_i \qquad (99)$$

[with Γ defined in Eq. (67) and Γ_i defined in Eq. (78)] indicated that for realistic aspect ratios and $\eta_i > 2/3$, the dominant modes have phase velocities in the direction of the ion diamagnetic drifts rather than the familiar electron direction. Such instabilities are driven by both resonant and non-resonant interactions with ions which have average bad magnetic drifts ($\overline{\omega_{Di}} < 0$). Growth rates for these modes were generally found to be smaller than those for trapped-ion instabilities with ordinary density profiles and mild temperature gradients ($\eta_i \lesssim 2/3$). Similar conclusions regarding the resonant de-stabilization of the ion drift branch have recently been reported by Tagger, et al. [133].

The 1D radial structure of the trapped-ion modes is governed by Eq. (78). Since there is no term in the effective radial potential, $Q(r, \omega)$, analogous to the ion sound term, this equation exhibits only one turning point if the untrapped ion resonances are ignored. Jablon, et al. [86] and Ross and Horton [87] have analysed this problem in the absence of magnetic shear and assumed various radial boundary conditions (at larger r) to provide a second turning point. Radially non-local modes were then obtained by standard WKB methods. Ross and Horton, however, also emphasized that it is important to take into account the influence of magnetic shear. This leads to a radial dependence in $k_\parallel$ which, in turn, implies that the ion transit resonances must be included (since they are strongly dependent on $k_\parallel$). In subsequent work, Gladd and Ross [34] retained the transit resonances (but ignored the drift resonances) in Eq. (78), and obtained numerical solutions of the non-local modes. It was found that strong ion-Landau damping close to the rational surfaces generates narrow peaks in $Q(r, \omega)$. As shown in Fig. 4, these lead to strong reflections which produce nodes in the eigenfunction, Φ. The authors have pointed out that the growth rates here can be significantly reduced below the radially local estimates, and that, in contrast to earlier work [86, 87], the eigenvalues appear to be virtually independent of the choice of outer boundary conditions. The influence of strong toroidal coupling, which would lead to a 2D-type analysis of the trapped-ion modes, has not as yet been determined.

Impurity effects on the trapped-ion modes have been investigated by Dobrowolny and Ross [35, 36, 124, 134]. The effective ion charge can be expressed as $Z_{eff} \equiv (n_i + \sum_I Z_I^2 n_I)/n_e$, and the impurities enter as separate ion species in the quasi-neutrality condition. The authors have noted that the obvious increase in the total collision frequencies of electrons and hydrogen ions is clearly stabilizing since it decreases the dissipative electron driving term ($\propto 1/\nu_{eff,e}$) and increases the ion damping contribution $\{\propto (\nu_{eff,i})^{1/2} \times [\ell n (\omega/\nu_{eff,i})]^{-3/2}\}$. At low phase velocities, $\omega < k_\parallel v_I$, Dobrowolny [36] has emphasized that Landau damping on light impurities (i.e. carbon, oxygen, etc. in the plateau regime) can be a strong stabilizing effect if the density gradient of the impurities and main plasma are in the same direction. Analogous collisional damping effects are found for impurities in the Pfirsch-Schlüter regime. Of course, oppositely directed gradients are accordingly de-stabilizing in both collisionality regimes. At higher phase velocities, $k_\parallel v_I < \omega$, Dobrowolny and Ross [35] have concluded that aside from enhanced collision frequencies, the impurity effects are not significant. Banana regime impurities have also been considered [36, 134], but

their appearance is generally believed to be unlikely even under reactor conditions. A number of the preceding conclusions have also been noted by Bhadra [125] and by Coppi, et al. [113]. As a final point regarding the influence of impurities on trapped-ion modes, it should be mentioned that magnetic drift and radially non-local effects have not been considered.

3.2.3. *Collisionless trapped-particle modes*

In the very-high-temperature limit where collisional effects become negligibly small, the trapped-ion mode evolves [3, 33] into the fluid-like "interchange" trapped-particle instability [2, 37]. As pointed out by Kadomtsev and Pogutse [2], this purely growing non-resonant mode is driven by the unfavourable ∇B drifts of the trapped particles in the presence of density gradients. Rosenbluth [37] noted that the stability requirement of favourable average magnetic drifts can be simply expressed as $dJ/dr < 0$, the so-called "maximum-J" criterion with $J = \oint_T ds\, m\, v_{||}$ being the familiar longitudinal invariant. In subsequent work, Pogutse [135] and Liu [136] found that the presence of temperature gradients can lead to further de-stabilization.

Other investigations of the collisionless trapped-particle modes have focused on possible stabilizing effects associated with radially non-local effects, finite-β, non-circular magnetic surfaces, and impurities. The usual radial-eigenmode approach was followed by Liu and Bhadra [137, 38] and by Jablon, et al. [86] in investigating the radial effects. This problem was also analysed by Briggs and Lau [138] who formulated it in terms of the evolution of a localized wave packet. In general, it was found that the radial effects do not dramatically alter the linear stability of these modes. With regard to finite β, the "self-dug-well" effect, noted by Rosenbluth and Sloan [40], is stabilizing but typically quite weak [92]. Callen, et al. [12] concluded that the influence of non-circular magnetic surfaces is also negligibly small. However, Glasser et al. [41] and Dobrott and Greene [92] have emphasized the fact that the combined effects of finite β and vertical ellipticity can be strongly stabilizing. In recent work, Dobrowolny and Paravano [39] have noted that the presence of impurities (which are taken to be in the plateau and Pfirsch-Schlüter regimes) tends to be a favourable influence but is generally insufficient to effect total stabilization. As a final point, it should be remembered that the collisionless requirement, $\nu_{\mathrm{eff,e}} \ll \omega$, is very difficult to satisfy even in the reactor regime. Hence, the practical relevance of the interchange trapped-particle stability is rather limited.

3.2.4. *Odd modes*

The class of trapped-particle instabilities with odd symmetry around the magnetic-field minimum has been extensively investigated by Coppi and co-workers [43–47]. In the original derivation of these odd modes, the analysis was carried out in the collisionless limit [43, 44]. It was pointed out that in the presence of positive temperature gradients, inverse Landau damping can give rise to instabilities of this type, provided the criterion, $2/3 < \eta_j < 1$, is satisfied. Coppi [43] noted that in the trapped-electron regime the odd modes have characteristic frequencies close to the average electron bounce frequency ($\omega \lesssim \omega_{be}$) and typically short wavelengths, $k_\perp \rho_i > 1$. In the trapped-ion regime, Coppi and Minardi [44] found that such modes can occur at longer wavelengths, $k_\perp \rho_i < 1$, with characteristic frequencies close to the average ion bounce frequency, $\omega \lesssim \overline{\omega_{bi}}$.

To derive these instabilities, it is convenient to work with the form of the perturbed distribution function given in Eq. (50). The basic approach involves substituting this expression into the quasi-neutrality condition and then operating with $\oint Rq\, d\theta\, \phi^*/B$ to generate a quadratic form. For the trapped-ion odd modes, the electron response is taken to be adiabatic, and the ion response is expanded in harmonics of the bounce and transit frequencies to third order in $(\omega/\omega_{b,t})_i$. The resulting expression is then solved by standard variational methods [46]. A similar procedure is used in the trapped-electron regime except that the ion response is now taken to be fluid-like and the electron response is expanded to third order in $(\omega/\omega_{b,t})_e$. Details of these calculations have been summarized in Ref. [46].

In general, the growth rates for the odd modes are smaller than those for even modes. However, as emphasized by Coppi and Taroni [45], these instabilities can be far more effective in scattering the deeply trapped particles. This is due to the fact that the electric field generated by an odd mode has its maximum at B_{min}, the position where the trapped particles are most heavily concentrated. It is for this reason that these instabilities are also called "trapped-particle scattering modes." Coppi and Taroni have carried out numerical calculations of single-particle orbits in the presence of odd modes and have found that the radial excursions of the trapped particles can be considerably

larger than the usual banana excursion. Here, they have noted that the average ∇B-drifts associated with these so-called "quasi-banana" orbits appear to be more favourable. In addition, they have pointed out that the enhanced scattering could also favourably influence the usual dissipative trapped-particle instabilities

Subsequent work on odd modes has dealt with the effect of impurities, collisions, radially non-local effects, and current-driven effects. Impurity-driven odd modes have been studied by Coppi [47], who pointed out that both resonant and non-resonant instabilities of this type can occur. The specific conditions for their appearance in various frequency ranges have recently been summarized in Ref. [113]. With regard to collisions and radially non-local effects, Coppi and Rewoldt [46] have concluded that the odd modes are not strongly influenced by these mechanisms. Current-driven effects on both odd and even modes [including those falling in the higher frequency range, $\omega > (\omega_{b,t})_e$] have also been investigated [139, 127, 46]. Coppi and Pozzoli [139] have emphasized that in the usual range, $\omega/k_\parallel < v_e$, current-driven instabilities can be very effectively suppressed in the banana regime. This is due to the fact that the current-carrying (untrapped) electron population tends to be greatly reduced, with the result that $\partial F_e/\partial v_\parallel$ remains negative for $v_\parallel \lesssim v_e$. As noted, e.g. by Coppi and Rem [127], current-driven effects in general become significant only if the usual requirement that u_0/v_e be appreciable is satisfied (with u_0 being the current drift velocity). In other papers dealing with odd modes, Callen, et al. [12] found that a non-circular distortion of the magnetic surface leads to no significant modifications of these instabilities, and Coppi and Bhadra [58] have noted that the presence of odd modes could hinder the efficiency of the TCT systems discussed in Section 1.3. More recently, Coppi and Pegoraro [140] have reported that ion diamagnetic drift modes with odd symmetry can also appear in the trapped-electron regime. Finally, it should be mentioned that, in another recent calculation, Rewoldt, et al. [141] have found that odd modes with relatively small growth rates can appear for certain cases in their 2D studies of trapped-electron instabilities.

4. CONSEQUENCES OF LOW-FREQUENCY MODES ON CONFINEMENT

4.1. Non-linear analysis

In general, it can be concluded from the linear theory discussed in the preceding sections that various forms of low-frequency microinstabilities are likely to be present in tokamak systems. Hence, the determination of the rate of particle and energy transport generated by their presence is a crucially important problem. Unfortunately, the non-linear theory required to study these transport processes is far less developed than the corresponding linear theory. This is due primarily to the fact that a general self-consistent calculation of the saturation amplitudes is very difficult. Rough approximations for these amplitudes lead, of course, to correspondingly imprecise estimates of transport rates. In this section, various approaches to the non-linear analysis of low-frequency electrostatic instabilities will be discussed, and relevant papers will be surveyed. Most of the calculations have been based on simple geometric models which do not include recent refinements of the linear theory. For example, possible non-linear effects associated with finite-β corrections and with 2D modifications, such as toroidal coupling, have generally not been considered.

4.1.1. Basic approaches

A common approach to obtaining rough estimates of diffusion rates involves the use of phenomenological models based on qualitative arguments. For example, the diffusion coefficient, D, corresponding to a simple random-walk stochastic model is just $D \cong (\Delta x)^2/(\Delta t)$ with Δx being the effective step size and Δt being the associated time interval. Approximating this correlation time with the linear growth period, $1/\gamma$, and the step size with a typical perpendicular wavelength of the unstable spectrum, $1/k_\perp$, then yields the familiar result

$$D \simeq \gamma/k_\perp^2 \tag{100}$$

Another phenomenological argument leading to the same result involves the notion from strong turbulence theory that at sufficiently large amplitudes, the unstable waves can cause the usual straight-line equilibrium orbits to be strongly perturbed. This in turn gives rise to an effective cross-field diffusion of the orbits which is related to the non-linear $\vec{E} \times \vec{B}$ drifts in the familiar continuity equation. In a heuristic sense, a diffusion coefficient can be introduced here and the resultant equation can be expressed as

$$\frac{\partial}{\partial t} n_j = - \frac{\partial}{\partial \vec{x}} \cdot \vec{D} \cdot \frac{\partial}{\partial \vec{x}} n_j \sim k_\perp^2 D n_j \tag{101}$$

At saturation, the viscous damping term, $k_\perp^2 D$, can be equated to the linear growth rate to recover Eq. (100).

Qualitative concepts from weak-turbulence theory have also been invoked to arrive at the estimate in Eq. (100). Following the usual quasi-linear procedure [142], an expression for the radial particle flux, Γ_p, can be readily obtained by integrating the drift-kinetic equation over the velocity space and averaging over the fast time scale of the fluctuations. For a simple slab model, this gives

$$\Gamma_{pj} = \int d^3v \overline{\left(i \frac{c}{B} k_y \phi^* f_j^{(0)} \right)} \equiv -D \frac{\partial}{\partial x} n_o \tag{102}$$

with the phase difference between Φ and $f_j^{(0)}$ providing the real contribution to Γ_{pj}. The anomalous flux here is ambipolar (i.e. $\Gamma_{pi} = \Gamma_{pe}$) as a consequence of quasi-neutrality. Recalling that for drift modes, $f_i^{(0)} \simeq |e| (\Phi/T_e)(\omega_*/\omega) F_{Mi}$ with $\omega \simeq \omega_* + i\gamma$, and noting that the required phase difference comes from γ, Eq. (102) reduces to

$$D \simeq |e\Phi/T_e|^2 r_n^2 \gamma \tag{103}$$

In estimating $|e\Phi/T_e|$, the most commonly invoked heuristic argument is that the mode saturates when the gradient of the perturbations reaches the level of the equilibrium (ambient) gradients, i.e. when $|e\Phi/T_e| \simeq 1/k_\perp r_n$ [8, 82]. Substituting this back into Eq. (103) then gives the result of Eq. (100). Another approach leading to the same rough estimate for the saturation amplitude involves the familiar concept of free energy. Liu, et al. [17] have calculated the free energy that would be released by the plasma if it could adiabatically expand to uniform density over a radial distance determined by the usual shear-dependent turning point. Equating this to the drift wave energy density gives approximately

$$|e\Phi/T_e| \sim \sum_k |e\Phi_k/T_e| \sim 1/k_x r_n$$

For $k_x \cong k_y \cong k_\perp$, this "upper-bound" estimate of the saturation amplitude is consistent with the result from the ambient gradient argument.

The phenomenological models described in the preceding discussion obviously lack rigor and could be questioned even on heuristic points. At best they are useful in providing rough order-of-magnitude or possible upper-bound-type estimates of anomalous transport. For a more quantitative analysis, it is necessary to turn to a more systematic application of weak- and strong-turbulence theories. A detailed presentation of the formalism associated with such theories is outside of the scope of the present review. In what follows, the general features of these approaches (as applied to low-frequency instabilities) will be discussed.

As noted, e.g. by Sagdeev and Galeev [142], it is appropriate to apply the theory of weak turbulence to calculate the non-linear evolution of an unstable plasma provided the energy in the excited spectrum of modes is small compared with the total plasma energy. The basic approach involves Fourier decomposing the potential, $\Phi(\vec{x}, t)$, in the Boltzmann equation and then expanding the perturbed distribution function in powers of the wave amplitude, $\Phi_{\vec{k}}$. Here the non-linearity corresponding to the $(\vec{\epsilon} \times \vec{B}) \cdot \partial f/\partial \vec{v}$-term in the drift-kinetic equation provides the coupling mechanism which permits the interaction between the linear eigenmodes of the system. The resulting expression for the perturbed distribution together with either Poisson's equation or the quasi-neutrality condition then give the basic non-linear wave equation. Physical processes, which can be considered within this framework, are quasi-linear wave-particle interactions and mode coupling. In the first case, Landau resonances ($\omega = \vec{k} \cdot \vec{v}$) can introduce simultaneous changes in the amplitude of the waves and in the initial particle distribution which generated the instabilities. Retaining only amplitude-squared terms, $|\Phi_{\vec{k}}|^2$, in the non-linear wave equation, it is found that these "self-coupling" ($\vec{k}$ to $-\vec{k}$) interactions lead to so-called "quasi-linear profile modifications". This type of calculation does not allow for energy transfer over the spectrum. To include such effects, it is necessary to retain terms of order $|\Phi_{\vec{k}}|^4$ in the perturbation theory. At this level, one can consider non-linear wave-wave interactions (three-wave coupling) and non-linear wave-particle interactions (non-linear Landau damping). The resonant three-wave coupling process requires that $\omega_3 = \omega_1 \pm \omega_2$ with $\vec{k}_3 = \vec{k}_1 \pm \vec{k}_2$, while non-linear Landau damping requires that the particle retain a constant phase with respect to the beats of two waves, i.e. $(\omega_2 \pm \omega_1) = (\vec{k}_2 \pm \vec{k}_1) \cdot \vec{v}$. The former condition is difficult to satisfy in the presence of strong wave dispersion, which is usually the situation for the shorter-wavelength drift modes. In the latter case, the induced scattering of the waves by the particles can cause both a transfer of energy over the spectrum as well as a dissipation of the energy.

To carry out the weak-turbulence calculations described, the standard procedure [142] involves the

assumptions (i) that the growth rate relative to the mode frequency is small, i.e. $|\gamma_{\vec{k}}/\omega| \ll 1$ with $\gamma_{\vec{k}} \equiv \mathrm{Im}(\omega_{\vec{k}})$; and (ii) that the frequency spectrum is peaked around $\omega = \omega_{\vec{k}}$ with width of order $\gamma_{\vec{k}}$, i.e. $\Phi(\vec{k}, \omega) \cong \Phi_{\vec{k}}\delta(\omega - \omega_{\vec{k}})$ with $\omega_{\vec{k}}$ being the solution to the linear dispersion relation. If these requirements are satisfied, then one can estimate the saturation amplitude by balancing the linear growth rate against the rate of energy output from the mode due either to three-wave resonant mode coupling ("decay interaction") or to non-linear Landau damping (wave scattering by ions). As pointed out, e.g. by Tsytovich [143], scattering here involves not only the usual Compton scattering ("bare" particle scattering) but also the non-linear scattering associated with the polarization cloud generated by a moving charged particle. This shielding cloud can then interact with electromagnetic waves in the plasma and serve as an additional source of radiation. Tsytovich has emphasized that the scattering by the charge of the screening polarization cloud can be of the same order as scattering by the main charge. Application to the drift wave problem leads roughly to the result, $D \cong (\gamma/k_\perp^2)(\gamma/\omega_*)$, with the non-linear dissipation coming from the wave scattering process. Details of the weak-turbulence formalism can be found, e.g. in standard text-book treatments by Sagdeev and Galeev [142], Tsytovich [143], and Davidson [144].

In practical situations, it is often the case that the weak-turbulence assumptions cannot be satisfied. As emphasized, e.g. in numerous papers by Dupree [145], Galeev [146], and Weinstock [147], the usual linear particle orbits must be modified in a non-perturbative fashion when unstable waves grow to sufficiently large amplitudes. The starting point here is to again Fourier-decompose the potential in the Boltzmann equation. However, unlike the weak-turbulence approach, the effect of the background waves on the orbits is non-perturbatively retained by formally introducing an orbit propagator. To render the calculation tractable, it is necessary to average this orbit-Green's function operator, over the phases of the background waves [145]. Since phase information is eliminated, the orbit modifications here depend only on the amplitude of the unstable waves. As demonstrated by Dupree [145], this procedure leads to the conclusion that the unperturbed orbits are effectively modified by a factor, $\exp[-d(t - t')]$, with d being the frequency randomization generated by the background wave turbulence. Physically, the exponential damping here can be interpreted as a collisional damping resulting from the wave-induced turbulent viscosity. This effect can be introduced into the usual local dispersion relation for drift instabilities by simply replacing ω with $\omega + id$ in the denominator of the perturbed density responses. Saturation results when the linear growth rate of the fastest-growing mode is balanced by viscous damping. For an isotropic turbulent spectrum, where $k_x \cong k_y$, this again leads to the approximate form given in Eq. (100). It should be noted, however, that the initial assumption of a turbulent spectrum (i.e. a large number of unstable background waves) breaks down close to marginal stability. Conceptual arguments for the resolution of this difficulty have been given in Ref. [143], but a formally rigorous justification has not been presented to date. A more practical difficulty in the application of strong-turbulence theory involves the fact that the choice of the growth rate and wave number in the diffusion coefficient is somewhat arbitrary since the non-linear spectrum is unknown. Obtaining such information would require a much better understanding of mode coupling in the presence of strong turbulence. Phenomena such as the possible formation of convective cells [148] and clumps [149] could also play an important role here.

4.1.2. Strong turbulence and de-trapping effects

The strong-turbulence formalism developed by Dupree [145] for analysing low-frequency drift instabilities in a slab geometry has recently been extended by Waddell [150] and Ehst [151] to include trapped-particle effects. These authors have obtained solutions to the drift-kinetic equation [98] for a toroidal geometry and used the results to analyse the dissipative trapped-ion mode [151] and the collisionless or interchange trapped-particle mode [150]. Since $\omega < \omega_{bj}$ for these instabilities, Waddell has pointed out that it is convenient to work with a bounce-averaged form of the drift-kinetic equation to determine the trapped-particle responses. The main conclusions of both authors are that (i) the dominant saturation mechanism is again the wave-induced viscous damping, and (ii) the radial diffusion coefficient is approximately given by

$$D \simeq \gamma/2k_r^2 \tag{104}$$

where k_r is the radial wave number. In addition, Ehst has found that, at saturation, $|e\Phi/T| \lesssim \epsilon^{1/2}/|k_r r_n|$. Using a similar strong-turbulence formalism, Sugihara and Ogasawara [152] have also obtained the result of

Eq. (104) in a recent paper. However, it should be noted that the expression for the non-linear dispersion relation given in their work is in error since neither the usual collision terms, $\nu_{eff,j}$, nor the turbulent-damping factor, d, should appear in the numerator of the density response.

In addition to cross-field turbulent diffusion, "de-trapping" effects involving motion along the magnetic field line have also been considered as viable saturation mechanisms for trapped-ion modes. Electrostatic de-trapping has been investigated by Jablon [153], who concluded that the electric field generated by the instabilities can greatly enhance the de-trapping rate of the particles and can lead to lower saturation levels than turbulent radial diffusion. However, in recent work, Ehst [151] has reported that, owing, in large part, to the use of an incorrect perturbed orbit in his time integral, Jablon greatly overestimated the damping effect of this collisionless de-trapping process. Using a corrected form for the decorrelation frequency, he found that the effect is much weaker than the collisional de-trapping associated with the turbulent diffusion of particles along the magnetic field line in the presence of an electric field. This collisional de-trapping was in turn found to be considerably weaker than the viscous damping from perpendicular diffusion. The influence of electrostatic de-trapping (and trapping) on collisionless drift and trapped-electron instabilities has also been studied. Kadomtsev and Pogutse [154] noted that, at sufficiently large wave amplitudes, the collisional scattering of the electrostatically trapped electrons can produce a non-linear drift instability for $\eta_e = d\ln T_e/d\ln n_e < 0$. They also proposed that for $\eta_e > 0$ this same process could be an effective saturation mechanism for the dissipative trapped-electron modes. However, in subsequent studies, Ott and Manheimer [155] performed more detailed calculations with an improved model for collisions and found that this electrostatic de-trapping effect is very weak and is not likely to be competitive with other saturation mechanisms.

As noted earlier, Coppi, et al. [43–47] have pointed out that if odd modes can be excited, the de-trapping (scattering) of deeply trapped particles could be significantly enhanced. They also considered the influence of electric fields on the barely trapped and barely circulating particles in the collisionless limit by adopting a simplified single-mode picture [45]. Since the linear orbit approximation breaks down in the boundary layer (i.e. where $\omega \cong \omega_{bj}$), they numerically integrated the exact orbit equation and found that for a sufficiently large wave amplitude, a large orbit amplification can result. In a recent paper, Smith [156] has also considered this single-mode problem for the trapped-ion instability. Using a Hamiltonian formulation for the equations of motion, it was demonstrated both analytically and numerically that the non-linear stochastic effects in the boundary layer can be strong even for a relatively weak wave amplitude. These strong perturbations of the ion trajectories are attributed to the overlap of the bounce resonances ($\omega_b = \omega/n$). As noted by Dobrowolny and Negrini [157], enhanced de-trapping at multiples of the bounce frequency could also occur in the presence of ion-acoustic turbulence (i.e. for a many-wave picture). In addition, it has been suggested that enhanced de-trapping can be dynamically generated by externally imposing oscillations in the magnetic field configuration [158]. Finally, it should be mentioned that turbulent velocity-space scattering has been considered as a possible saturation mechanism for trapped-ion modes by Berk and Rosenbluth [159]. The notion here is that the trapped-ion instability can produce a loss-cone-type ion distribution which generates unstable ion-cyclotron modes. The presence of these high-frequency instabilities in turn raises the effective ion collision frequency. Although the stability of the longer azimuthal-wavelength modes is enhanced by this non-linear process, the authors concluded that the overall effect on the rough $D \cong \gamma/k_\perp^2$ diffusion estimate is not appreciable.

4.1.3. Fluid models and mode coupling

As pointed out by Kadomtsev and Pogutse [2, 3] the non-linear analysis of low-frequency drift instabilities can be considerably simplified by using fluid-type equations to approximate the essential kinetic effects. In their application of this approach to the trapped-ion instability, collisions were treated with a Krook-type operator, the untrapped responses were taken to be adiabatic, and, after bounce averaging, a greatly simplified form of the drift-kinetic equation was integrated over velocity-space to generate the following two-dimensional continuity equation for the trapped-particle fluid densities, n_j^T:

$$\frac{\partial}{\partial t} n_j^T + \nabla \cdot \left(n_j^T \vec{v}_j^T \right) = -\frac{1}{\varepsilon} \nu_j \left(n_j^T - \varepsilon^{1/2} n_o \exp(e\Phi/T)_j \right) \tag{105}$$

One should remember here that the gradient operator in the second term does not act on the relative fraction of trapped-particles in n_j^T because this factor arises from the velocity-space integration, i.e. the gradient operator formally appears inside the velocity-space integral [160, 161]. Note that the right-hand side of Eq. (105) models the collisional relaxation of n_j^T toward a Boltzmann equilibrium, the fluid velocities, $\vec{v}_j$, are determined by the usual momentum balance equation, and the potential, Φ, is related to n_j^T by the quasi-neutrality condition:

$$n_e^T + (1 - \varepsilon^{1/2}) n_o \exp(e\Phi/T)$$

$$= n_i^T + (1 - \varepsilon^{1/2}) n_o \exp(-e\Phi/T) \quad (106)$$

with $T_e = T_i \equiv T$. By taking $|e\Phi/T| \equiv \tilde{\Phi} << 1$, ignoring ∇B-drift effects, considering the slab limit [$r \to x$ and $r(\theta - \zeta/q) \to y$], and invoking the usual approximations appropriate to the dissipative trapped-ion modes, Eqs (105) and (106) can be readily combined to give

$$\left(\frac{\partial}{\partial t} + v_* \frac{\partial}{\partial y} + \frac{v_*^2}{\nu_-} \frac{\partial^2}{\partial y^2} + \nu_+\right)\tilde{\Phi}$$

$$= - \frac{v_*}{\varepsilon^{1/2}} (1 - \eta_i) \frac{\partial}{\partial y} (\tilde{\Phi})^2$$

$$- \frac{2v_*^2 r_n}{\varepsilon^{1/2} \nu_-} \left(\frac{\partial \tilde{\Phi}}{\partial x} \frac{\partial^2 \tilde{\Phi}}{\partial y^2} - \frac{\partial \tilde{\Phi}}{\partial y} \frac{\partial^2 \tilde{\Phi}}{\partial x \partial y} \right) \quad (107)$$

with $\nu_{+,-} \equiv \nu_{i,e}/\varepsilon$ and $v_* \equiv (\varepsilon^{1/2}/2)(cT/eBr_n)$. The non-linear terms on the right-hand side of this equation come from the convective steepening terms $\{\propto \nabla \cdot [n_j^T (c\vec{\varepsilon} \times \vec{B}/B^2)]\}$ in the continuity equation. When set to zero, the left side just gives the usual linear result, $\omega_0 \simeq k_y v_* + i(k_y^2 v_*^2/\nu_-) - i\nu_+$, for $\tilde{\Phi} \propto \exp[i(k_y y - \omega t)]$. Wimmel [161] has noted that a parallel electric field can be readily incorporated in this fluid model.

In analysing Eq. (107), Kadomtsev and Pogutse pointed out that the two-dimensional non-linear term acts to convect energy from the longer wavelength modes to the shorter wavelength modes. As the energy is transferred to the larger wavenumbers, a broad turbulent spectrum could rapidly develop. The authors then argued that this justifies replacing the non-linear mode coupling term with an effective turbulent diffusion term, $D[(\partial^2/\partial x^2) + (\partial^2/\partial y^2)]\tilde{\Phi}$. Balanced against the linear growth term, this leads again to the familiar result, $D \simeq \gamma/k_\perp^2$, for $k_\perp \simeq k_x \simeq k_y$. However, Saison and Wimmel [162] have recently reported that numerical solutions to the same non-linear equation [i.e. Eq. (107)] show no evidence of such turbulent processes. Considering the limit, $\eta_i \cong 1$, which effectively eliminates the radially local wave-steepening term [$\propto (\partial/\partial y)(\tilde{\Phi})^2$], the authors treated this problem as a time-dependent initial-value calculation. Their numerical results indicated that the saturation mechanism appears to be a coherent process which generates modifications in the equilibrium density profiles. Such an effect could result, e.g. from the effect of the zero-frequency harmonic generated by the non-linear beating of an unstable mode with itself [142]. The associated transport coefficient was found to exhibit a Bohm-like scaling which could exceed the familiar Kadomtsev and Pogutse estimates, $D_{K\text{-}P}$, by an order of magnitude, or more, for relevant parameters.

LaQuey, et al. [163] and Cohen, et al. [160, 89, 164] have also analysed the dissipative trapped-ion instability by using the basic Kadomtsev-Pogutse fluid model but have additionally incorporated kinetic effects which act as energy sinks at short wavelengths. It is well known from the linear analysis described earlier that Landau damping by circulating [29, 30] and trapped [31] ions exerts a strong stabilizing influence at short wavelengths provided $\eta_i < 2/3$. LaQuey, et al. [163] introduced this kinetic effect into the fluid model by perturbatively adding to Eq. (107) the term,

$$\gamma_{LD} = A' (1 - 3\eta_i/2) k_y^4 v_*^4 / \bar{\omega}_{bi}^3$$

with A' being a numerical factor (typically ~ 40). Recalling the fact that $|\omega_0/\nu_-| \ll 1$ for the dissipative trapped-ion modes, these authors noted that it is relevant to analyse the radially-local, one-dimensional problem which results when the two-dimensional non-linear term in Eq. (107) is negligibly small, i.e. when $|k_x r_n \omega_0/\nu_-| << 1$. After a transformation to the drift frame moving with speed v_*, the equation can be cast in the dimensionless form

$$\left(\frac{\partial}{\partial\tau} + \frac{\partial}{\partial\xi^2} + \nu + \alpha\frac{\partial^4}{\partial\xi^4}\right)\psi + \frac{\partial}{\partial\xi}(\psi)^2 = 0 \qquad (108)$$

with the last term providing the convective non-linear steepening. LaQuey, et al. obtained two types of analytic solutions, i.e. "two-mode" equilibria and "multi-mode" or "solitary-wave" equilibria.

In subsequent investigations, Cohen, et al. [160] demonstrated both analytically and numerically that the multi-mode equilibria are irrelevant since they are neither stable nor accessible. On the other hand, it was found that the two-mode equilibria could satisfy these requirements even in the presence of wave dispersion which inhibits the mode coupling process. It was noted that the corresponding transport coefficient could be considerably smaller than $D_{K\text{-}P}$. However, the authors have also emphasized that their analysis is valid only if the width of the unstable spectrum is sufficiently narrow. In more recent work, Cohen and Tang [164, 89] have pointed out that the local equilibria could be unstable to radial perturbations associated with the 2D non-linear term in Eq. (107). From linear kinetic theory it is known that the presence of magnetic shear can enhance the circulating ion-Landau damping effects and that finite-ion-banana-width corrections to ω_0 tend to decrease the growth rates [34]. These perturbative effects were accordingly added to the 2D fluid model to provide an energy sink at short radial wavelengths. The authors have found that the additional coupling to stable modes provided by the 2D non-linear term apparently leads to smaller saturation amplitudes than the 1D situation. This calculation again can only be applied when the spectrum of unstable modes is sufficiently narrow.

Fluid-type 2D slab models have also been employed in the non-linear analysis of drift and trapped-electron instabilities. Here the basic approach [165–169] has been to consider only the linear response for the electrons and to obtain the non-linear ion response from the familiar fluid equations, i.e. the continuity equation and the momentum balance equation. Taking the electron response to be adiabatic to lowest order and using the quasi-neutrality condition, Tasso and others [165–167] have shown that in the radially local limit the non-linear drift wave equation reduces approximately to

$$\left(\frac{\partial}{\partial t} + v_d\frac{\partial}{\partial y}\right)\tilde{\Phi} - \frac{1}{2}\eta_e v_d\frac{\partial}{\partial y}(\tilde{\Phi})^2 = 0 \qquad (109)$$

where $\tilde{\Phi} \equiv e\Phi/T_e$, $v_d \equiv cT_e/eBr_n$ is just the diamagnetic drift velocity, and the non-linearity arises again from the non-linear $\vec{E} \times \vec{B}$ convective flow. In the absence of wave dispersion and energy sinks, this non-linearity produces a steepening of the wave form which leads to solitary-wave solutions [165–166]. Manheimer, et al. [167] subsequently applied this type of analysis to the simplest form of the dissipative trapped-electron instability. If ∇B-drift effects are ignored, the dominant portion of the unstable spectrum falls in the non-dispersive long-wavelength region. Moreover, at shorter wavelengths, the dissipative stabilization for $\eta_e > 0$ provides an effective energy sink. Numerical calculations of saturation amplitudes from this mode coupling process indicated considerably smaller transport levels than the usual $\gamma/k_\perp^2$ estimate. However, as acknowledged by the authors, this picture is irrelevant in practice since the ∇B-drift de-stabilization of the shorter-wavelength modes eliminates their energy sink and extends the unstable spectrum into the highly dispersive region.

In more recent work, Horton [168, 169] focused attention on the two-dimensional non-linearity in the ion fluid response and cast the non-linear drift wave equation in the form

$$i\frac{\partial}{\partial t}\tilde{n} = L\tilde{\Phi} + D_B\left(\frac{\partial\tilde{n}}{\partial x}\frac{\partial\tilde{\Phi}}{\partial y} - \frac{\partial\tilde{n}}{\partial y}\frac{\partial\tilde{\Phi}}{\partial x}\right) \qquad (110)$$

Here $\tilde{n} \equiv n_i/n_0$, $D_B \equiv cT_e/eB$, and L is the usual linear operator, i.e. in the absence of the non-linear term Eq. (110) reduces to the usual linear eigenmode equation for drift and trapped-electron modes in a 2D slab. The analysis was carried out in the spirit of the weak-turbulence approach [142] described earlier, and the derivation of the final form of the non-linear wave equation studied is characterized by the following features: (i) the potential, $\tilde{\Phi}$, and density fluctuations, $\tilde{n}$, are expressed in terms of a time-dependent superposition of linear eigenmodes; (ii) the radial dependence of these eigenmodes is taken to have the localized, single-rational-surface structure of the Pearlstein-Berk solutions; (iii) harmonic components generated by self-interaction in normal modes are neglected; (iv) the usual weak-turbulence assumptions of random phase, peaking of frequency spectrum about $\omega \cong \omega_k$, small growth rate relative to the mode frequency ($|\gamma_k/\omega| \ll 1$), and small amplitude ($|\tilde{\Phi}| \ll 1$) are invoked; and (v) the perturbation expansion is carried out to third order in the wave amplitude.

An equation for the saturation amplitude was obtained by balancing the linear growth rate against

the rate of energy output from the non-linear dissipation. Here it was concluded that the dominant saturation mechanism is provided by a wave scattering term which appears to be analogous to the Compton ("bare" particle) scattering contribution to the non-linear Landau damping term from standard weak-turbulence kinetic theory [142, 143]. As in the kinetic calculation, the mode coupling term transfers energy from the short to the long-wavelength regime, where ion-Landau damping is invoked as the energy sink. However, in this fluid calculation there is no term analogous to the part of the kinetic non-linear Landau damping term associated with the scattering by the charge of the shielding cloud [143]. Using only the non-linear scattering factor (obtained from the fluid analysis) along with the growth term, Horton found that the spectral density, $I(k_y \rho_s)$, could be approximated by

$$I(k_y\rho_s) \simeq \frac{1}{\pi k_y \rho_s} \left(\frac{\rho_s}{r_n}\right)^2 \frac{L_s}{r_n} \left| \mathrm{Im}\, D_k(\omega_k) \right| \tag{111}$$

where $D_k(\omega_k)$ is the imaginary part of the usual linear dispersion relation. The corresponding spectral density of the potential fluctuations is given by

$$\left\langle \tilde{n}^2 \right\rangle \simeq \left\langle \tilde{\Phi} \right\rangle^2 \simeq \int d\, k_y \rho_s\, I(k_y \rho_s) \tag{112}$$

and the turbulent energy density by

$$W \simeq n_e T_e \left\langle \tilde{n}^2 \right\rangle \tag{113}$$

Comparison with strong turbulence and free energy [17] upper-bound estimates of W_{max} showed that the ratio, $\alpha \equiv W/W_{max}$, falls roughly in the range $0.1 < \alpha < 0.7$ for typical parameters [169]. With the amplitudes determined, the anomalous particle and thermal fluxes can be readily estimated from standard quasi-linear expressions [170]. In applying the preceding analysis to recent experimental data, Horton calculated the magnitude and shape of density fluctuation spectra for measured parameters. Despite the fact that a number of the approximations made in the theory are not satisfied in the actual experiments, comparisons indicated good qualitative agreement with the measured fluctuation spectra [169]. This is illustrated in Fig. 8.

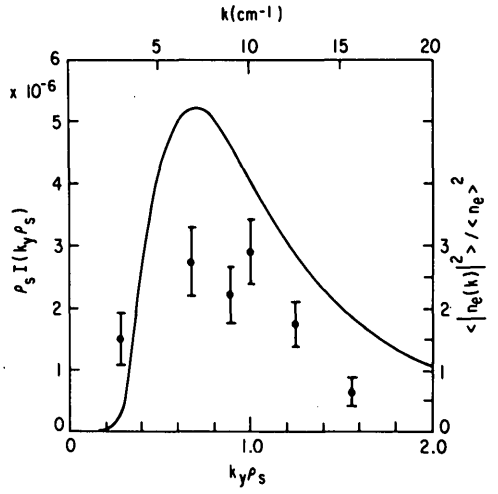

FIG. 8. Comparison of the theoretically calculated spectral distribution, $I(k_y\rho_s)$, given in Eq.(111) and Refs [168, 169], with the electron density fluctuation spectrum obtained from microwave scattering in the ATC experiment given in Ref.[208].

As noted earlier, Tsytovich [143] has emphasized in the past that the shielding-cloud effect can be an important factor in the non-linear ion-Landau damping term. In particular, at long wavelengths, the kinetic theory indicates that the non-linear scattering term is down in magnitude by roughly $k_\perp^2 \rho_i^2$ from the result using only the Compton (unshielded) scattering contribution. A kinetic analysis including the shielding effect leads to a drift wave equation similar to Eq.(110) except that the non-linear factor (for $k_\perp \rho_i < 1$) is now approximately given by

$$D_B a_i^2 \frac{\partial}{\partial y} \left(\frac{\partial \tilde{\Phi}}{\partial x} \frac{\partial^2 \tilde{\Phi}}{\partial y^2} - \frac{\partial \tilde{\Phi}}{\partial y} \frac{\partial^2 \tilde{\Phi}}{\partial x \partial y} \right)$$

Hasselberg, et al. [171] have recently studied this mode coupling term within the framework of standard weak turbulence theory as applied to the collisionless drift and trapped-electron modes. Using a 2D slab model, they expanded to third order in the wave amplitude and found that the primary contribution of this non-linearity is to introduce an additional amplitude-dependent factor into the coefficient of the usual radial derivative, $\rho_i^2 (\partial^2 \tilde{\Phi}_k / \partial x^2)$, in the drift-wave equation. Assuming that all but the lowest (n = 0) radial eigenmodes are shear stabilized, these authors obtained solutions which have the same structure as the usual linear eigenfunctions,

$\tilde{\Phi}_k \propto \exp(-i\sigma_k x^2/2)$. However, the shear length, L_s, in the corresponding eigenvalue conditions, was found to be effectively replaced by an amplitude-dependent shear length,

$$\ell_s^2 = L_s^2[1 - f(\tilde{\Phi})^2] \qquad (114)$$

with $f(\tilde{\Phi})^2 \propto \sum_{k'} |\tilde{\Phi}_{k'}|^2 > 0$. Noting that the modified shear length decreases with increasing turbulence, Hasselberg, et al. have concluded that this non-linear enhancement of shear stabilization can lead to lower saturation amplitudes than commonly predicted. It should be pointed out, however, that such favourable processes could be effectively suppressed by the linear 2D toroidal coupling effects discussed earlier [88–90].

Mode coupling effects associated with the possible interaction of low-frequency drift instabilities with high-frequency modes in the plasma have been investigated by Satya and Kaw [172] and by Chen, et al. [173]. Following standard weak-turbulence formalism [174, 142], Satya and Kaw considered the effect of background electron-plasma-wave turbulence on the dispersion relation for low-frequency drift waves. For such effects to be important, the amplitude of the high-frequency turbulence must be considerably higher than typical levels in tokamak systems. Motivated by the interest in using RF waves near the lower hybrid frequency as a supplementary heating scheme, Chen et al. [173] have recently investigated the influence of a self-consistent lower hybrid pump on trapped-particle instabilities. In their analysis, the pump could either be a single coherent wave or a spectrum of turbulent waves. The familiar three-wave-coupling weak-turbulence formalism [142] was applied, and modifications to the local dispersion relations for the simplest forms of the dissipative trapped-electron and trapped-ion modes were obtained. The parametric coupling to the pump was found to be primarily due to the parallel ponderomotive force acting on the untrapped electrons. Estimates using amplitudes from typical lower hybrid pump fields indicated that these effects can either be significantly stabilizing or de-stabilizing, depending on the orientation of the wave vectors, $\vec{k}$, for the drift waves. The authors noted that, as a rough criterion, the effects are usually de-stabilizing for $k_\parallel/k_\perp < (m_e/M_i)^{1/2}$. It was accordingly concluded that the influence of lower hybrid heating tends to be unfavourable for the trapped-electron modes and favourable for the trapped-ion modes.

4.1.4. Marginal stability considerations

In analysing the transport properties of systems close to marginal stability, an approach, which is generally different from those described in the preceding sections, has also been employed [8, 175]. The basic concepts involved are explained, e.g. in a paper by Simon [175]. He considered a linearly stable, time-dependent equilibrium state which is driven unstable by a slight change (Δ) in the external parameters of the system. It then evolves to a new equilibrium state which can oscillate in time. As demonstrated in Ref. [175], the amplitudes of these final oscillating states along with the associated transport rates and frequency shifts can be calculated as a function of Δ. This approach was applied to the analysis of dissipative drift modes in a straight system with a uniform magnetic field by Hinton and Horton [176] and by Monticello and Simon [177]. In these calculations the external parameter was taken to be the magnetic field, i.e. $\Delta = (B - B_c)/B_c$ with B_c being the critical field for the onset of instability in the linear theory. Working with the Braginskii fluid equations [10], Hinton and Horton considered the mode coupling effects (treated in earlier work by Stix [178]) together with ion viscous effects. The latter were found to provide the dominant saturation mechanism. However, the density profile modifications generated by the non-linear beating of the unstable mode with itself were not included. In subsequent work, Monticello and Simon [177] found that this effect could lead to lower saturation amplitudes. They reported that the comparison of their theoretical results with experimental data from Q-machines indicates good agreement. More recently, Simon and Gross [179] have applied the same marginal stability approach to the Vlasov equation with the purpose of determining the threshold behaviour of collisionless drift modes in straight systems. As before, the non-linear evolution of a single unstable mode in a uniform magnetic field was studied, and the saturated amplitude was found in terms of $\Delta = (B - B_c)/B_c$. The authors have concluded that the saturation mechanism here appears to be an increase in the ion-Landau damping caused by a non-linear decrease in the phase velocity of the wave along the cylindrical axis. It should be noted, however, that such effects have not been observed in particle simulations of collisionless drift waves in similar configurations [108].

Marginal stability concepts have also been applied by Manheimer, et al. [180] to estimate anomalous transport effects associated with the simplest form of

the dissipative trapped-electron instability [20] in a slab geometry. As in the earlier studies [175–179], the starting point involves assuming a steady-state equilibrium configuration at marginal stability. However, in this case, the magnetic fields are non-uniform and the modes of interest are driven by temperature gradients. Attention was accordingly focused on marginally stable temperature profiles and the changes in these profiles generated by external mechanisms. The basic approach here is to first use linear theory to calculate the marginally stable temperature profile. Assuming classical resistivity, this also determines the current profile since $j \propto T^{3/2}$. If the input and outflow of energy together with other relevant fluid properties of the confined plasma are also known, then the temperature and current profiles can be used to calculate the steady-state energy flux in the system. The saturation amplitude of the instability can, in turn, be estimated by using this information with the usual quasi-linear expression for the energy flux [170].

In applying the preceding approach to the dissipative trapped-electron mode, Manheimer, et al. [180] began by recalling that the familiar shear stabilization criterion [82, 83] for the simplest form of this instability can be expressed as

$$[1 + 2(T_i/T_e)](r/R)^{1/2}(1/q^2)(dq/dr) = -0.25(1/T_e)(dT_e/dr) \quad (115)$$

If the resistivity is taken to be classical, then Ampère's law can be used to generate another equation relating q to T_e, i.e.

$$dq/dr = (2q/r) \times \{1 - [T_e/T_e(0)]^{3/2}[q/q(0)]\} \quad (116)$$

Because of the singularity at r = 0, these coupled equations were solved by numerically integrating from r = 0.1 a to r = a with a being the edge of the plasma. The authors found that the results for the relative temperature profiles, $T_e(r)/T_e(0)$, can be expressed in terms of q(a), which in turn is determined by the total plasma current (i.e. by the external circuit). It was reported that, for typical tokamak parameters, this procedure leads to estimates of fluctuation amplitudes in reasonable agreement with measured values. Unfortunately, in an actual toroidal system, the simple shear stabilization criterion given in Eq.(115) is not likely to be applicable. For example, magnetic-drift effects can lead to critical shear requirements which cannot be satisfied [22, 23]. Moreover, recent 2D calculations have indicated that toroidal coupling effects can significantly modify and possibly eliminate the stabilizing influence of magnetic shear [88–90]. Nevertheless, the general marginal stability approach described here provides an interesting alternative to the conventional non-linear appraoches.

4.1.5. Particle simulations

It is well known that particle simulations have provided very useful information in the investigation of transport processes for confined plasmas in thermal equilibrium. Results from these numerical calculations have served as helpful guidelines in the development of analytic non-linear theories in this area. A review of such theories as well as a description of relevant computational techniques can be found in a survey-type article by Dawson, et al. [181]. More recently, particle codes have been developed to study non-linear effects associated with the presence of low-frequency drift instabilities in a cylindrical geometry. As noted earlier, these have involved investigations of collisionless drift and trapped-electron modes [108, 128, 169, 182, 183].

In the "$2\frac{1}{2}$–D" (x, y, v_x, v_y, v_z) models developed by Lee, Okuda, and Matsuda [108, 128], the plasma is taken to be non-uniform and bounded by conducting plates in the x-direction and to be uniform in the y- and z-directions with periodic boundary conditions. As shown in Fig. 9a, the magnetic field lies in the y-z plane and is tilted at a small angle, α, off the z-axis. Since $k_{\|} = \vec{B} \cdot \vec{k}/B = k_y \sin\alpha$, the ratio of $k_{\|}$ to k_y is a constant fixed by the choice of α. In the collisionless-drift-wave simulations [108], temperature gradients are not considered, but allowance is made for the presence of magnetic shear by adding the component, $\vec{B}_s(x) = \hat{y}B_0(x - x_0)/L_s$, with x_0 being a reference

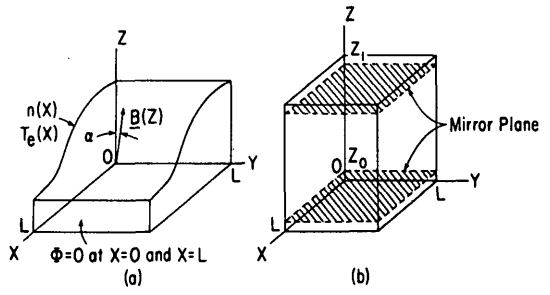

FIG. 9. A sketch of the $2\frac{1}{2}$-D model used in particle code simulation of collisionless drift and dissipative trapped-electron instabilities.

point in x. Now the constant ratio, $k_{\|}/k_y$, is determined primarily by the choice of L_s. It was reported that, for the linear stage of the simulations, growth rates in the shear-free limit were found to be in good agreement with analytic theory, and shear stabilization thresholds apparently exhibit the scaling $|r_n/L_s| \propto (m_e/M_i)^{1/3}$. In addition, the results tended to support the existence of the energy transport mechanism suggested by Coppi [103], i.e. that energy is transferred from the parallel electron temperature to the waves through inverse Landau damping in the unstable regions. The corresponding quasi-linear modifications [142] in the velocity-space distribution of the electrons were also observed. However, no evidence for ion-Landau damping in the form of ion heating was detected. As emphasized by the authors, the dominant saturation process appears to be the quasi-linear modification of the density profile. The associated particle transport for most cases investigated was found to be roughly a factor of four less than the familiar $\gamma/k_\perp^2$-estimate.

Matsuda and Okuda [128] used a shearless version of the $2\frac{1}{2}$-D model to study dissipative trapped-electron modes. As indicated in Fig.9, temperature gradients are included, and the magnetic-trapping effects are artificially introduced by reflecting some particles at the planes $z = z_0$ and $z = z_1$. Specifically, particles, whose ratio, $|v_{\|}/v_\perp|$, falls below a given value at $z = z_0$ and $z = z_1$, are reflected along the field lines. Monte-Carlo collisions are employed here to model the electron-ion pitch-angle scattering. In accordance with conventional theoretical predictions, it was found that, in the presence of magnetic trapping and collisions, drift waves tend to be de-stabilized by positive electron temperature gradients ($\eta_e > 0$) and finite-ion-gyroradius effects. These fluctuations were observed to disappear if either $\eta_e < 0$ or if collisions are suppressed. In the non-linear stage of the simulations, it was found that the saturation of the instabilities is primarily effected by a quasi-linear flattening of the temperature profile. The authors reported that this process tends to occur before the density profile changes significantly, and that the estimated thermal transport is roughly a factor of five less than the $\gamma/k_\perp^2$-estimate. It was also noted that the quasi-linear velocity-space effects seen in the collisionless-drift-wave simulations are effectively suppressed here because the presence of collisions serves to maintain a Maxwellian distribution for the electrons. Typically, in both the collisionless drift and trapped-electron simulations, the saturation amplitude of the instabilities, $|\tilde{\Phi}|$, was of order 10% with $k_y\rho_i \sim 0.5$ for the most unstable modes.

In very recent work, Cheng and Okuda [182] have developed a fully 3D (x, y, z, v_x, v_y, v_z) model to simulate collisionless drift modes in a cylindrical geometry. Here the system is bounded in x and y and periodic in z. There are no initial temperature gradients, and the magnetic field is taken to be uniform and to lie in the z-direction. However, in these 3D simulations there are now distinct Fourier modes in the z-direction,i.e. the ratio of $k_{\|}$ to k_y is no longer constrained to be a fixed quantity as in the $2\frac{1}{2}$-D case. In addition to finding reasonable qualitative agreement with most of the earlier $2\frac{1}{2}$-D results, the authors have reported that convective cells (characterized by $\omega = 0$ and $k_{\|} = 0$) can be non-linearly excited by unstable drift waves. It is proposed here that the observed anomalous particle diffusion is initially caused by the drift modes but that at later stages it is due to non-linearly excited convective cells, which can continue to enhance diffusion even after the drift instability is saturated. The physical picture suggested by the authors is based on the notion that the ions and the electrons respond differently to the electric field, E_θ, generated by the drift instabilities. This difference in the cE_θ/B-drifts causes local charge separation producing an effective E_r-field. The resulting two-dimensional electric fields then give rise to vortex flows [148].

Recalling that the simple linear theory of drift instabilities indicates that $\omega_r \equiv \mathrm{Re}(\omega)$ can have the same value for two different values of $k_y\rho_i$, Okuda and Cheng [183] have reported that a standard application of weak-turbulence mode-coupling theory [142] indicates that these convective cells (with $\omega = 0$ and $k_{\|} = 0$) can be generated non-linearly. With regard to the consequences of such phenomena, it was pointed out [182] that, in the absence of convective cells, non-linear processes, such as quasi-linear profile modification, can saturate drift modes without completely flattening the density gradient. However, in the presence of these vortex flows, anomalous diffusion was found to persist until the gradient is entirely eliminated, thus leading to larger saturation amplitudes. For typical cases, both the simulation results for the overall diffusion coefficient and the estimates of convective-cell diffusion [148] indicated rough agreement with the $\gamma/k_\perp^2$ predictions, i.e. quantitatively, $D_\perp(\mathrm{cm}^2\cdot\mathrm{s}^{-1}) \sim O(10^{-2})$. It was also noted that in the presence of convective cells the power spectrum exhibits peaks at both $\omega \cong 0$ and $\omega \cong \omega_*$. This qualitative behaviour has been experimentally observed, e.g. in the FM-1 spherator [184] for sufficiently weak magnetic shear. Within this context, it should be

emphasized, as a final point, that the presence of shear can severely inhibit the formation of convective cells. Cheng and Okuda [182] have introduced this effect into their 3D simulations and have found that convective-cell phenomena become negligibly small for $L_s/r_n < 25$.

4.2. Confinement estimates and transport modelling

To assess the danger of enhanced anomalous transport in tokamaks, it is necessary to obtain an estimate of the effective confinement time, τ, in the presence of microinstabilities. It is well known that the starting point here involves taking the velocity moments of the Boltzmann equation and working with the resulting conservation equations for each species [10]. The basic equation governing radial transport of particles has the form

$$\frac{\partial}{\partial t} n_j = \frac{1}{r} \frac{\partial}{\partial r} rD \frac{\partial}{\partial r} n_j + S_I \qquad (117)$$

where S_I is a source term accounting for ionization. At the simplest heuristic level, one can assume D to be a slowly varying function of radius, $|r d \ln D/dr| \ll 1$, and to consider a steady-state situation, $\partial n_j/\partial t = 0$. For $n_j = n_0(1 - r^2/a^2)$ and $S_I = -n_0/\tau$, Eq.(117) yields the often-quoted [185] estimate, $\tau = a^2/4D$, where $a \equiv$ plasma (or limiter) radius. Since the equation governing thermal transport has roughly the same structure as Eq.(117), this result is also used to estimate energy confinement, i.e.

$$\tau_E = a^2/4\chi \qquad (118)$$

with χ being the heat transport coefficient. Another rough approximation for τ can be obtained by taking $n_j = \hat{n}_j(r)\exp(-t/\tau) + n_{0j}$ and associating τ with the e-folding density decay time in the absence of a source term ($S_I = 0$). If D is again assumed to vary weakly in r, Eq.(117) reduces to a Bessel equation with solution, $\hat{n}_j(r) = J_0(\alpha r)$ where $\alpha \equiv (\tau D)^{-1/2}$. Recalling that the first zero occurs at $\alpha r = 2.4$ and invoking the boundary condition, $\hat{n}_j(a) = 0$, then leads to the result, $\tau = a^2/(5.76D)$.

Using Eq.(118) along with the familiar $\gamma/k_\perp^2$ approximation for the transport coefficients, Dean, et al.[185] obtained rough estimates for tokamak confinement in the presence of collisional drift modes and dissipative trapped-electron and trapped-ion instabilities in their simplest forms. The results for representative parameters were quoted by Furth [1] in his review article

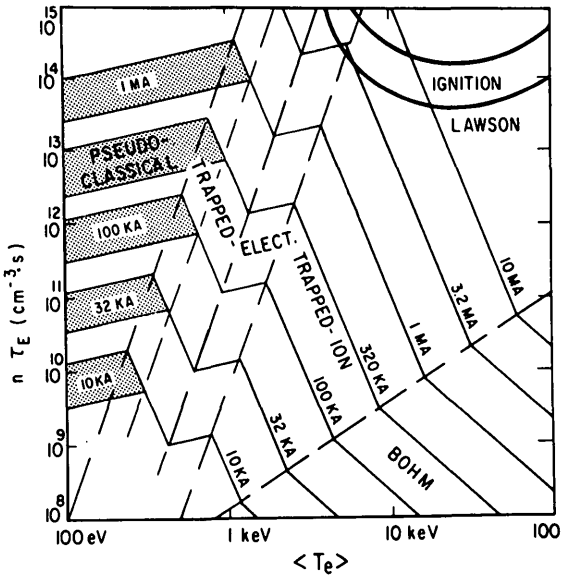

FIG.10. Rough estimates of confinement as a function of plasma current given in Refs [1, 185]. Here, $B_T = 50$ kG, $\beta_{pe} = 1$, $R/a = 3$, $Z_{eff} = 1$, $T_e = T_i$, and $\langle T_e \rangle$ is the average electron temperature.

on general aspects of tokamak research and were displayed there in the form shown on Fig.10. "Pseudo-classical" refers to the use of the transport coefficient introduced by Yoshikawa [11] in the collisional-drift-wave regime, and "Bohm" refers to the diffusion resulting in the irrelevant very-high-temperature regime where the collisionless (interchange) trapped-ion modes could appear. The two labelled curves indicate the criteria for reaching energy "break-even" (Lawson criterion) and for attaining "ignition" conditions in a deuterium-tritium plasma assuming 40% thermal conversion efficiency. For $B_T = 50$ kG, $\beta_{pe} = 1$, $R/a = 3$, $Z_{eff} = 1$, $r_n = a$, $\epsilon = 2/9$, $\eta = 1$, and $T_e = T_i$, the equations used to generate Fig.10 are [185]:

$$(n\tau_E)_{PSEUDO} \simeq 3 \times 10^{14} I^2 \langle T_e \rangle^{1/2} \qquad (119)$$

$$(n\tau_E)_{TE1} \simeq 3 \times 10^{14} I^4 \langle T_e \rangle^{-11/2} \qquad (120)$$

$$(n\tau_E)_{TE2} \simeq 1 \times 10^{13} I^2 \langle T_e \rangle^{1/2} \qquad (121)$$

and

$$(n\tau_E)_{TI} \simeq 3 \times 10^{16} I^4 \langle T_e \rangle^{-11/2} \qquad (122)$$

with $\langle T_e \rangle$ being the average electron temperature in units of keV and the current, I, in MA.

Even at the simple level of the preceding estimates, it is important to realize that the TE2 regime, which scales favourably with $\langle T_e \rangle$ according to Eq.(121), does not exist in practice. As emphasized, e.g. by Adam, et al. [23], ∇B-drift effects can be strongly de-stabilizing in this higher-temperature range of the trapped-electron modes. Following basic quasi-linear procedures [82, 170], the mean energy flux, Q, across a magnetic surface can be estimated from

$$Q \simeq \frac{\rho_i}{r_n}\left(\frac{cT_e^2}{eB}\right)\frac{(2b)^{1/2}}{(k_x^2\rho_i^2 + 2b)}\,\mathrm{Im}\,[I_Q(b)]\,\frac{\partial n}{\partial r} \tag{123}$$

where

$$I_Q(b) = (2\epsilon)^{1/2}\left(\frac{2}{\pi^{1/2}}\right) \times \int_0^\infty d\bar{E}\,\bar{E}^{1/2}\exp(-\bar{E})\frac{(\omega - \omega_{Te}^*)}{(\omega - \overline{\omega_{De}} + i\nu_{f,e})}$$

$b = k_\theta^2\rho_i^2/2$, $\bar{E} = E/T_e$, and $\overline{\omega_{De}} \cong \epsilon_n\omega_*\bar{E}$ for $rq'/q \cong 1$. Use has been made here of the ambient gradient approximation for saturation, $|e\Phi|/T_e \cong 1/k_\perp r_n$, and k_x is determined by the simple slab result for the radial structure [82], i.e. $k_x^2\rho_i^2 \sim (r_n/L_s)(\omega_*/\omega)$. The integral, $I_Q(b)$, can be readily evaluated numerically [23]. Taking $Q \cong \chi_e(\partial T_e/\partial r)$, $\tau_E \sim a^2/4\chi_e$, and $\epsilon = 1/4$ leads to the estimate

$$(n\tau_E)_{TE} \simeq 6 \times 10^{13}\, I^2 \langle T_e \rangle^{-5/2}(\hat{Q})^{-1} \tag{124}$$

with $\hat{Q}$ being a numerical factor falling roughly in the range $0.1 < \hat{Q} < 0.7$. Comparison with the results of Dean, et al. [185] is illustrated in Fig.11. It is seen, e.g. in the 1-MA case, that the $n\tau_E$-estimate at $\langle T_e \rangle \cong 4$ keV is nearly a factor of 5 worse. The results, in general, indicate that anomalous transport due to trapped-electron modes is likely to remain important up to $\langle T_e \rangle \sim 10$ keV. Hence, in the expected operating regimes of the larger tokamaks, such as T-10 and PLT, both the trapped-electron and trapped-ion instabilities could significantly affect confinement.

The crude estimates described in the preceding discussion can be significantly improved by numerically solving the radial transport equations. Beginning around 1969, considerable effort has gone into the development of one-dimensional radial-transport codes. In the early work of Dnestrovskii, et al. [186, 187], Mercier and Soubbaramayer [188], and Düchs, et al. [189], attention was focused on classical and neoclassical transport processes. Subsequent studies have dealt with the effect of impurities, neutral gas, atomic processes, various neutral-beam injection schemes, and microinstabilities. In a recent review article, Hogan [190] has summarized the basic features of 1D tokamak transport codes and has also discussed in some detail the numerical methods used.

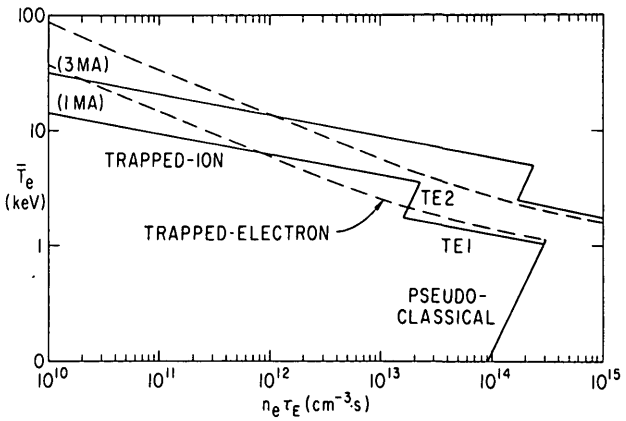

FIG.11. Modifications to Fig.10 introduced by the inclusion of the ∇B-drift destabilization of trapped-electron modes discussed in Ref.[23]. The solid lines represent results calculated as in Fig.10, and the dashed lines represent the ∇B-drift-modified results.

To treat anomalous transport caused by micro-instabilities the most common approach has been to use in the codes transport coefficients (D, χ) obtained from either simple $\gamma/k_\perp^2$-estimates or from quasi-linear estimates of particle and energy fluxes (Γ, Q). As a decreasing function of collisionality, these coefficients are typically taken to pass through a Bohm-diffusion range ($\sim cT/16eB$), a transition zone ($\sim \nu^{1/3}$), and the "pseudoclassical" regime ($\sim \nu$) of dissipative drift waves. In the last case, D and χ can be "empirically" adjusted to fit experimental observations. At still lower collision frequencies, the relevant transport coefficients are taken to reflect the presence of trapped-electron and trapped-ion instabilities. In recent work by Rutherford, et al. [123], the ∇B-drift enhancement of transport due to trapped-electron modes has been taken into account. Their code also allows for the possible presence of collisionless and current-driven drift instabilities as well as enhanced transport caused by MHD effects when q falls below unity near the magnetic axis. The authors have reported that their computed results agree with observed magnitudes of

particle and energy confinement in present-day experiments to within a factor of 3. However, even with the inclusion of a simple form of current-driven drift modes, the scaling of energy confinement time with density (observed, e.g. in the ALCATOR experiment) has not been adequately reproduced with the code.

As a final note, it should be mentioned that Krall and Liewer [191] have recently considered the possibility that additional terms, commonly neglected in the 1D energy transport equation, could be important. In particular, they have proposed that such terms would lead to a substantial reduction in the usual estimates of energy loss caused by the dissipative trapped-electron modes. However, in subsequent work, Manheimer, et al. [192] concluded that these instabilities cannot give rise to such anomalous heating. Using the total energy equation along with the electron momentum equation, these authors found that the only effect here is an anomalous energy exchange between electrons and ions.

4.3. Experimental results

Much of the early experimental evidence for the existence of low-frequency microinstabilities was obtained from linear devices such as Q-machines. For example, conclusive identification of collisional drift instabilities in such systems was established by Hendel, et al. [193]. In subsequent work, Ellis and Motley [194] presented compelling evidence for the presence of the current-driven form of these dissipative modes. At lower collisionality, "universal" or collisionless drift instabilities were found by Politzer and also by Stott, et al. [195]. As noted earlier, Deschamps, et al. [114] and Prager, et al. [130] have concluded that both the temperature-gradient-driven ($\eta_e > 0$) and finite-ion-gyroradius-driven forms of dissipative trapped-electron modes are likely to be present in their linear experiments. Finally, in a straight system in which the ions are unmagnetized, Primmerman, et al. [196] have reported detecting odd modes with characteristic frequencies $\omega \lesssim \omega_{be}$. Especially in the case of the dissipative drift instabilities, the comparison of the experimental results in the references cited with corresponding theoretical estimates generally indicates reasonable agreement.

With regard to toroidal-type systems, most of the experimental investigations of low-frequency microinstabilities have been carried out on internal conductor devices such as the spherator, levitron, and various multipoles. The basic features of these machines as well as a summary of significant results obtained before 1973 can be found in a review paper by Yoshikawa [197]. For example, it was pointed out in this article that data from the spherator experiment, obtained by Pacher, et al. [198], correlate very well with the theoretically predicted effect of shear on collisional drift instabilities.

Subsequent studies in the FM-1 spherator have been focused on the investigation of anomalous effects in the electron banana regime. By using pulsed heating, Ejima and Okabayashi [199] demonstrated that fluctuation levels can be dramatically reduced in the presence of oppositely directed density and temperature gradients ($\eta_e < 0$). This, of course, is indicative of a particular property of the dissipative trapped-electron instability, which distinguishes it from ordinary drift modes. For $\eta_e > 0$, the measured ratio of particle to energy transport was reported to be in reasonable agreement with the usual quasi-linear theoretical estimates, i.e. $(\chi/D) \sim 3$. As discussed in some detail by Sauthoff [200], the mode structure of these instabilities can be investigated with the use of Langmuir probes. The basic approach here involves displacing pairs of these probes in the radial, toroidal, and poloidal directions and then determining the corresponding structures by correlation techniques. The measured phase shifts and amplitude variations were found to be in poor agreement with theoretical results from simple shear-dependent slab models. Better correlation would likely require a complicated 2D calculation taking into account the particular features of the spherator geometry.

Current-driven drift and ion-acoustic modes have also been investigated in the FM-1 device. Analysing the scattering of microwaves by density fluctuations, Arunasalam, et al. [201] found that in the electron banana regime these instabilities are easily suppressed by electron trapping effects. This is in agreement with the earlier theoretical conclusions of Coppi and Pozzoli [139]. More recently, Okabayashi and Arunasalam [184] have applied similar microwave scattering techniques to the measurement of density fluctuations generated by the usual low-frequency drift instabilities. For the experimental conditions considered, the authors have noted that the results correlate reasonably well with simple linear theoretical dispersion relations for collisional, collisionless, and dissipative trapped-electron modes in a strongly sheared magnetic field. By varying the shear strength, they were able to obtain stability criteria in rough qualitative agreement with the Pearlstein-Berk-type scaling, $(r_n/L_s)_{crit} \propto (m_e/M_i)^{1/3}$, discussed earlier. When the shear was decreased, it was found that very-low-

frequency fluctuations ($\omega \ll \omega_*$) could be enhanced considerably. In the moderately-weak-shear range, the frequency power spectrum exhibited peaks near both $\omega \cong \omega_*$ and $\omega \cong 0$. As noted earlier, the qualitative behaviour here resembles the simulation results for convective cells reported by Cheng and Okuda [182, 183]. However, in the limit of very weak shear, a state of isotropic turbulence was observed. Specifically, the density fluctuations in this regime showed a strong dependence on frequency but no discernible dependence on wave number. The strongly turbulent behaviour observed here was also produced for the stronger-shear cases at sufficiently high temperatures. The authors have found no compelling theoretical interpretations for these experimental observations. With regard to the final saturation amplitudes, the measured levels (typically, $|\delta n/n| \sim 3\%$) were not appreciably affected by changes in the shear strength and temperature and tended to be in agreement with the familiar ambient-gradient estimate of $|\delta n/n| \sim |1/k_\perp r_n|$.

In the Culham levitron experiment, attention has been primarily focused on the collisionless current-driven drift modes. Alcock, et al. [202] have recently reported observing enhanced plasma loss rates when current is induced parallel to the main magnetic field with the characteristic drift velocity in the range $5 \times 10^{-3} \lesssim u_0/v_e \lesssim 10^{-2}$. The particle confinement time was found to scale as $(u_0/v_e)^{-1}$ and appeared to be insensitive to magnetic shear. Measurements of the radial-mode structure yielded mode widths, which are also unaffected by shear and are considerably narrower than those predicted by simple-slab-geometry calculations. These results served to motivate calculations by Taylor [88] and Cordey and Hastie [107], who took into account the strong variation of shear and other equilibrium quantities in the poloidal direction and (as discussed in Sections 2.2.3 and 3.1) were able to find unstable modes insensitive to shear. Alcock, et al. [202] have pointed out that further measurements are required before conclusive comparisons with such modes can be made. As a general note, it should be remembered that the characteristic density and temperature of the plasma in both the spherator and levitron experiments are much lower than those in present-generation tokamak experiments. Typical average values are $n \sim 2 \times 10^{11}$ cm^{-3} with $T_e \sim T_i \sim 2$ to 5 eV in FM-1, and $n \sim 6 \times 10^{11}$ cm^{-3} with $T_e \sim T_i \sim 5$ to 10 eV in the Culham levitron.

With regard to recent octupole experiments, Drake, et al. [203] have reported that, for a purely poloidal magnetic field, vortex diffusion has been observed in the Wisconsin levitated octupole. The experimental results here indicated that the radial diffusion coefficient scales as $n^{-1/2}$ and appears to be in qualitative agreement with theoretical estimates for convective-cell diffusion [148]. In the presence of a toroidal field both the Wisconsin and the General Atomic octupoles have shown evidence for the existence of trapped-electron and trapped-ion modes [204]. These experiments were carried out at much lower densities ($n < 10^9$ cm^{-3}) than those in the spherator and levitron and could therefore fall in a more collisionless regime. It was reported that the measured fluctuation levels can be quite large ($|\delta n/n| \sim 40\%$), and that unstable trapped-ion modes propagating in the ion rather than the conventional electron diamagnetic direction have been observed. A compelling correlation between these experimental results and viable theoretical estimates remains to be determined.

Investigations of low-frequency drift waves have also been carried out in stellarator experiments. Kawahata and Fujiwara [205] have reported that data obtained from the JIPP stellarator indicate the presence of collisional drift instabilities. Operating at average densities and temperatures in the range $n \sim 10^9$ to 10^{10} cm^{-3}, $T_e \sim 0.5$ to 3 eV, they found that these modes can be readily suppressed by shear values as weak as $|a/L_s| \sim 0.01$, and that, for most of the cases considered, only a few unstable modes are dominant. In a subsequent paper, Hatori, et al. [206] noted that the experimental data in such cases are consistent with theoretical estimates obtained from non-linear two-fluid equations near marginal stability. Their calculation indicated that the saturation mechanism can be associated with a flattening of the density profile. More recently, Hamberger, et al. [207] have performed microwave scattering measurements of low-frequency density fluctuations on the TORSO stellarator. Here the average operating parameters ($n \sim 10^{13}$ cm^{-3}, $T_e \sim 10^2$ eV, $B \sim 10$ kG) begin to approach conditions in present-generation tokamaks. Fluctuation levels in the drift wave regime were typically found to be of the order of several percent. It was observed that as the current parameter, u_0/v_e, increases, these levels also tend to rise. Noting that the particle confinement time accordingly scales as $(u_0/v_e)^{-1}$, the authors have suggested that collisionless current-driven drift instabilities could be responsible for the fluctuations.

The first detailed measurements of small-scale density fluctuations in a tokamak were carried out by Mazzucato [208] on the ATC device. A spectral analysis of scattered microwaves produced a frequency spectrum which is consistent with the presence of drift

waves, and, as illustrated in Fig.8, exhibits its largest amplitudes for wavelengths in the range 0.5 to 1 cm. This corresponds to values for $k_\perp \rho_i$ of order unity. Subsequent measurements [209] with an improved microwave scattering system indicated that the total density fluctuations, $|\delta n/n|$, are of order 10^{-2}. The typical uncompressed ATC discharge studied had characteristic parameters, $n \sim 10^{13}$ cm^{-3}, $T_e \lesssim 0.8$ keV, $T_i \sim 0.2$ keV, $a \sim 16$ cm, $R \sim 80$ cm, $q(a) \sim 3.5$, and $Z_{eff} \gtrsim 2$. Corresponding values of ν_{*e} and L_s indicated that collisionless drift modes as well as trapped-electron modes could be present. In fact, turbulence levels near the magnetic field minimum (where the trapped particles would be concentrated) were observed to be higher by nearly a factor of 3 than levels near the field maximum. It has also been noted that the turbulent spectrum gives some evidence of being isotropic in $\vec{k}$-space, and that if the heuristic random-walk-type estimate for turbulent diffusion caused by drift waves is employed, a large fraction of the electron energy losses observed in the ATC experiment could be accounted for [208, 209].

Another method for measuring small-scale density fluctuations involves the use of CO_2 laser scattering at small angles. Surko and Slusher [210, 209] have applied such an approach to the ATC tokamak and have corroborated the spectral information and fluctuation amplitudes reported by Mazzucato. The evidence here also favours the picture of a turbulent spectrum which is nearly isotropic in $\vec{k}_\perp$. In particular, it is stressed by the authors that instead of a single frequency, a broad range of frequencies is associated with a particular wave vector, i.e. in contrast to the usual weak turbulence picture, here $|\Delta\omega/\omega|$ is of order unity. Moreover, the k_r-spectra give no evidence of the drift wave mode structure predicted by simple slab model linear theory. The authors have also noted that a non-linear process, recently investigated by Hasegawa [211], could be relevant to the present experiment. The notion here is that the coupling of radial and poloidal modes by the $\vec{\epsilon} \times \vec{B}_T$ drift of ions can produce large frequency shifts comparable to ω when $|\delta n/n|$ is of order 10^{-2}. As a final point regarding these CO_2 laser scattering measurements it should be mentioned that, in sharp contrast to Mazzucato's results, the density fluctuations were found to be nearly 50% greater near the field maximum than levels observed near the field minimum [209]. This result is difficult to reconcile with conventional theoretical predictions.

Other tokamak experiments, which typically operate near the transition between the plateau and electron-banana regimes, include TFR [212] and ORMAK [213]. Both machines give evidence of anomalous energy transport leading to lower confinement times than predicted by "pseudoclassical" estimates. The τ_E-scaling in these experiments suggest some correlation with enhanced transport caused by dissipative trapped-electron modes but could also be related to the presence of MHD activity. In contrast to the ATC, TFR, and ORMAK systems, the ALCATOR device [214] operates at much higher fields ($B_T \sim 80$ kG) and can generate higher-density ($n \gtrsim 10^{14}$ cm^{-3}) plasmas. At these densities the energy confinement time appears to increase linearly with increasing n. Coppi,et al. [215, 216] have recently noted that the presence of current-driven drift modes could account for such scaling. Although trapped-particle instabilities are ruled out in this high-collisionality regime, it is argued that, in the presence of an applied electric field, magnetic-trapping effects can nevertheless produce a positive slope in the electron distribution. This in turn can lead to substantial growth rates even when u_0/v_e is relatively small. These authors have reported that for certain ranges of wave numbers and temperature gradients ($\eta_e > 0$), such an effect can cause the current-driven de-stabilizing term to dominate over the combined influence of finite-ion-gyroradius and temperature-gradient terms [215].

5. NON-ELECTROSTATIC AND HIGH-FREQUENCY MODES

Up until the past few years, relatively little attention has been paid to possible non-electrostatic and high-frequency microinstabilities in tokamaks. However, significant progress toward higher plasma temperatures and densities together with the development of very promising neutral-beam heating schemes have recently served to stimulate considerable interest in these types of instabilities. Mikhailovskii [49], e.g. has emphasized that the de-stabilization of electromagnetic (non-electrostatic) shear-Alfvén modes by toroidal effects can become important as β_p (ratio of plasma pressure to the pressure of the poloidal magnetic field) begins to exceed unity. In addition, since neutral-beam-injected tokamak fusion reactor concepts generally involve the introduction of velocity-space anistropy, the investigation of related electrostatic as well as electromagnetic high-frequency instabilities has also become important [55]. With regard to actual fusion conditions, the production of alpha particles can be still another source of velocity-space anisotropy. The

fast magnetosonic (compressional Alfvén) and shear-Alfvén waves, which can be de-stabilized by such effects, are often called "thermonuclear" micro-instabilities [60–62].

5.1. Shear-Alfvén modes

It is well known that, under normal circumstances, pressure-gradient-driven shear-Alfvén modes in cylindrical systems are relatively unimportant since they have very small growth rates and are easily suppressed by shear [95, 9]. Mikhailovskii, however, has pointed out that in tokamaks toroidal curvature [49] and magnetic trapping [50] effects can lead to significant de-stabilization of these waves when β_p exceeds unity. The basic notion here is that the inclusion of $\vec{v}_D$ (∇B-drift velocity) in either the Vlasov equation or in corresponding fluid equations will lead to an additional de-stabilizing term in the shear-Alfvén branch of the usual dispersion relation for low-frequency, pressure-gradient-driven modes [8, 9]. In carrying out the calculation, an ansatz similar to Eq.(17) was employed for the perturbed quantities. It was then additionally assumed that the slow poloidal variation could be represented by a Fourier series truncated at m = ± 1, i.e.

$$\psi \simeq [\psi_m + \psi_{m+1}\exp(i\theta) + \psi_{m-1}\exp(-i\theta)]\exp[i(m\theta - n\zeta)] \quad (125)$$

with $\psi \equiv \Phi - (A_\parallel \omega/k_\parallel c)$. As discussed in Section 2.2.3, such an approximation cannot be applied if the toroidal coupling is strong, i.e. ballooning of the mode structure along the field line must be sufficiently weak. Using the form in Eq.(125), Mikhailovskii found that the ∇B-term introduces an "effective" parallel wavelength of order $1/qR$. He then reported that for $\beta_p > 1$, low-frequency electromagnetic modes could be de-stabilized by inverse-ion-Landau damping ($\omega \sim v_i/qR$) in the presence of density and temperature gradients.

In a subsequent paper [50], long-wavelength ($k_\perp \rho_i < 1$) shear-Alfvén waves with characteristic frequencies falling in the range $v_i/qR < \omega \sim v_A/qR < \omega_{be}$ were considered. Here it was pointed out that the collisional scattering of magnetically trapped electrons could drive these modes unstable (in analogy with the electrostatic dissipative trapped-electron instability). Working with the drift-kinetic equation and applying the procedures introduced by Rosenbluth, et al. [29] to deal with collisional effects, Mikhailovskii found that the appearance of such modes requires $\beta_p > T_i/T_e$ and $\nu_{eff,e} < \omega \sim \omega_* \sim v_A/qR < \omega_{be}$. This radially local calculation indicated that the corresponding growth rates are roughly given by $\gamma \sim \epsilon^2 \beta_p (\nu_e v_A/qR)^{1/2}$. It has also been noted that short-wavelength ($k_\perp \rho_i \gtrsim 1$) instabilities of this type can appear [217] for $\beta_p > 1$. Mikhailovskii [120], however, has recently reported that such short-wavelength modes should be readily suppressed if β_p exceeds $\epsilon^{-1/2}$.

Since $\omega \cong k_\parallel v_A$ for shear-Alfvén modes, and $k_\parallel$ is in fact a non-local quantity, a realistic assessment of the influence of these instabilities on toroidal confinement requires a proper treatment of the associated radial structure in the presence of magnetic shear. This problem has been investigated within the context of high-energy neutral-beam injection (TCT) studies by Rosenbluth and Rutherford [57]. Their calculation was motivated by earlier radially local work [55] which indicated that shear-Alfvén modes could be strongly de-stabilized by Landau resonances with beam ions that have unfavourable ∇B-drifts. In addition to the radially non-local nature of these instabilities, the authors also took into account the spatial variation ($\propto \cos\theta$) along the field line of the beam drift velocity and the presence of trapped electrons. However, temperature gradients were ignored. The basic approach involved calculating the perturbed distribution functions from the drift-kinetic equation with finite-ion gyroradius effects included through the polarization drift velocity, $\vec{v}_p = (M/eB^2)[1 + (3/4) \times \rho_\perp^2 \nabla_\perp^2](\partial\vec{\epsilon}/\partial t)$. Analogous to the procedures described in Section 2.3, an expression for the total parallel current was obtained by integrating this equation over velocity space. The result was then combined with the quasi-neutrality condition to generate a fourth-order radial differential equation which is approximately given by

$$\left\{\omega^2 \rho_i^2 \left(\frac{7}{4} - i\delta\right) \frac{\partial^4}{\partial r^4} + \frac{1}{r^3}\frac{\partial}{\partial r} r^3 \times [\omega^2(1 + i\Lambda_b) - \omega_A^2] \frac{\partial}{\partial r} - \left(\frac{m^2 - 1}{r^2}\right) \times [\omega^2(1 + i\Lambda_b) - \omega_A^2]\right\}\xi = 0 \quad (126)$$

where Φ, $A_\parallel$ are assumed to vary as $\exp[-i(m\theta - n\zeta + \omega t)]$, $\xi = -m\Phi/rB$ denotes the fluid-displacement variable, $\omega_A(r) \equiv k_\parallel(r) v_A$, $\delta \equiv \epsilon^{-1/2} \omega \nu_e [\omega^2 + (\nu_e/\epsilon)^2]^{-1}$ is the damping contribution from trapped electrons,

and $\Lambda_b \equiv [1-(\omega_{*b}/\omega)](n_b T_b)/(n_i M_i \omega^2 R^2)$ is the de-stabilizing beam contribution.

In analysing Eq.(126) Rosenbluth and Rutherford focused attention on fast-varying solutions amenable to a WKB-type treatment. Around the singular-layer region, where $\omega = \omega_A(r_0)$, such solutions are characterized by oscillatory behaviour for $0 < r < r_0$ and are evanescent for $r > r_0$. The authors reported that the stability criterion (obtained from the WKB eigenvalue condition) indicates that for $\omega < \omega_{*b}$ and sufficiently small r_0, unstable shear-Alfvén modes can appear. This implies that the beam could be anomalously flattened in radial density profile over the innermost region (e.g. $r_0 < 15$ cm for typical proposed TCT parameters). The effects here are considerably less severe than radially local estimates [55]. However, in discussing their results, Rosenbluth and Rutherford noted that in the analogous situation for alpha-particles in a reactor, the stability requirements (e.g. $r_0 > 80$ cm for typical parameters) are apparently difficult to satisfy. Hence, more careful studies relaxing some of the approximations made and including temperature gradient effects should be of interest.

5.2. High-frequency modes

As noted earlier, high-energy neutral-beam injection tends to produce strong velocity-space anisotropy which can lead to high-frequency electrostatic and electromagnetic modes. In addition, the slowing-down process for the injected ions can cause the plasma to have a sheared mean velocity along the magnetic field. Stix [53] has pointed out that for sufficiently large values of this parallel velocity shear, low-frequency modes, such as the Kelvin–Helmholz and ordinary drift instabilities, can be excited. Subsequently, Catto, et al. [218] carried out a more detailed analysis including magnetic shear and obtained specific criteria for the appearance of such instabilities.

With regard to the high-frequency modes, Berk, et al. [55] have performed extensive calculations in the infinite uniform-medium limit. Working with representative steady-state distributions obtained from approximate solutions of the Fokker-Planck equation, these authors found that for parallel injection the associated perpendicular velocity-space anisotropy is insufficient to de-stabilize the ion-cyclotron, lower-hybrid, and electron-plasma waves. They have additionally pointed out that compressional Alfvén instabilities should be avoidable since the injection velocity, v_b, typically falls below the Alfvén speed, v_A, i.e. the coupling between the beam and these Alfvén waves is suppressed if $v_b < v_A$. In subsequent work, Perkins [56] concluded that beam-driven electromagnetic ion-cyclotron modes can also be avoided under typical steady-state operating conditions for TCT systems. However, during the transient pre-heat phase, the fast-ion distribution can be sufficiently peaked to de-stabilize these waves.

Regarding peaked transient distributions, Mai and Horton [219] have obtained stability criteria for a variety of electrostatic instabilities. It was found that if the density of the fast-ion component is low compared to the main plasma component (i.e. n_b/n small), stabilizing effects, such as electron Landau damping, tend to keep these modes from becoming significantly disruptive. Although an extremely peaked transient distribution [$F_b \propto \delta(v-v_b)$] can be strongly de-stabilizing [220, 219], the spread generated by the resulting velocity-space diffusion should quickly suppress further disturbances [55, 219]. It is likely that this spreading of the distribution will also exert a strong stabilizing influence on the short-wavelength shear-Alfvén modes, which were recently analysed by Beasley, et al. [221] using $F_b \propto \delta(v - v_b)$.

For the case of perpendicular instead of parallel injection, Cordey and Houghton [54] have emphasized that a large variety of high-frequency waves, such as ion-cyclotron loss-cone modes, could be easily de-stabilized. Jassby [52], however, has subsequently noted that these instabilities are unlikely to persist under steady-state conditions, provided effects, such as charge exchange and large orbit losses of decelerating ions, do not severely deplete the lower-energy portion of the distribution. Although the linear stability compared to parallel injection is much worse, perpendicular-injection schemes provide the possibility of more efficient penetration of energetic ions. In particular, Jassby and Goldston [222] have recently proposed that perpendicular injection into vertically asymmetric toroidal field ripples can serve this purpose. The basic notion here is that the energetic ions, formed from the beam by ionization and charge exchange, will be mirror-trapped in the ripples and drift upward (i.e. into the plasma interior) with the ∇B-drift. By appropriately shaping the ripple, the ions can be de-trapped near the centre of the system, where they assume banana orbits and thermalize. Motivated by these considerations, Krommes, et al. [223] investigated the related high-frequency micro-instabilities. By taking into account the stabilizing influence of the radial convection of energy (associated, e.g. with magnetic-shear effects), the authors found that the beam density threshold, n_b/n, for the onset

of lower hybrid and convective loss-cone modes could be avoided if the beam is sufficiently spread. Above the linear stability threshold, quasi-linear estimates of the velocity ($v_\perp$) diffusion indicated that for typical parameters a sufficient spread in the distribution is reached before the instabilities grow to significant amplitudes.

Before leaving the subject of high-frequency tokamak microinstabilities, it should be noted that in the presence of an applied electric field, $\epsilon_\parallel$ (below the critical runaway field), the resulting velocity-space anisotropy generated in the electron distribution can also excite such modes. Coppi, et al. [59, 216] have extensively investigated this problem in the radially local, collisionless limit. Using a single-particle analysis, the authors numerically integrated a collisionless form of the drift-kinetic equation to obtain non-Maxwellian distributions. In the direction of acceleration by $\epsilon_\parallel$, it was found that an interval of positive slope could develop, while in the opposite direction a "loss-cone" tended to result. These so-called "slide-away" electron distributions were in turn found to give rise to electrostatic instabilities with characteristic frequencies close to the electron-cyclotron (Ω_e) and ion plasma (ω_{pi}) frequencies. The authors have proposed that the presence of such modes could account for the observation of increased ion temperatures and emission at the electron-cyclotron and ion plasma frequencies on the ALCATOR experiment.

5.3. Alpha-particle-driven modes

High-energy alpha-particles produced in fusion reactions can provide still another source of velocity-space anisotropy. The resulting "thermonuclear" instabilities are analogous to the fast-ion-driven modes discussed in the preceding section. Just as in the case of high-energy beams, spatial gradients associated with the alpha-particles can also be an accessible source of free energy. For example, Mikhailovskii [62] has pointed out that alpha-particle density gradients can drive shear-Alfvén modes unstable. He has found that such modes can be dangerous even for isotropic velocity distributions provided $v_\alpha > v_A$, i.e. if the alpha-particle velocity exceeds the Alfvén speed. Also, as noted in Section 5.1, shear-Alfvén modes can be additionally de-stabilized by resonant interactions with alpha particles that have unfavourable ∇B drifts [57].

Investigations of unstable modes driven by the velocity-space anisotropy of the alpha particles have primarily been focused on the fast magnetosonic (compressional Alfvén) waves. In particular, Kaladze and Mikhailovskii [60] have noted that these waves can be de-stabilized by resonant interactions with trapped alpha-particles at the alpha-particle gyro-frequency. Using a delta-function distribution, the authors found the growth rates to be proportional to the alpha-particle density. In subsequent studies, Lominadze and Mikhailovskii [61] showed that thermal spread in the distribution exerts a strong stabilizing influence, and Kaladze, et al. [224] demonstrated that vertical ellipticity in the plasma cross-section also favours stability. With the exception of Ref. [57], all of the alpha-particle-related calculations mentioned in the present section were carried out in the radially local limit.

6. CONCLUSIONS

As is obvious from the large amount of material discussed in this review, the investigation of micro-instabilities in tokamaks has remained an active area of theoretical studies in recent years. The purpose of this final section is to summarize the current status of research on the more actively analysed modes and to comment on important aspects of these instabilities which remain to be investigated.

In the area of linear low-frequency microinstability theory, the dissipative (collisional) and universal (collisionless) drift modes together with the trapped-electron and trapped-ion modes have received the most attention. Many important features, such as the inclusion of essential geometric and collisional effects, have been incorporated to provide more reliable estimates of stability criteria and growth rates. In particular, toroidal effects associated with ∇B-drifts have led to significantly more pessimistic predictions for stability.

With regard to the electrostatic analysis of dissipative and universal drift instabilities, the most interesting recent development is that, for a sheared slab model (1D-radial limit), these eigenmodes have been found to be stable [19a, 19b]. The calculations here were carried out in the long-wavelength ($k_r\rho_i < 1$) regime and involved retaining the complete de-stabilizing electron response in a non-perturbative analysis. Although unstable normal modes can be recovered by considering highly peaked density profiles [14], the requirement here that the width of the ω_*-profile be of the order of a few ion gyroradii is not likely to be satisfied in most experiments of current interest. In the light of these recent results, it would be of interest to re-examine impurity-driven

[18] and current-driven [12] drift eigenmodes in a sheared-slab geometry.

Despite the slab model results, drift instabilities can still readily appear in tokamaks as a consequence of the toroidal coupling effects, emphasized by Taylor [88] and discussed in detail in Section 2.2.3. The important point here is that the effective potential in the differential equation governing the eigenmodes in the long-wavelength regime can be converted from its "anti-well" character to that of a well by the toroidal terms. This, in turn, can prevent the stabilizing propagation of energy away from the unstable region, and leads to a localized ("ballooning") mode structure along the field line. Although the rough analytic models indicate the requirement that $rq'/q < 1/2$, for the toroidal coupling effects to be significant, recent 2D numerical calculations [141] seem to indicate that even at larger values of shear ($rq'/q > 1/2$), unstable drift eigenmodes can persist in a torus. The specific influence of shear on drift instabilities for arbitrary wavelengths in a toroidal geometry remains under investigation. In any case, for tokamak systems, it can be concluded at the present time that it is possible for dissipative drift modes to appear in the Pfirsch-Schlüter regime ($\nu_e^* > \epsilon^{-3/2}$) and the universal modes in the plateau regime ($1 < \nu_e^* < \epsilon^{-3/2}$). If present, the most unstable eigenmodes will tend to have a localized or ballooning structure along the field line and characteristic wave numbers and frequencies falling in the familiar ranges, $k_\perp \rho_i \lesssim 1$ and $v_i/Rq < \omega < v_e/Rq$ with $\omega \lesssim \omega_{*e}$.

In the area of trapped-particle instabilities, the most significant theoretical developments have involved (i) the understanding of the role of ∇B-drift effects; and (ii) the fully two-dimensional analysis of the trapped-electron modes in a toroidal geometry. Specifically, the inclusion of the ∇B-drift term in the non-adiabatic electron response leads to strongly de-stabilizing resonant [23] and non-resonant [24] effects on the trapped-electron modes. As a result, these instabilities can persist in the higher-temperature (more collisionless) regimes where they were previously believed to be stable. In particular, if design parameters are achieved, it is possible that both trapped-electron and trapped-ion instabilities could contribute to anomalous transport in large tokamaks such as T-10 and PLT.

With regard to the 2D analysis of trapped-electron eigenmodes, the results from these studies [27, 89, 90] have demonstrated that the toroidal effects (including the contributions from the trapped electrons and ion ∇B-drifts) produce a ballooning-type mode structure along the field line. These eigenmodes, which extend over many rational surfaces, appear to be insensitive to shear stabilization for $rq'/q \leqslant 1$ [141]. The determination of their actual radial extent is currently under investigation and involves the inclusion of the slow radial variations in equilibrium quantities and their gradients. With regard to the trapped-ion instabilities, the complete 2D mode structure in a toroidal geometry has yet to be determined. As a consequence, the true influence of shear on these eigenmodes remains an open question.

Summarily, the current status of the theory of trapped-particle instabilities indicates that within the banana regime, $\nu_{*j} < 1$, both trapped-electron and trapped-ion modes are likely to be present. Although the trapped-electron analysis is valid for arbitrary wavelengths, the fastest growing modes appear to have roughly the same characteristic wave numbers and frequencies as the drift instabilities, i.e. $k_\perp \rho_i \lesssim 1$ and $\omega \lesssim \omega_{*e}$. On the other hand, trapped-ion mode calculations have only been carried out in the long-wavelength limit where $k_\perp \rho_{Bi} < 1$ with ρ_{Bi} being the average ion radial banana width. Local and radial 1D calculations indicate that these long-wavelength, low-frequency instabilities ($\omega < \epsilon^{1/2} v_i$) will be very difficult to stabilize if sufficiently large ion temperature gradients ($\eta_i > 2/3$) are present to eliminate the favourable ion Landau damping effects.

With the continued progress toward reactor conditions, the subject of finite-beta effects on tokamak microinstabilities has become a prime area of interest. For low-frequency electrostatic modes, modifications in the form of enhanced favourable curvature [40, 92, 94] and coupling to shear-Alfvén waves [48, 28] tend to favour stability. However, it has also been pointed out that the shear-Alfvén branch itself can be destabilized by finite-beta effects (for $\beta_p > 1$) in the presence of toroidal curvature [49, 50]. Since $\omega \sim k_\parallel v_A$ for these modes and $k_\parallel$ is a non-local quantity, future work in this area should focus on the radial structure. In addition, with regard to both shear-Alfvén modes and finite-beta modified drift waves, further investigations of ballooning effects associated with ∇B-drifts and the presence of trapped particles are needed. High-energy ions from neutral-beam injection and alpha-particles from fusion reactions can additionally contribute to the de-stabilization of the shear-Alfvén waves [57, 62]. With regard to high-frequency instabilities driven by energetic beam ions, extensive studies [54–56] have indicated that for steady-state operation the system should be stable to such disturbances if parallel injection is employed.

As a final note, it should be mentioned that the basic kinetic-theory formalism applied to the investigation of microinstabilities has also been applied to the study of collisional electromagnetic instabilities such as tearing modes [225]. Since these modes generally fall in the category of MHD instabilities, they have not been discussed in the present review. Nevertheless, it is of interest to note that the magnetic perturbations generated by these modes, as well as by the shear-Alfvén and finite-β-modified drift waves, could lead to the formation of turbulent magnetic islands. As a result, plasma transport properties would be accordingly affected [226]. Hence, the kinetic treatment of the collisional electromagnetic modes is currently a subject of active research [227].

The non-linear theory required to determine the influence of microinstabilities on confinement is far less developed than the corresponding linear theory. Numerous approaches ranging from phenomenological models to formal weak- and strong-turbulence descriptions have been extensively studied. However, a compelling self-consistent non-linear theory remains elusive. Most estimates of anomalous transport and related confinement times are still either based on or do not markedly differ from the rough, upper-bound-type $D \sim \gamma/k_\perp^2$ approximation [2]. Exceptions for specific instabilities have been discussed in some detail in Section 4.

Fluctuation levels and spectral characteristics obtained from particle code simulations as well as from recent toroidal experiments have helped to indicate the relevance (or lack of relevance) of assumptions made in the non-linear theories. For example, even though the measured fluctuation amplitudes are small ($|\delta n/n| \lesssim 10^{-2}$), the large frequency spread, $|\Delta\omega/\omega|$, observed in the ATC experiment [208–210] is difficult to reconcile with most weak-turbulence calculations. In general, careful measurements of frequency and wave spectra have provided compelling evidence that low-frequency drift-type instabilities are likely to be present in toroidal systems. Although the fluctuation amplitudes are consistent with the observed anomalous transport, a definitive explanation of the empirical scalings, $D \propto 1/n$ and $(n)_{max} \propto B/R$, found, e.g. in the ALCATOR experiment [214], remains to be determined [228].

ACKNOWLEDGEMENTS

The author thanks Drs E.A. Frieman, J.L. Johnson, and P.H. Rutherford for suggesting this project and for their interest and encouragement. Very helpful discussions with Dr. G. Rewoldt and numerous other research personnel at Princeton are also gratefully acknowledged. Finally, special thanks go to Ms Rebecca Bell for her excellent work on this lengthy manuscript.

REFERENCES

[1] FURTH, H.P., Nucl. Fusion 15 (1975) 487.

[2] KADOMTSEV, B.B., POGUTSE, O.P., Nucl. Fusion 11 (1971) 67.

[3] KADOMTSEV, B.B., POGUTSE, O.P., in Reviews of Plasma Physics (LEONTOVICH, M.A., Ed.) Consultants Bureau, New York (1970) Vol. 5, 249.

[4] MOROZOV, A.I., SOLOVEV, L.S., Sov. Phys., Doklady 4 (1959) 1031.

[5] GALEEV, A.A., SAGDEEV, R.Z., Sov. Phys., JETP 26 (1968) 233.

[6] ROSENBLUTH, M.N., HAZELTINE, R.D., HINTON, F.L., Phys. Fluids 15 (1972) 116.

[7] HAZELTINE, R.D., HINTON, F.L., Revs. Mod. Phys. 48 (1976) 239.

[8] KADOMTSEV, B.B., Plasma Turbulence, Academic Press, New York (1965) 79.

[9] MIKHAILOVSKII, A.B., Theory of Plasma Instabilities, Consultants Bureau, New York, (1974) Vol. 2.

[10] BRAGINSKII, S.I., in Reviews of Plasma Physics (LEONTOVICH, M.A., Ed.) Consultants Bureau, New York (1965) Vol. 1, 205.

[11] YOSHIKAWA, S., Phys. Rev. Lett. 25 (1970) 353; ARTSIMOVICH, L.A., JETP Lett. 13 (1971) 70.

[12] See for example, CALLEN, J., COPPI, B., DAGAZIAN, R., GAJEWSKI, R., SIGMAR, D., in Plasma Physics and Controlled Nuclear Fusion Research (International Atomic Energy Agency, Vienna, 1971) Vol. 2, 451.

[13] GALEEV, A.A., ORAEVSKY, V.N., SAGDEEV, R.Z., Sov. Phys., JETP 17 (1963) 615.

[14] KRALL, N.A., ROSENBLUTH, M.N., Phys. Fluids 8 (1965) 1488; KRALL, N.A., in Advances in Plasma Physics (SIMON, A., THOMPSON, W., Eds.) Wiley, New York (1968) Vol. 1, 153.

[15] PEARLSTEIN, L.D., BERK, H.L., Phys. Rev. Lett. 23 (1969) 220.

[16] GLADD, N.T., HORTON, C.W., Phys. Fluids 16 (1973) 879.

[17] See for example, LIU, C.S., ROSENBLUTH, M.N., HORTON, C.W., Phys. Rev. Lett. 29 (1972) 1489.

[18] COPPI, B., FURTH, H.P., ROSENBLUTH, M.N., SAGDEEV, R.Z., Phys. Rev. Lett. 17 (1966) 377.

[19] See for example, Ref. [8], 85.

[19a] ROSS, D.W., MAHAJAN, S.M., Phys. Rev. Lett. 40 (1978) 325; TSANG, K.T., CATTO, P.J., WHITSON, J.C., SMITH, J., Phys. Rev. Lett. 40, (1978) 327.

[19b] CHEN, L., GUZDAR, P.N., HSU, J.Y., KAW, P.K., OBERMAN, C., WHITE, R.B., Preprint, Princeton Plasma Phys. Lab. Rept. PPPL-1423 (June, 1978).

[20] KADOMTSEV, B.B., POGUTSE, O.P., Sov. Phys., Doklady 14 (1969) 470.

[21] LIU, C.S., ROSENBLUTH, M.N., TANG, W.M., Phys. Fluids 19 (1976) 1040.

[22] TANG, W.M., RUTHERFORD, P.H., FURTH, H.P., ADAM, J.C., Phys. Rev. Lett. 35 (1975) 660.

[23] ADAM, J.C., TANG, W.M., RUTHERFORD, P.H., Phys. Fluids 19 (1976) 561.

[24] COPPI, B., REWOLDT, G., Phys. Rev. Lett. 33 (1974) 1329; Phys. Lett. 54A (1975) 301.

[25] YOSHIKAWA, S., OKABAYASHI, M., Phys. Fluids 17 (1974) 1762.

[26] See for example, Ref. [23].

[27] REWOLDT, G., TANG, W.M., FRIEMAN, E.A., Phys. Fluids 20 (1977) 402.

[28] TANG, W.M., LIU, C.S., ROSENBLUTH, M.N., CATTO, P.J., CALLEN, J.D., Nucl. Fusion 16 (1976) 191.

[29] ROSENBLUTH, M.N., ROSS, D.W., KOSTOMAROV, D.P., Nucl. Fusion 12 (1972) 3.

[30] SAGDEEV, R.Z., GALEEV, A.A., Sov. Phys., Doklady 13 (1968) 562.

[31] TANG, W.M., Nucl. Fusion 13 (1973) 883.

[32] TANG, W.M., Phys. Fluids 17 (1974) 1249.

[33] TANG, W.M., ADAM, J.C., ROSS, D.W., Phys. Fluids 20 (1977) 430.

[34] GLADD, N.T., ROSS, D.W., Phys. Fluids 16 (1973) 1706.

[35] DOBROWOLNY, M., ROSS, D.W., Phys. Fluids 18 (1975) 717.

[36] DOBROWOLNY, M., Nucl. Fusion 14 (1974) 599.

[37] ROSENBLUTH, M.N., Phys. Fluids 11 (1968) 869.

[38] BHADRA, D.K., LIU, C.S., Phys. Fluids 14 (1971) 2152.

[39] DOBROWOLNY, M., PARAVANO, A., Plasma Phys. 18 (1976) 761.

[40] ROSENBLUTH, M.N., SLOAN, M.L., Phys. Fluids 14 (1971) 1725.

[41] GLASSER, A.H., FRIEMAN, E.A., YOSHIKAWA, S., Phys. Fluids 17 (1974) 181.

[42] ADAM, J.C., LAVAL, G., PELLAT, R., Nucl. Fusion 13 (1973) 47.

[43] COPPI, B., Phys. Rev. Lett. 29 (1972) 1076.

[44] COPPI, B., MINARDI, E., Plasma Phys. 16 (1974) 1021.

[45] COPPI, B., TARONI, A., Plasma Phys. 16 (1974) 161; Plasma Phys. 17 (1975) 951.

[46] COPPI, B., REWOLDT, G., in Advances in Plasma Physics (SIMON, A., THOMPSON, W., Eds.) Wiley, New York (1976) Vol. 6, 421.

[47] COPPI, B., Phys. Rev. Lett. 31 (1973) 1443.

[48] CATTO, P.J., EL-NADI, A.M., LIU, C.S., ROSENBLUTH, M.N., Nucl. Fusion 14 (1974) 405.

[49] MIKHAILOVSKII, A.B., Nucl. Fusion 13 (1973) 259.

[50] MIKHAILOVSKII, A.B., Sov. J. Plasma Phys. 1 (1975) 38.

[51] DAWSON, J.M., FURTH, H.P., TENNEY, F.H., Phys. Rev. Lett. 26 (1973) 1156; FURTH, H.P., JASSBY, D.L., Phys. Rev. Lett. 32 (1974) 1176.

[52] JASSBY, D.L., Nucl. Fusion 17 (1977) 309.

[53] STIX, T.H., Phys. Fluids 16 (1973) 1922; Plasma Phys. 14 (1972) 367.

[54] CORDEY, J.G., HOUGHTON, M.J., Nucl. Fusion 13 (1973) 215.

[55] BERK, H.L., HORTON, W., ROSENBLUTH, M.N., RUTHERFORD, P.H., Nucl. Fusion 15 (1975) 819.

[56] PERKINS, F.W., Phys. Fluids 19 (1976) 1012.

[57] ROSENBLUTH, M.N., RUTHERFORD, P.H., Phys. Rev. Lett. 34 (1975) 1428.

[58] COPPI, B., BHADRA, D.K., Phys. Fluids 18 (1975) 692.

[59] COPPI, B., PEGORARO, F., POZZOLI, R., REWOLDT, G., Nucl. Fusion 16 (1976) 309.

[60] KALADZE, T.D., MIKHAILVOSKII, A.B., Sov. J. Plasma Phys. 1 (1975) 128.

[61] LOMINADZE, D.G., MIKHAILOVSKII, A.B., Sov. J. Plasma Phys. 1 (1975) 291.

[62] MIKHAILOVSKII, A.B., Sov. Phys., JETP 41 (1976) 890.

[63] HASTIE, R.J., TAYLOR, J.B., HAAS, F.A., Ann. Phys. 41 (1967) 302; HASTIE, R.J., TAYLOR, J.B., Plasma Phys. 13 (1968) 275.

[64] RUTHERFORD, P.H., FRIEMAN, E.A., Phys. Fluids 11 (1968) 569.

[65] JAMIN, E., Ph.D. Dissertation, Princeton University (1971).

[66] CATTO, P.J., TSANG, K.T., Phys. Fluids 20 (1977) 396.

[67] CONNOR, J.W., HASTIE, R.J., Plasma Phys. 17 (1975) 97.

[68] ROSENBLUTH, M.N., MACDONALD, W.M., JUDD, D.L., Phys. Rev. 107 (1957) 1.

[69] CALLEN, J.D., BEASLEY, C.O., FISCHER, S.K., HICKS, H.R., SEELY, J.F., Bull. Am. Phys. Soc. 19 (1974) 863.

[70] HINTON, F.L., ROSS, D.W., Nucl. Fusion 16 (1976) 329.

[71] HORTON, W., Phys. Fluids 19 (1976) 711.

[72] CATTO, P.J., TSANG, K.T., CALLEN, J.D., TANG, W.M., Phys. Fluids 19 (1976) 1596.

[73] BHATNAGAR, P.L., GROSS, E.P., KROOK, M., Phys. Rev. 94 (1954) 511; GROSS, E.P., KROOK, M., Phys. Rev. 102 (1956) 593.

[74] See for example, ROGISTER, A., HASSELBERG, G., Phys. Rev. Lett. 37 (1976) 906; Nucl. Fusion 16 (1976) 943.

[75] DOUGHERTY, J.P., Phys. Fluids 7 (1964) 1788.

[76] MIKHAILOVSKII, A.B., POGUTSE, O.P., Sov. Phys., Tech. Phys. 11 (1966) 153.

[77] See for example, Ref. [3], 265.

[78] COPPI, B., in Advances in Plasma Physics (SIMON, A., THOMPSON, W.B., Eds.) Wiley, New York (1971) Vol. 4, 173.

[79] ROBERTS, K.V., TAYLOR, J.B., Phys. Fluids 8 (1965) 315.

[80] LIEWER, P.C., MANHEIMER, W.M., TANG, W.M., Phys. Fluids 19 (1976) 276.

[81] MIKHAILOVSKII, A.B., JETP Lett. 23 (1976) 395.

[82] GALEEV, A.A., in Proceedings of the Third International Symposium on Toroidal Plasma Confinement, Garching, FRG, 26-30 March 1973, paper E1-1; SAGDEEV, R.Z., GALEEV, A.A., Comments on Plasma Phys. and Controlled Fusion 1 (1972) 23.

[83] HORTON, W., ROSS, D.W., TANG, W.M., BERK, H.L., FRIEMAN, E.A., LAQUEY, R.E., LOVELACE, R.V., MAHAJAN, S.M., ROSENBLUTH, M.N., RUTHERFORD, P.H., in Plasma Physics and Controlled Nuclear Fusion Research (International Atomic Energy Agency, Vienna, 1975) Vol. 1, 541.

[84] FRIED, B.D., CONTE, S.D., The Plasma Dispersion Function, Academic Press, New York (1961).

[85] ROSENBLUTH, M.N., CATTO, P.J., Nucl. Fusion 15 (1975) 573.

[86] JABLON, C., LAVAL, G., PELLAT, R., Phys. Rev. Lett. 27 (1971) 83.

[87] ROSS, D.W., HORTON, C.W., Phys. Rev. Lett. 28 (1972) 484.

[88] TAYLOR, J.B., in Plasma Physics and Controlled Nuclear Fusion Research (International Atomic Energy Agency, Vienna, 1977), Vol. 2, p. 323.

[89] TANG, W.M., ADAM, J.C., COHEN, B.I., FRIEMAN, E.A., KROMMES, J.A., REWOLDT, G., ROSS, D.W., ROSENBLUTH, M.N., RUTHERFORD, P.H., CATTO, P.J., TSANG, K.T., CALLEN, J.D., in Plasma Physics and Controlled Nuclear Fusion Research (International Atomic Energy Agency, Vienna, 1977), Vol. 2, p. 489.

[90] ROSS, D.W., MINER, W.H., Phys. Fluids 20 (1977) 1957.

[91] MUKHOVATOV, V.S., SHAFRANOV, V.D., Nucl. Fusion 11 (1971) 605.

[92] DOBROTT, D.R., GREENE, J.M., Plasma Physics 17 (1975) 929.

[93] SHAFRANOV, V.D., in Reviews of Plasma Physics (LEONTOVICH, M.A., Ed.) Consultants Bureau, New York, (1966) Vol. 2, 103.

[94] NEWBERGER, B.S., Ph.D. Dissertation, Princeton University (1976).

[95] MIKHAILOVSKII, A.B., RUDAKOV, L.I., Sov. Phys., JETP 17 (1963) 621.

[96] MISHIN, E.V., Sov. Phys., JETP 32 (1971) 148.

[97] CHEUNG, L., HORTON, W., Ann. Phys. 81 (1973) 201.

[98] HAZELTINE, R., Plasma Phys. 15 (1973) 77.

[99] RUKHADZE, A.A., SILIN, V.P., Sov. Phys. Uspekhi 11 (1969) 659.

[100] RUTHERFORD, P.H., FRIEMAN, E.A., Phys. Fluids 10 (1967) 1007.

[101] MANHEIMER, W., Phys. Fluids 19 (1976) 335.

[102] LAU, Y.Y., BRIGGS, R.J., Nucl. Fusion 15 (1975) 103.

[103] COPPI, B., Phys. Rev. Lett. 25 (1970) 851.

[104] ROSENBLUTH, M.N., LIU, C.S., Phys. Fluids 15 (1972) 1801.

[105] LIU, C.S., Phys. Rev. Lett. 27 (1971) 1637.

[106] HORTON, W., Phys. Rev. Lett. 28 (1972) 1506.

[107] CORDEY, J.G., HASTIE, R.J., Nucl. Fusion 17 (1977) 523.

[108] LEE, W.W., OKUDA, H., Phys. Rev. Lett. 36 (1976) 870.

[109] WONG, S.K., Phys. Fluids 18 (1975) 391.

[110] ONG, R.S.B., YU, M.Y., J. Plasma Phys. 4 (1970) 729.

[111] BHADRA, D.K., Phys. Fluids 14 (1971) 977; Plasma Phys. 11 (1969) 247.

[112] KOCH, R.A., HORTON, W., Phys. Fluids 18 (1975) 861.

[113] COPPI, B., REWOLDT, G., SCHEP, T., Phys. Fluids 19 (1976) 1144.

[114] DESCHAMPS, P., GRAVIER, R., RENAUD, C., SAMAIN, A., Phys. Rev. Lett. 31 (1973) 1457.

[115] SAUTHOFF, N.R., OKABAYASHI, M., SCHMIDT, J.A., Phys. Fluids 18 (1975) 915.

[116] HORTON, W., ESTES, R., KWAK, H., CHOI, D., Phys. Fluids (in press).

[117] TANG, W.M., RUTHERFORD, P.H., FRIEMAN, E.A., LIU, C.S., Bull. Am. Phys. Soc. 19 (1974) 866.

[118] TSANG, K.T., CALLEN, J.D., CATTO, P.J., Phys. Fluids 20 (1977) 2113.

[119] COPPI, B., LAVAL, G., PELLAT, R., ROSENBLUTH, M.N., Plasma Phys. 10 (1968) 1.

[120] MIKHAILOVSKII, A.B., Sov. Phys. Doklady 21 (1976) 339.

[121] ROSS, D.W., TANG, W.M., ADAM, J.C., Phys. Fluids 20 (1977)613.

[122] CHU, K.R., MANHEIMER, W.M., Nucl. Fusion 18 (1978) 29.

[123] DÜCHS, D.F., POST, D.E., RUTHERFORD, P.H., Nucl. Fusion 17 (1977) 565.

[124] ROSS, D.W., Nucl. Fusion 14 (1974) 447.

[125] BHADRA, D.K., Phys. Fluids 18 (1975) 380.

[126] BUSSAC, M.N., LAVAL, G., PELLAT, R., Phys. Rev. Lett. 30 (1973) 588.

[127] COPPI, B., REM, J., Phys. Fluids 17 (1974) 184.

[128] MATSUDA, Y., OKUDA, H., Phys. Rev. Lett. 36 (1976) 474.

[129] SEN, A., SUNDARAM, A.K., Nucl. Fusion 16 (1976) 303.

[130] PRAGER, S.C., SEN, A.K., MARSHALL, T.C., Phys. Rev. Lett. 33 (1974) 692.

[131] CHEN, F.F., FURTH, H.P., Nucl. Fusion 9 (1969) 364.

[132] FURTH, H.P., RUTHERFORD, Phys. Fluids 12 (1969) 2638.

[133] TAGGER, M., LAVAL, G., PELLAT, R., Nucl. Fusion 17 (1977) 109.

[134] DOBROWOLNY, M., Plasma Phys. 16 (1974) 996.

[135] POGUTSE, O.P., Nucl. Fusion 9 (1969) 157.

[136] LIU, C.S., Phys. Fluids 12 (1969) 1489.

[137] LIU, C.S., BHADRA, D.K., Phys. Rev. Lett. 25 (1970) 1706.

[138] BRIGGS, R.J., LAU, Y.Y., Phys. Rev. Lett. 28 (1972) 1248.

[139] COPPI, B., POZZOLI, R., Plasma Phys. 16 (1973) 223.

[140] COPPI, B., PEGORARO, F., Nucl. Fusion 17 (1977) 969.

[141] REWOLDT, G., TANG, W.M., FRIEMAN, E.A., Phys. Fluids (in press).

[142] SAGDEEV, R.Z., GALEEV, A.A., Nonlinear Plasma Theory, Benjamin, New York (1969).

[143] TSYTOVICH, V.N., Nonlinear Effects in Plasma, Plenum, New York (1970).

[144] DAVIDSON, R.C., Methods in Nonlinear Plasma Theory, Academic Press, New York (1972).

[145] DUPREE, T.H., Phys. Fluids 11 (1968) 2680; Phys. Fluids 10 (1967) 1049; Phys. Fluids 9 (1966) 1773.

[146] GALEEV, A.A., Phys. Fluids 10 (1967) 1041.

[147] WEINSTOCK, J., Phys. Fluids 12 (1969) 1045; Phys. Fluids 11 (1968) 1977.

[148] See for example, OKUDA, H., DAWSON, J.M., Phys. Fluids 16 (1973) 408.

[149] DUPREE, T.H., Phys. Fluids 17 (1974) 100; Phys. Fluids 15 (1972) 334; Comments on Plasma Phys. and Controlled Fusion 1 (1972) 33.

[150] WADDELL, B.V., Nucl. Fusion 15 (1975) 803.

[151] EHST, D.A., Ph.D. Dissertation, Massachusetts Institute of Technology (1976); Phys. Fluids 20 (1977) 2076.

[152] SUGIHARA, M., OGASAWARA, M., Journal of Phys. Soc. of Japan 41 (1976) 1370.

[153] JABLON, C.J., Phys. Rev. Lett. 28 (1972) 880.

[154] KADOMTSEV, B.B., POGUTSE, O.P., Sov. Phys., Doklady 14 (1970) 863; Sov. Phys., Doklady 14 (1970) 881.

[155] OTT, E., MANHEIMER, W.M., Phys. Fluids 19 (1976) 1035.

[156] SMITH, G.R., Phys. Rev. Lett. 38 (1977) 970.

[157] DOBROWOLNY, M., NEGRINI, P., Phys. Rev. Lett. 28 (1972) 132.

[158] JABLON, C., RUTHERFORD, P.H., Phys. Fluids 14 (1971) 2033; DOBROWOLNY, M., POGUTSE, O.P., Phys. Rev. Lett. 25 (1970) 1608; ROSS, D.W., POGUTSE, O.P., Nucl. Fusion 11 (1971) 127.

[159] BERK, H.L., ROSENBLUTH, M.N., Nucl. Fusion 15 (1975) 1013.

[160] COHEN, B.I., KROMMES, J.A., TANG, W.M., ROSENBLUTH, M.N., Nucl. Fusion 16 (1976) 971.

[161] WIMMEL, H.K., Plasma Phys. 18 (1975) 321; Plasma Phys. 18 (1975) 693.

[162] SAISON, R., WIMMEL, H.K., in Plasma Physics and Controlled Nuclear Fusion Research (International Atomic Energy Agency, Vienna, 1977), Vol. 2, 481.

[163] LAQUEY, R.E., MAHAJAN, S.M., RUTHERFORD, P.H., TANG, W.M., Phys. Rev. Lett. 34 (1975) 391.

[164] COHEN, B.I., TANG, W.M., Nucl. Fusion (to be published).

[165] TASSO, H., Phys. Lett 24A (1967) 618; ORAEVSKII, V.N., TASSO, H., WOBIG, H., in Plasma Physics and Controlled Nuclear Fusion Research (International Atomic Energy Agency, Vienna, 1969) Vol. I, 671.

[166] OTT, E., MANHEIMER, W.M., BOOK, D.L., BORIS, J.P., Phys. Fluids 16 (1973) 885.

[167] MANHEIMER, W.M., CHU, K.R., OTT, E., BORIS, J.P., CALLEN, J.D., Nucl. Fusion 16 (1976) 203.

[168] HORTON, W., Phys. Rev. Lett. 37 (1976) 1269.

[169] HORTON, W., OKUDA, H., CHENG, C.Z., KUO, Y.Y., LEE, W.W., MATSUDA, Y., TRUE, M., in Plasma Physics and Controlled Nuclear Fusion Research (International Atomic Energy Agency, Vienna, 1977), Vol. 2, 467.

[170] See for example, DOBROWOLNY, M., NOCENTINI, A., Plasma Phys. 16 (1974) 433; Nucl. Fusion 13 (1973) 629.

[171] HASSELBERG, G., ROGISTER, A., EL-NADI, A., Phys. Fluids 20 (1977) 982.

[172] SATYA, Y.S., KAW, P.K., Phys. Rev. Lett 31 (1973) 1453.

[173] CHEN, L., KAW, P.K., TANG, W.M., Nucl. Fusion 16 (1976) 661.

[174] VEDENOV, A.A., GORDEEV, A.V., RUDAKOV, L.I., Plasma Phys. 9 (1967) 719.

[175] SIMON, A., Phys. Fluids 11 (1968) 1181.

[176] HINTON, F.L., HORTON, C.W., Phys. Fluids 14 (1971) 116.

[177] MONTICELLO, D.A., SIMON, A., Phys. Fluids 17 (1974) 791.

[178] STIX, T.H., Phys. Fluids 12 (1969) 627.

[179] SIMON, A., GROSS, L.S., Phys. Fluids 20 (1977) 946.

[180] MANHEIMER, W.M., CHU, K.R., OTT, E., BORIS, J.P., Phys. Rev. Lett. 37 (1976) 286; MANHEIMER, W.M., BORIS, J.P., Comments Plasma Phys. 3 (1977) 15.

[181] DAWSON, J.M., OKUDA, H., ROSEN, B., in Methods in Computational Physics, Academic Press, New York (1976) Vol. 16, 281.

[182] CHENG, C.Z., OKUDA, H., Phys. Rev. Lett. 38 (1977) 708.

[183] CHENG, C.Z., OKUDA, H., Nucl. Fusion 18 (1978) 587.

[184] OKABAYASHI, M., ARUNASALAM, V., Nucl. Fusion 17 (1977) 497.

[185] DEAN, S.O., CALLEN, J.D., FURTH, H.P., CLARKE, J.F., OHKAWA, T., RUTHERFORD, P.H., "Status and Objectives of Tokamak Systems for Fusion Research," USAEC Rept. WASH-1295, U. S. Atomic Energy Commission, Washington, D.C. (1974).

[186] DNESTROVSKII, Y.N., KOSTOMAROV, D.P., Sov. At. Energy 29 (1970) 1205.

[187] DNESTROVSKII, Y.N., KOSTOMAROV, D.P., PAVLOVA, JETP Lett. 13 (1971) 493.

[188] MERCIER, C., SOUBBARAMAYER, in Plasma Physics and Controlled Nuclear Fusion Research (International Atomic Energy Agency, Vienna, 1971) Vol. I, 425.

[189] DÜCHS, D.F., FURTH, H.P., RUTHERFORD, P.H., in Plasma Physics and Controlled Nuclear Fusion Research (International Atomic Energy Agency, Vienna, 1971) Vol. I, 369.

[190] HOGAN, J.T., in Methods in Computational Physics, Academic Press, New York (1976) Vol. 16, 131.

[191] KRALL, N.A., LIEWER, P.C., Phys. Rev. Lett. 36 (1976) 1041.

[192] MANHEIMER, W.M., OTT, E., TANG, W.M., Phys. Fluids 20 (1977) 806.

[193] HENDEL, H.W., CHU, T.K., POLITZER, P.A., Phys. Fluids 11 (1968) 2426.

[194] ELLIS, R.F., MOTLEY, R.W., Phys. Fluids 17 (1974) 582.

[195] POLITZER, P.A., Phys. Fluids 14 (1971) 2410; STOTT, P.E., LITTLE, P.F., BURT, J., Phys. Rev. Lett. (1970) 996.

[196] PRIMMERMAN, C.A., LIDSKY, L.M., POLITZER, P.A., Phys. Rev. Lett. 33 (1974) 957; PRIMMERMAN, C.A., Ph.D. Dissertation, Massachusetts Institute of Technology (1975).

[197] YOSHIKAWA, S., Nucl. Fusion 13 (1973) 433.

[198] PACHER, H.D., PACHER, G.W., YOSHIKAWA, S., Phys. Rev. Lett. 25 (1970) 1559; PACHER, H.D., VON GOELER, S., Phys. Fluids 14 (1971) 1268.

[199] EJIMA, S., OKABAYASHI, M., Phys. Fluids 18 (1975) 904.

[200] SAUTHOFF, N.R., Ph.D. Dissertation, Princeton University (1975).

[201] ARUNASALAM, V., OKABAYASHI, M., HAWRYLUK, R.J., SUCKEWER, S., Phys. Rev. Lett. 36 (1976) 726; Phys. Fluids 20 (1977) 95.

[202] ALCOCK, M.W., ASHBY, D.E.T.F., CORDEY, J.G., EDLINGTON, T., FLETCHER, W.H.W., JONES, E.M., MALMBERG, J., RIVIERE, A.C., START, D.F.H., SWEETMAN, D.R., in Plasma Physics and Controlled Nuclear Fusion Research (International Atomic Energy Agency, Vienna, 1977), Vol. 2, 321.

[203] DRAKE, J.R., GREENWOOD, J.R., NAVRATIL, G.A., POST, R.S., Phys. Fluids 20 (1977) 148; NAVRATIL, G.A., POST, R.S., EHRHARDT, A.B., Phys. Fluids 20 (1977) 156.

[204] DRAKE, J.R., KERST, D.W., NAVRATIL, G.A., POST, R.S., EJIMA, S., LAHAYE, R., MOELLER, C., OHKAWA, T., PETERSEN, P.I., PRATER, R., WONG, S.K., in Plasma Physics and Controlled Nuclear Fusion Research (International Atomic Energy Agency, Vienna, 1977), Vol. 2, 343.

[205] KAWAHATA, K., FUJIWARA, M., J. Phys. Soc. Japan 40 (1976) 1150.

[206] HATORI, T., NISHIKAWA, K.I., TERASHIMA, Y., DODO, T., OKADA, O., in Plasma Physics and Controlled Nuclear Fusion Research

(International Atomic Energy Agency, Vienna, 1976), Vol. 2, 351.

[207] HAMBERGER, S.M., SHARP, L.E., LISTER, J.B., MROWKA, S., Phys. Rev. Lett. 37 (1976) 1345.

[208] MAZZUCATO, E., Phys. Rev. Lett. 36 (1976) 792.

[209] GOLDSTON, R.J., MAZZUCATO, E., SLUSHER, R.E., SURKO, C.M., in Plasma Physics and Controlled Nuclear Fusion Research (International Atomic Energy Agency, Vienna, 1977) Vol. I, 371.

[210] SURKO, C.M., SLUSHER, R.E., Phys. Rev. Lett. 37 (1976) 1747.

[211] HASEGAWA, A., Phys. Lett. 57A (1976) 143.

[212] EQUIPE TFR, in Plasma Physics and Controlled Nuclear Fusion Research (International Atomic Energy Agency, Vienna, 1977) Vol. I, 35; "Ohmic Heating and Electron Power Balance in TFR," 3rd Symposium on Plasma Heating in Toroidal Devices, Varenna, Italy (Sept., 1976) private communication.

[213] BERRY, L.A., (ORMAK GROUP), in Plasma Physics and Controlled Nuclear Fusion Research (International Atomic Energy Agency, Vienna, 1977) Vol. I, 49.

[214] APGAR, E., (ALCATOR GROUP), in Plasma Physics and Controlled Nuclear Fusion Research (International Atomic Energy Agency, Vienna, 1977) Vol. I, 247.

[215] COPPI, B., LAMPIS, G., PEGORARO, F., Phys. Lett. 59A (1976) 118.

[216] BASU, B., COPPI, B., MOLVIG, K., PEGORARO, F., HABER, I., HUI, B., PALMADESSO, P., PAPADOPOULOS, K., WINSOR, N., in Plasma Physics and Controlled Nuclear Fusion Research (International Atomic Energy Agency, Vienna, 1977), Vol. 2, 455.

[217] MIKHAILOVSKII, A.B., FRIDMAN, A.M., Nucl. Fusion 16 (1976) 837.

[218] CATTO, P.J., ROSENBLUTH, M.N., LIU, C.S., Phys. Fluids 16 (1973) 1719.

[219] MAI, L.P., HORTON, W., Phys. Fluids 18 (1975) 356.

[220] KORABLEV, L.V., RUDAKOV, L.I., Sov. Phys. JETP 27 (1968) 439.

[221] BEASLEY, C.O., LOMINADZE, J.G., MIKHAILOVSKII, A.B., Sov. J. Plasma Phys. 2 (1976) 95.

[222] JASSBY, D.L., GOLDSTON, R.J., Nucl. Fusion 18 (1975) 356.

[223] KROMMES, J.A., ROSENBLUTH, M.N., TANG, W.M., Nucl. Fusion 17 (1977) 667.

[224] KALADZE, T.D., LOMINADZE, J.G., MIKHAILOVSKII, A.B., POKHOTELOV, D.A., Nucl. Fusion 16 (1976) 465.

[225] See for example, COPPI, B., Phys. Fluids 7 (1964) 1501.

[226] CALLEN, J.D., Phys. Rev. Lett. 39 (1977) 1540.

[227] DRAKE, J., LEE, Y.C., Phys. Fluids 20 (1977) 1431; CHEN, L., RUTHERFORD, P.H., TANG, W.M., Phys. Rev. Lett. 39 (1977) 460.

[228] ROSENBLUTH, M.N., Theoretical Summary of Magnetic Confinement, 6th IAEA Conference on Plasma Physics and Controlled Nuclear Fusion Research, Berchtesgaden, FRG, (Oct., 1976) Nucl. Fusion 16 (1976) 1051.